이학박사 학위논문

GaN microstructures and nanostructures grown on graphene for transferable device applications

그래핀 상에 성장한 질화갈륨 마이크로 및 나노구조물과 이의 이동가능한 소자 응용

2015년 2월

서울대학교 대학원
물리 천문 학부
정 건 욱

Doctoral Thesis

GaN microstructures and nanostructures grown on graphene for transferable device applications

Kunook Chung
Department of Physics and Astronomy
Seoul National University
2015

GaN microstructures and nanostructures grown on graphene for transferable device applications

그래핀 상에 성장한 질화갈륨 마이크로 및
나노구조물과 이의 이동가능한 소자 응용

지도교수 이 규 철

이 논문을 이학박사학위논문으로 제출함
2014년 12월

서울대학교 대학원
물리·천문학부
정 건 욱

정건욱의 박사학위논문을 인준함
2014년 12월

위 원 장	홍 승 훈	(인)
부 위 원 장	이 규 철	(인)
위 원	김 대 식	(인)
위 원	이 탁 희	(인)
위 원	홍 영 준	(인)

DMS 200920428 정건욱 KunooK Chung, GaN microstructures and nanostructures grown on graphene for transferable device applications, 그래핀 상에 성장한 질화갈륨 마이크로 및 나노구조물과 이의 이동가능한 소자 응용, Department of Physics and Astronomy, and Institute of Applied Physics, 2015, P 196, Adviser: Prof. Gyu-Chul Yi, Text in English

Abstract

Current inorganic semiconductor devices, including light emitting diodes (LEDs), are based mostly on groundbreaking achievements in semiconductor technology, such as fabrication of heterostructures used in high performance devices (Nobel Prize in 2000) and invention of efficient LEDs (Nobel Prize in 2014). Recently, due to the demand for electronic and optoelectronic devices with large-size and flexibility, many efforts have been made to fabricate the devices in a foldable form using inorganic, organic semiconductors, and their hybrids. For the fabrication of high performance devices, inorganic semiconductors have many advantages over organic semiconductors because of their high radiative recombination rates, high carrier mobility as well as long term stability and reliability. However, problems associated with high-quality inorganic material preparation on flexible and large-size substrates are one of the major obstacles to use inorganic semiconductors in flexible and large-scale device applications. In particular, the limited size and rigidity of typical inorganic semiconductor growth substrates require further developments of novel material system and device

fabrication process suitable for the recent trend. Here, this dissertation introduces a novel material system of hybrid heterostructure, which composed of epitaxial inorganic semiconductor thin films and catalyst-free one dimensional (1D) micro- and nanostructures directly grown on graphene films, for transferable and flexible inorganic semiconductor device applications.

This thesis consists of 7 parts. Following by general introduction in chapter 1, chapter 2 reviews preparation methods and characteristics of graphene briefly and discusses about graphene as an inorganic growth substrates for transferable and flexible device applications. In chapter 3, the detailed experimental set-ups and procedures, including growth, fabrication and characterization methods, are described. Chapter 4 presents a method to grow epitaxial GaN films on graphene films. GaN films were grown on various graphene films, such as mechanically exfoliated graphene layers from the graphite powder and chemical vapor deposition grown graphene films. The optical and structural characteristics of GaN films grown on various graphene substrates are also discussed. In addition to the GaN films, 1D GaN micro- and nanorods were grown on graphene films with high optical and structural quality, which are described in chapter 5. Using these hybrid heterostructures, transferable, large-scale, and flexible optoelectronic devices were fabricated in chapter 6. Finally, chapter 7 presents the summaries of this thesis with suggestion for future works.

Table of Contents

List of Figures

List of Tables

Introduction

1

The preparation of high-quality inorganic compound semiconductors on flexible and large-size substrates, such as glass, metal, and plastic substrates, represents a significant breakthrough in fabrication technology, which may enable next-generation optoelectronic and electronic devices that are flexible and can be manufactured using large-scale and low-cost processes.[1-4] A number of difficulties remain in the fabrication of high-quality compound semiconductors on these substrates, however. Because of the limited thermal budget or lack of epitaxial growth on these substrates, growth of compound semiconductors is not straightforward. In addition, conventional inorganic semiconductor transfer techniques, such as laser-lift-off, require complicated processes—including numerous lithography and etching steps—to fabricate and assemble devices.[5] To overcome these problems, strategies using unconventional etching and release techniques have been used. [1, 6]

One powerful solution has been exploiting the growth of hybrid heterostructures composed of inorganic semiconductors grown on two dimensional (2D) layered materials, such as graphene and hexagonal boron nitride.[2, 3, 7] In particular, the 2D layers offer weak atomic bonding to the underlying substrate, as well as excellent mechanical flexibility, which can enable transfer of compound semiconductors to create transferable and flexible inorganic devices. Moreover, a combination of different inorganic semiconductors and 2D

layers may lead to a range of flexible devices with diverse functionality, including solar cells, field effect transistors, field-emission devices, optical communication devices, and light-emitting diodes (LEDs).

Among various inorganic compound semiconductors, nitride semiconductors (AlN, GaN, InN, and their alloys) can be one of the most promising candidates for the fabrication of inorganic semiconductor/graphene hybrid heterostructures. For example, because of the excellent optical and electrical characteristics of nitride semiconductors, full-color-spectrum nitride LEDs with high efficiency and reliability and long-term stability are now commercially available. [8-10] Nevertheless, problems of limited substrate size, high cost, high-resistance ohmic contacts, and poor heat dissipation remain, primarily because of the requirement of a sapphire substrate for nitride film growth. Additionally, for large-area or flexible-device applications, the device must be fabricated on glass, plastic, or metal substrates. However, high-quality, epitaxial nitride films can be grown only on a lattice-matched single-crystal substrate at a high growth temperature, above 1000°C;[8] glass and plastic substrates have no tolerance for such high temperatures, and, as amorphous materials, cannot be used for epitaxial growth of a crystalline film.[11] For this reason, previous techniques, most notably epitaxial growth and lift-off, have separated thin films from their growth substrates to make flip-chip devices on metal substrates.[12] However, difficulties in separating the films from a single-crystal substrate arising from strong bonding between GaN and sapphire and their high mechanical and chemical stability have limited the use of such techniques. This difficulty can be

resolved readily using substrates composed of graphene layers because the graphene-layer structure makes it possible to transfer the epitaxial film grown on graphene layers.

The present research focused on the growth of high quality GaN films and 1D GaN micro- and nanostructures on graphene films for transferable and flexible optoelectronic device applications. For the material growths, metal-organic chemical vapor deposition (MOCVD) growth techniques were employed, which is desirable because of advantages such as the feasibility of large area growth as well as a relatively simple and accurate doping and thickness control. In addition, various graphene films, including mechanically exfoliated graphene layers from the graphite powder and graphene films synthesized on Cu and Ni foils by chemical deposition method (CVD), was used for the growth substrates. In particular, the large-size graphene films have become available over 30 inches,[13] the hybrid heterostructures would open up diverse opportunities to fabricate various electronic and optoelectronic devices such as flexible and wearable LED displays in large-scale.

Heteroepitaxial nitride thin films were grown on graphene films using high-density vertically aligned ZnO nanowalls as an intermediate layer. The GaN films showed high structural and optical characteristics, such as stimulated emission at room temperature and a highly *c*-axis oriented crystal structure. As one of the examples for device applications, LEDs, emitting strong electroluminescence (EL) emission under room illumination, were fabricated. In

addition, the layered structure of a graphene substrate made it possible to transfer GaN-based LEDs onto foreign substrates such as glass, metal, or plastic easily.

Moreover, graphene offers a hexagonal basal plane of atomic lattices, which enables to grow high-quality GaN films without using expansive and size limited single crystal substrates. The simple technique to obtain high quality inorganic semiconductors even on amorphous substrates would enables to fabricate LEDs on large-area non-crystalline solid substrates, generally providing and manufacturing large and cost-effective optoelectronic and electronic devices. Methods of growing high-quality GaN films on large-scale CVD graphene films and fabricating light-emitting devices directly on the films prepared on amorphous silica substrates are presented. Furthermore, position controlled GaN micro-film/graphene heterostructure arrays can be fabricated over the entire substrates of SiO_2 or metal films.

For flexible device applications, the growth of 1D GaN micro- and nanorods and coaxial quantum-well heterostructures on graphene films were investigated. Highly Si-doped, *n*-type GaN micro-rods were grown on the CVD graphene films with excellent vertical alignments. In addition, the nanorod LEDs exhibited intense emission of visible light, even after transfer onto the flexible polymer substrate, and reliable operation was achieved following numerous cycles of mechanical deformation.

Background and literature survey

2

This chapter reviews physical characteristics and preparation methods of graphene films, and introduces graphene films as an inorganic semiconductor growth substrate. Very recently, graphene have been paid much attention in the field of material science due to the high electrical characteristics as well as optical transparency and mechanical flexibility.[14-17] Following this high interest, inventors of graphene received Nobel Prize in Physics 2010. However, it is hard to fabricate optoelectronic devices, such as LEDs and solar cells, using graphene because of the zero band-gap. Meanwhile, single crystal ZnO nanorods were grown on few-layer-graphene in 2009,[18] which opens the new possibility of fabricating graphene-based optoelectronic devices by hybridization of inorganic compound semiconductors on graphene. Moreover, as a view of inorganic semiconductor growth substrates, graphene have many advantages for inorganic semiconductor device applications by providing transferability, flexibility, and large-scale synthesis to the devices. For a comparison, current research on transferable and flexible inorganic semiconductor devices is also presented in this chapter.

2.1. Preparation methods and characteristics of graphene films

Graphene is a monolayer of graphite, which consists of weakly bonded layers of hexagonally arranged carbon atoms held together by strong covalent bonds. Professors Geim and Novoselov, who won Nobel Prize in Physics 2010, firstly succeed to prepare single-layer-graphene and investigated electrical characteristics of graphene in 2004.[14] Figures 2.1a and 2.2b show optical microscopy image of multi-layer-graphene and atomic force microscopy (AFM) image of single-layer-graphene, respectively. Atomically thin graphene layers were prepared by a simple preparation method: single-layer-graphene was prepared by repeated peeling of graphite powder using sticky tape. In addition, high electrical characteristics of graphene were demonstrated, exhibiting high electron mobility as high as 10,000−15,000 cm^2/Vs for mono-layer-graphene or multi-layer-graphene even at room temperature. More interestingly, Kim *et al*. observed half-integer quantum Hall effect in graphene as shown in Fig. 2.1c, which effect had been observed only from the well-defined quantum wells in semiconductor interfaces.[15] Because of easy preparation and excellent electrical characteristics, graphene opens up a new field of 2D layered materials and are drawing attention as an upcoming next generation electronics materials.

In addition to the excellent electrical characteristics, other physical characteristics of graphene were investigated by other groups. The elastic properties and intrinsic breaking strength of graphene layers were investigated using AFM.[16] The free-standing graphene layers, which were prepared by mechanically exfoliation of the graphite, exhibited Young's modulus of 1.0 TPa

and the intrinsic strength of 130 GPa. Furthermore, graphene shows high optical transparency because it is atomically thin. Figure 2.1d shows the optical transparency of graphene layers. According to the experimental result, one layer of graphene absorbs 2.3 % fraction of incident white light, and this value was consistent with the theoretical prediction.[17] As the layer number of graphene increased from 1 to 5, the transmittance of graphene layers decreased with the 2.3 % fraction. These results strongly suggested that graphene-based devices can be fabricated in transparent and flexible form.

Since graphene showed very interesting physical properties, many efforts have been paid on the preparation of large-scale graphene films for practical applications. Among various methods, chemical vapor deposition (CVD) on metal foil (or metal film) has been widely used for growing large-scale graphene films because of their easy synthesis and relative high quality. Many diverse metal substrates were used for the graphene growths by CVD method, including Ni, and Cu foils. In particular, Hong *et al*. demonstrated flexible and large-scale CVD graphene films as large as 30 inches, as shown in Fig. 2.2a, which was extremely larger than mechanically exfoliated graphene layers from the graphite flake.[13] Furthermore, when the number layer of CVD graphene films is less than 4, they exhibited high optical transmittance over 90 % for visible light with a sheet resistance of 50−270 Ω/□, as shown in Fig. 2.2b.

The major difference in CVD graphene films with mechanically exfoliated graphene layers is that CVD graphene films have multi-domain with random in-plane orientations.[19-21] Figure 2.2c shows the domain size and orientations of

CVD graphene films synthesized on Cu foil by direct observation using tunneling electron microscopy (TEM).[20] According to these results, CVD-grown graphene films exhibited typical grain size of few to tens of μm, and high angle grain boundaries were observed between graphene domains. Meanwhile, electrical characteristics of CVD graphene films were investigated using CVD graphene prepared by different growth conditions which resulted in different mean grain sizes, as shown in Fig. 2.2d.[21] The room temperature mobility of CVD graphene films with the grain sizes of 250, 470, and 1700 nm were 1000, 7300, and 5300 cm^2/Vs, respectively. This result suggested that graphene grain size did not significantly affect to the electrical characteristics. Furthermore, the mobility of CVD graphene films was much higher than those of single crystal silicon (1500 cm^2/Vs) although it depends on the growth conditions of CVD graphene. However, single crystal graphene growth is still main issues in CVD graphene because defective grain boundaries can affect to non-uniform electrical and mechanical characteristics of graphene.

Meanwhile, Samsung and Sungkyunkwan University reported wafer-scale growth of single crystal graphene as shown in Figs. 2.3a-c.[22] The single crystal graphene films were grown on Si wafer using hydrogen terminated Ge buffer layer, exhibiting homogeneous surface morphology without any wrinkles and high mobility as high as 10,000 cm^2/Vs. This result would provide many advantages for developing graphene-based electronic and optoelectronic devices in large-scale.

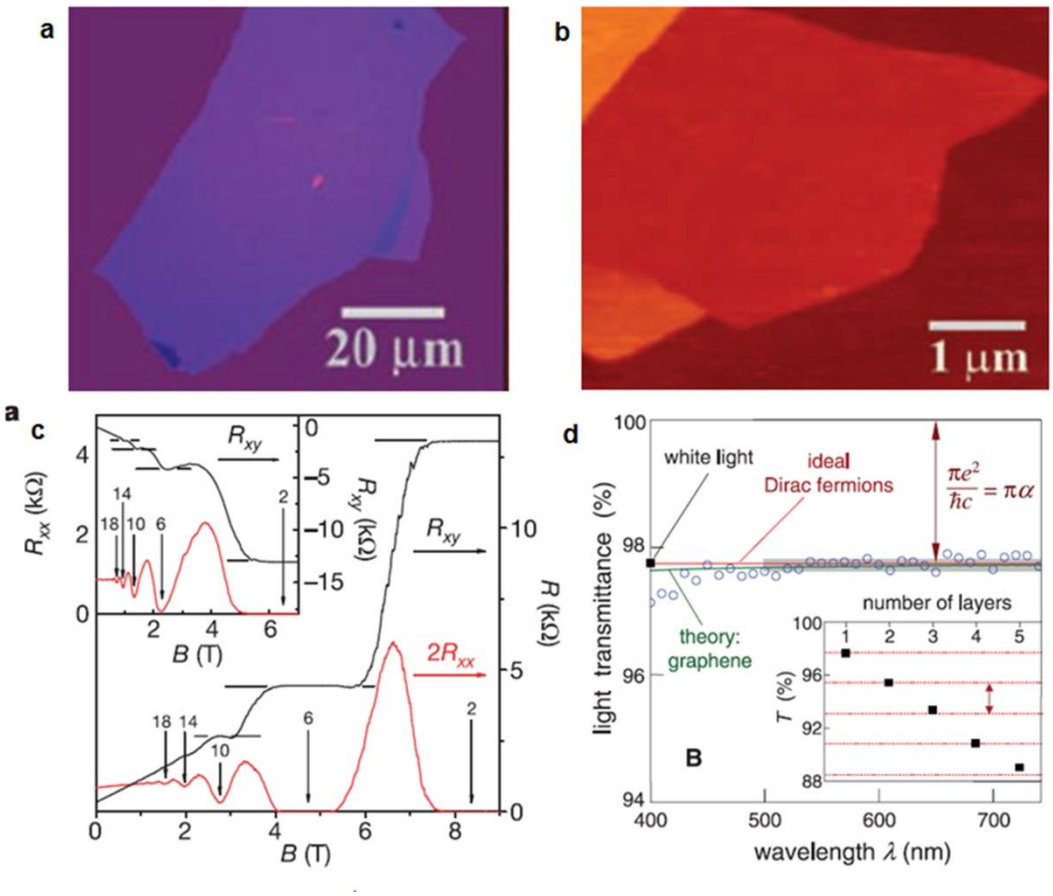

Fig. 2.1. Surface morphologies and physical characteristics of mechanically exfoliated graphene layers. (a) Optical image of multi-layer-graphene transferred onto SiO_2/Si substrate (ref. 14). (b) AFM image of mono-layer-graphene (ref. 14). (c) Hall resistance and magnetoresistance measured in single layer graphene at temperature of 30 mK and gate voltage of 15 V (ref. 15). (d) Optical transparency of graphene layers (ref. 17).

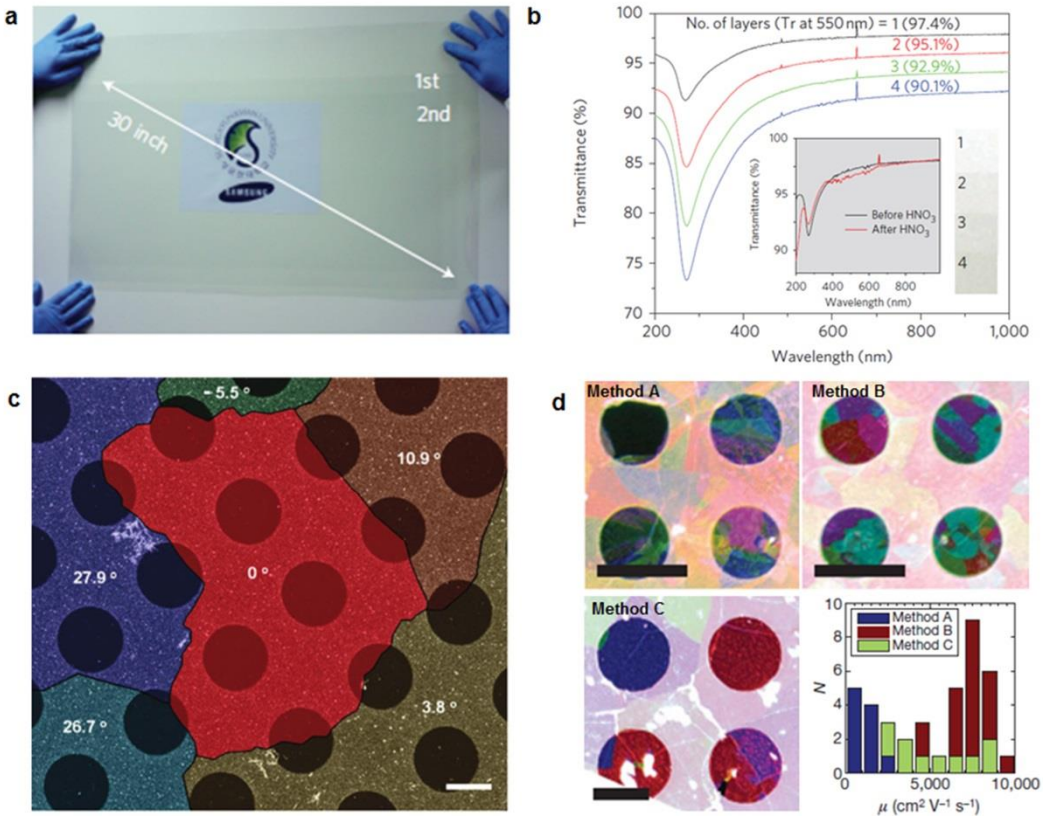

Fig. 2.2. Large-scale graphene films grown on metal substrates using CVD method. (a) Optical image of large-scale graphene films transferred onto plastic substrate (ref. 13). (b) Optical transparency of few-layer CVD-grown graphene (ref. 13). (c) TEM image of CVD-grown graphene (ref. 20). (d) TEM images and Hall mobility of CVD-grown graphene at different growth conditions of A, B, and C (ref. 21).

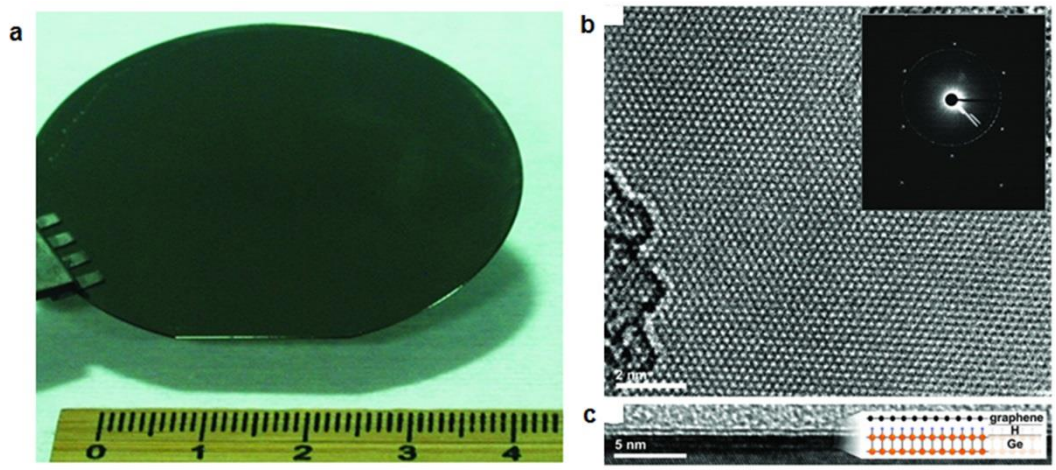

Fig. 2.3. Single crystal graphene grown on Si wafer using hydrogen-terminated Ge intermediate layer (ref. 22). (a) Optical image of graphene grown on Ge/Si substrate. (b) HR-TEM image of graphene and its diffraction patterns. (c) Cross-sectional TEM image.

2.2. Inorganic semiconductor growths on graphene

Among various inorganic semiconductors, ZnO nanostructures, such as nanorods and nanowalls, were firstly grown on mechanically exfoliated graphene using catalyst-free MOCVD.[18] Since nanostructures do not require strict epitaxial relations with the growth substrates due to their extremely small diameter, high quality nanostructures have been grown even on amorphous glass or polycrystalline metal films.[23-26] Accordingly, single crystal ZnO nanostructures with good vertical alignments were easily grown on graphene layers. Nevertheless, growth behavior of ZnO nanostructures on graphene was interesting compared to other growth substrates, as shown in Figs. 2.4a and 2.4b. ZnO nanorods grown on pristine graphene layers exhibited good vertical alignments with low density. The low density growth is presumably due to the lack of chemical reactivity of graphene surfaces. However, growth densities of ZnO nanostructures showed drastic increase at the graphene step edges: ZnO nanowalls or high density nanorods were grown along the graphene step edges. This result suggested that various morphologies of inorganic semiconductor nanostructures can be prepared on graphene layers if the graphene step edges are controllable. More importantly, it was notable that the ZnO nanostructures grown on graphene showed high optical characteristics. As shown in Fig. 2.4c, free exciton emission peaks were observed from the low temperature photoluminescence (PL) spectra.

Meanwhile, epitaxial relations of ZnO nanostructures on graphene were investigated using TEM.[27] As illustrated in Fig. 2.5a, graphene were transferred on TEM grid firstly, and ZnO nanostructures were then grown on the graphene

films for the sample preparation. Since graphene has excellent electron beam transparency and high mechanical strength, no additional sampling processes was required for the TEM measurements, which makes it possible to investigate the growth behavior with high sensitivity. As shown in Fig. 2.5b, the high resolution TEM image and diffraction patterns of ZnO and graphene clearly revealed that they are lattice matched. Typically, wurtzite ZnO exhibited a 3:4 lattice match with graphene. This work clearly showed that inorganic semiconductors can be grown on graphene films with epitaxial relations and lattice matched crystal structure, which is one of the import features for using graphene as inorganic semiconductor growth substrates.

From the high optical characteristics ZnO nanostructures grown on graphene and their lattice matched epitaxial relationships, it is clear that graphene films can be a good candidate for inorganic semiconductor growth substrates. Furthermore, graphene films can satisfy other requirements for the inorganic semiconductor growth substrate. Graphene have high mechanical and thermal stability at high temperature for high quality inorganic semiconductor growths. Excellent electrical and thermal characteristics of graphene would be used as a good electrode and heat dissipation layer for the inorganic semiconductors devices.

Additionally, graphene substrates can have many potential advantages for large-scale and flexible device applications. First of all, large-scale graphene films are available, which is much larger than any formal inorganic semiconductor substrates. Secondly, it is easy to prepare position controlled inorganic semiconductors on graphene due to the chemical reactivity of graphene. In general,

pristine graphene have extremely few dangling bonds, resulting low chemical reactivity with inorganic semiconductors. However, nucleation of inorganic semiconductors can be enhanced by simple plasma treatment because the plasma makes graphene rough.[28] Furthermore, since graphene is very reactive with the plasma treatment, few-layer-graphene can be entirely etched within a minute. Accordingly, position-controlled inorganic semiconductors can be prepared on graphene films by selective etching of graphene surface (Fig. 2.6).[29] Meanwhile, additional SiO_2 or Si_xN_{1-x} layers have been strongly required to fabricate position controlled inorganic semiconductors on a typical growth substrate,[30] which requires additional process and time consuming to fabricate position controlled inorganic semiconductor arrays. The last thing I want to mention about graphene substrates is that the layered structure of graphene films offers easy lift-off and transfer processes of the inorganic semiconductors onto foreign substrates. This interesting feature provides graphene-based inorganic hybrid heterostructures as a unique material system for transferable and flexible device application.

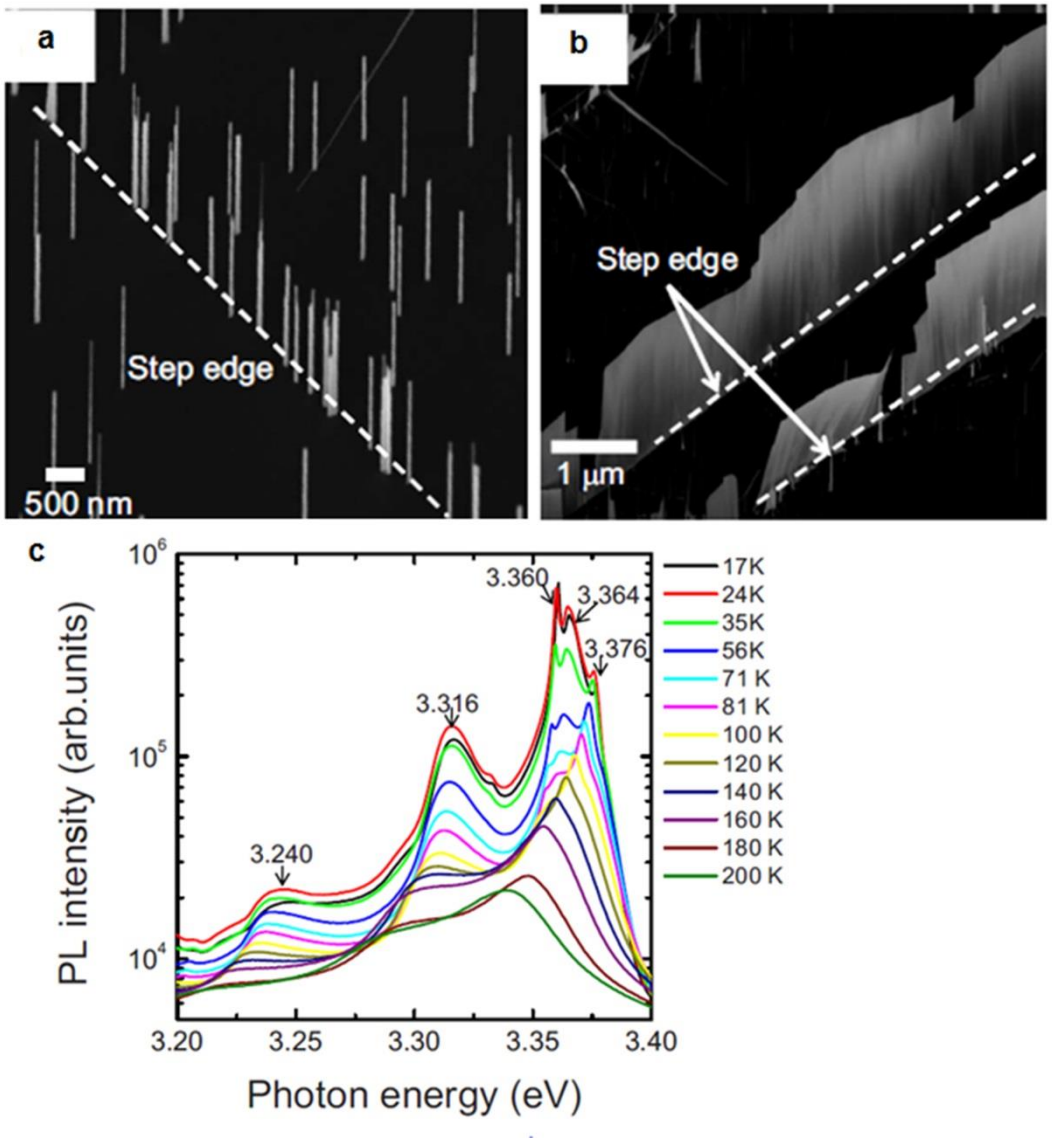

Fig. 2.4. (ref. 18) SEM images of ZnO (a) nanorods and (b) nanowalls grown on few-layer-graphene. (c) Temperature dependent PL spectra of ZnO nanostructures grown on graphene layers.

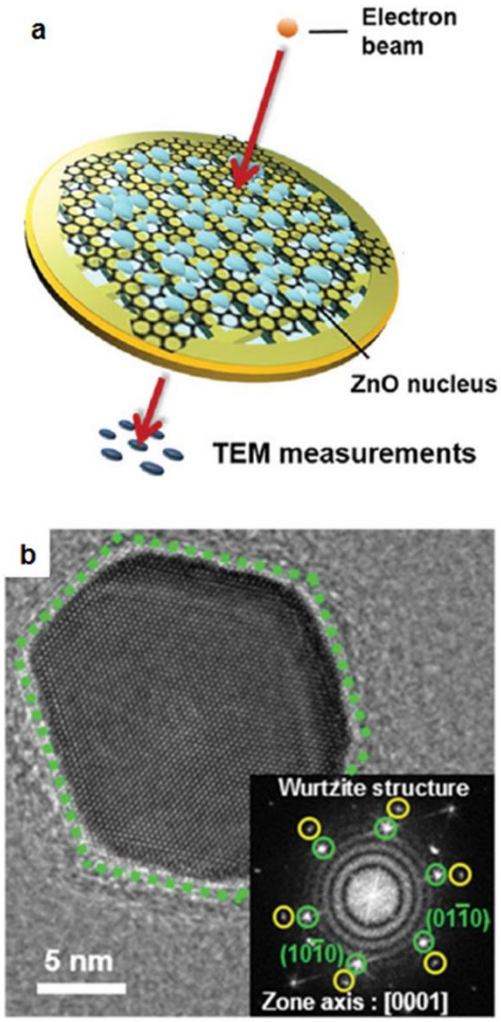

Fig. 2.5. (ref. 27) (a) Schematic illustration of ZnO nanostructures grown on graphene coated TEM grid for TEM analysis. (b) HR-TEM image of ZnO grown on graphene. The inset shows diffraction patterns of ZnO and graphene.

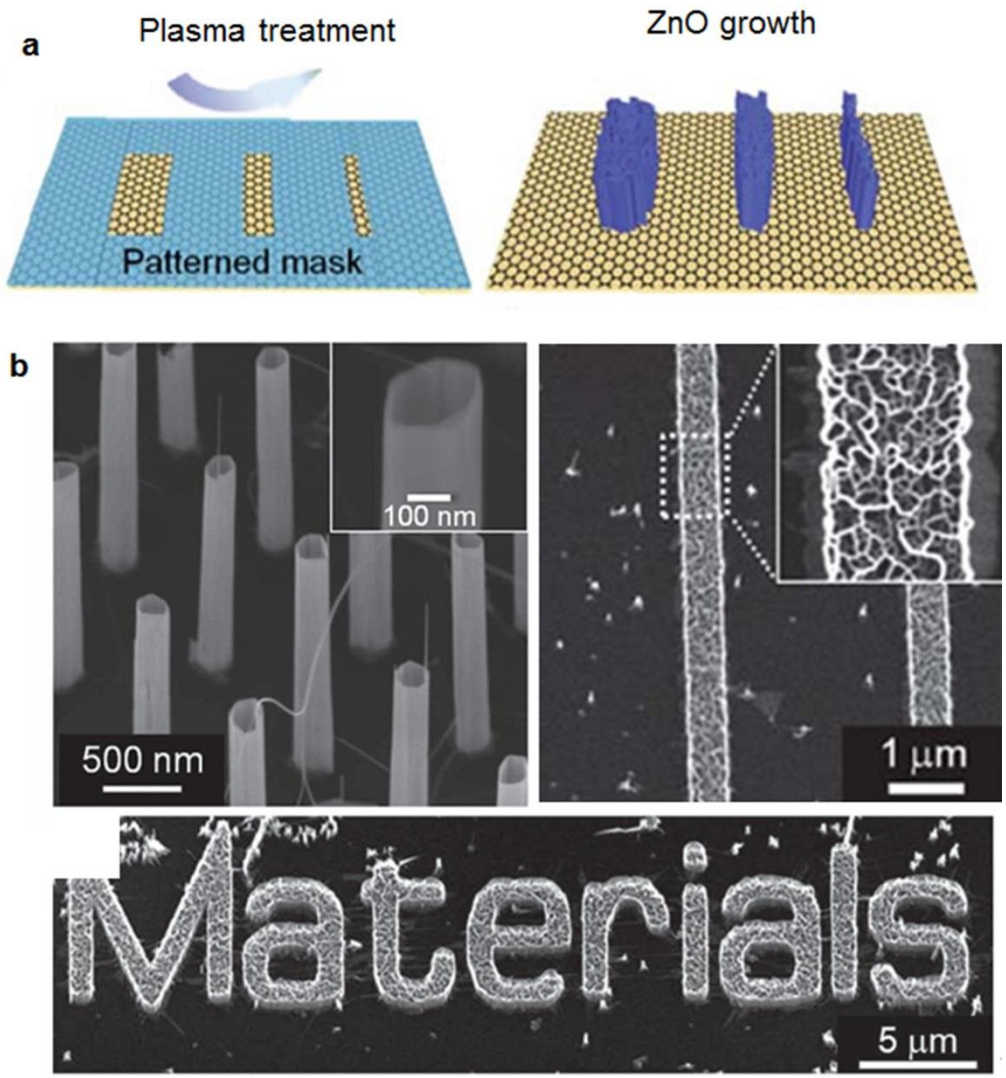

Fig. 2.6. (ref. 29) (a) Schematic illustration of position controlled growth ZnO nanostructures on graphene layers. (b) Various ZnO nanostructures grown on graphene layers, including position controlled nanotubes and nanowalls.

2.3. Methods to fabricate transferable devices

Many diverse inorganic semiconductor devices, such as LEDs, solar cells, and field effect transistors (FETs), are now commercially available which show superior device performance compare to its competitors due to well-developed thin film technologies. The thin film technology can be classified into two categories. One is top-down lithography which offers precise controls of positions and dimensions of materials in nanometer scale. The other is high quality thin film growth which is promising for the fabricating high performance inorganic semiconductor devices. Specifically, high quality thin films can be prepared on a lattice matched single crystalline substrates using epitaxial growth, exhibiting high purity crystals with low defects and impurities. Furthermore, by using this thin film growth technique, inorganic semiconductor heterostructures and quantum structures can be fabricated for high efficiency devices, such as two-dimensional electron gas in high electron mobility transistors and quantum wells in LEDs. However, along the same reason, it is difficult to prepare high quality inorganic semiconductors on large-scale or flexible substrates, such as metal and glass, due to the lack of epitaxial relationships between inorganic semiconductor thin films and the substrates. For this reason, applications of the inorganic semiconductor devices had been strongly restricted to the limit of the growth substrate although there are great interests in the fabrication of large-scale and foldable devices.

To overcome the substrate limitation, many efforts have been paid attention to separate inorganic semiconductors from the growth substrates. In this

case, inorganic semiconductor thin films are grown epitaxially on the lattice matched single crystalline substrates firstly and the thin films are then separated from the substrates. Accordingly, inorganic semiconductor devices can be fabricated on diverse substrates taking advantages of the high material quality. However, since inorganic semiconductors are strongly bonded to the substrates, the key requirement of this technique is to prepare free-standing inorganic semiconductors without damages.

The lift-off process can be categorized into two types: physical method and chemical method. One example of physical lift-off techniques is laser lift-off (LLO), which is widely used in the thin film lift-off technology. The LLO method was demonstrated by Kelly *et al*. for the first time in 1996.[31] For the separation GaN epitaxial thin films from sapphire substrates, a pulsed Nd:YAG laser (355 nm) was illuminated through the double polished sapphire substrate and used for thermal decomposition of GaN layers at the interface, as shown schematically in Fig. 2.7a. In addition, Wong *et al.* reported separation of GaN films and LEDs from sapphire substrate using a KrF excimer laser (248 nm), similar method to the previous technique, and confirmed that material quality or device performance before and after the lift-off process are nearly identical.[5, 12] The other lift-off technique is wet chemical etching of sacrificial layer. Yablonovitch *et al.* first demonstrated the chemical lift-off of $Al_xGa_{1-x}As$ films from GaAs substrate wafers using a 500-Å-thick AlAs sacrificial layer in 1987.[32] Recently, this method re-examined by Rogers *et al*. As shown in Fig. 2.7b, high yield GaAs micro-film chips were prepared by growing multilayers of GaAs/AlAs heterostructures.[1, 33]

Following by assembly process of GaAs micro-film chips, flexible LEDs and solar cells were demonstrated with good reliability (Figs. 2.7c and 2.7d).

Although the previous growth and lift-off techniques successfully demonstrated transferable inorganic semiconductor devices, the essential requirement of the single crystal substrate strongly limit their uses because of high cost and limited substrate size. Furthermore, difficulties of separating thin films from the growth substrates still remain unresolved. For example, it is hard to utilize GaN-based devices in large-scale and flexible form using previous techniques. The LLO method has been widely used to fabricate GaN-based high power devices on metal substrate. However, it is difficult to prepare free-standing GaN films in wafer-scale using this method because lasers can only separate GaN films in small area. Therefore, it might be desirable to investigate alternative substrates, which have advantages for large-scale scalability, transferability, and flexibility, for the diverse applications of inorganic semiconductor devices .

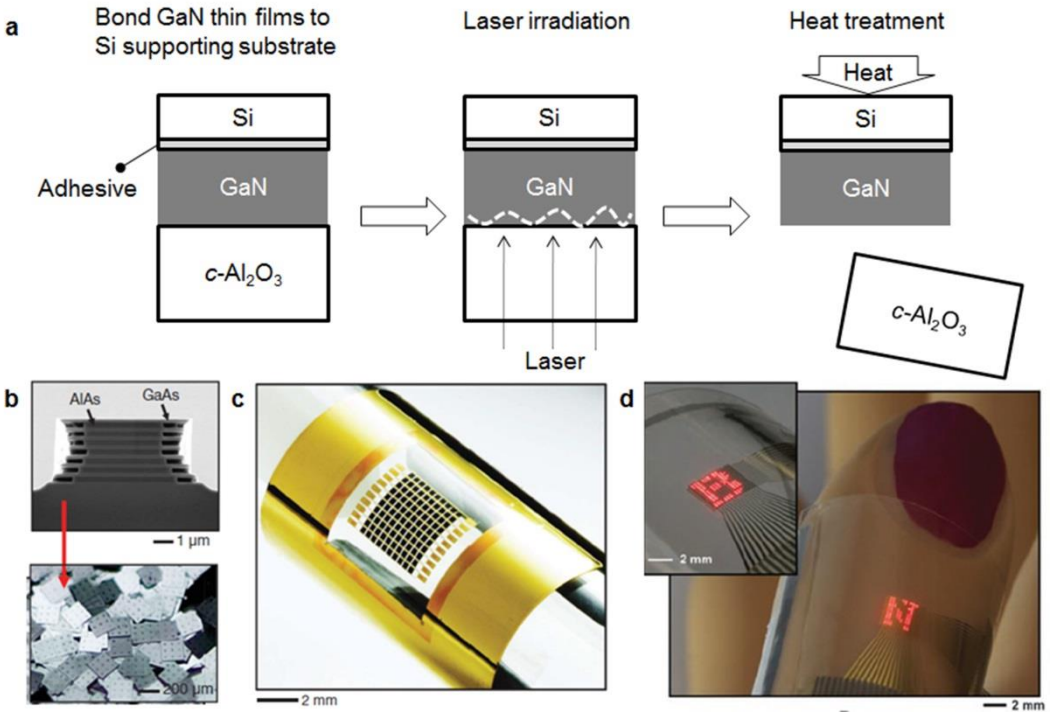

Fig. 2.7. Various inorganic semiconductor lift-off techniques. (a) Process of laser lift-off technique: bond GaN films to Si supporting substrate, laser irradiation through the sapphire substrate, heat treatment above the Ga melting point for the substrate separation. (b) GaAs/AlAs multi-heterostructures for high yield free-standing GaAs thin films. Optical images of transferable (c) solar cell (ref. 33) and (d) LED arrays (ref. 1).

Experimental methods

3

This chapter describes apparatus and methods to fabricate GaN/graphene heterostructures. MOCVD system was employed for the growth of various GaN microstructures and nanostructures, including GaN films and 1D GaN micro- and nanorods. Furthermore, GaN based *p-n* junction diodes were fabricated with $In_xGa_{1-x}N$/GaN quantum wells (QWs) for optoelectronic device applications.

3.1. Metal-organic chemical vapor deposition

This section describes apparatus used to grow GaN and ZnO, including GaN thin films and 1D microstructures, $In_xGa_{1-x}N$/GaN QWs, Si- and Mg-doped GaN layers, and ZnO nanostructures. Three MOCVD systems were employed for the growths of nitride semiconductors and ZnO nanostructure, where two MOCVDs had precursors of Ga, In, Mg, Si for the nitride semiconductor growths, and the other MOCVD had precursor of Zn for the growth of ZnO nanostructures. However, all MOCVDs consist of gas delivery system, growth chamber, substrate heating system, and low pressure pumping and exhaust system.

3.1.1. Gas delivery system

Figure 3.1 shows gas delivery system of nitride semiconductor MOCVD. All gases, reactants, and dopants are delivered to the reactor chamber using this

system. The gas directions and flow rates were controlled by air actuated pneumatic valves (Fujikin Inc. FPR-UDDFCL-7106.35) with 12 channel pneumatic gas manifold control card (Clippard Instrument Laboratory Inc., No. EMC-08-24-30) and mass flow controls (MFCs) (Tylan Co. FC-280S, Celerity Co. TN280, Mykrolis Co. FC-280S) with 12-channel MFC controller (DFC4000), respectively. Line pressures of reactants and dopants were controlled using bellows-shield metering valve (Swagelok Inc. SS4BMG), and their pressures were measured by baratron pressure gauge (MKS Co. 870B). All gas lines were made of 1/4" or 1/2" electro-polished 316-stainless steel (SS) tubing. The tube connections were made with VCR fittings with SS gaskets (SS-4-VCR-2, Swagelok, Co.).

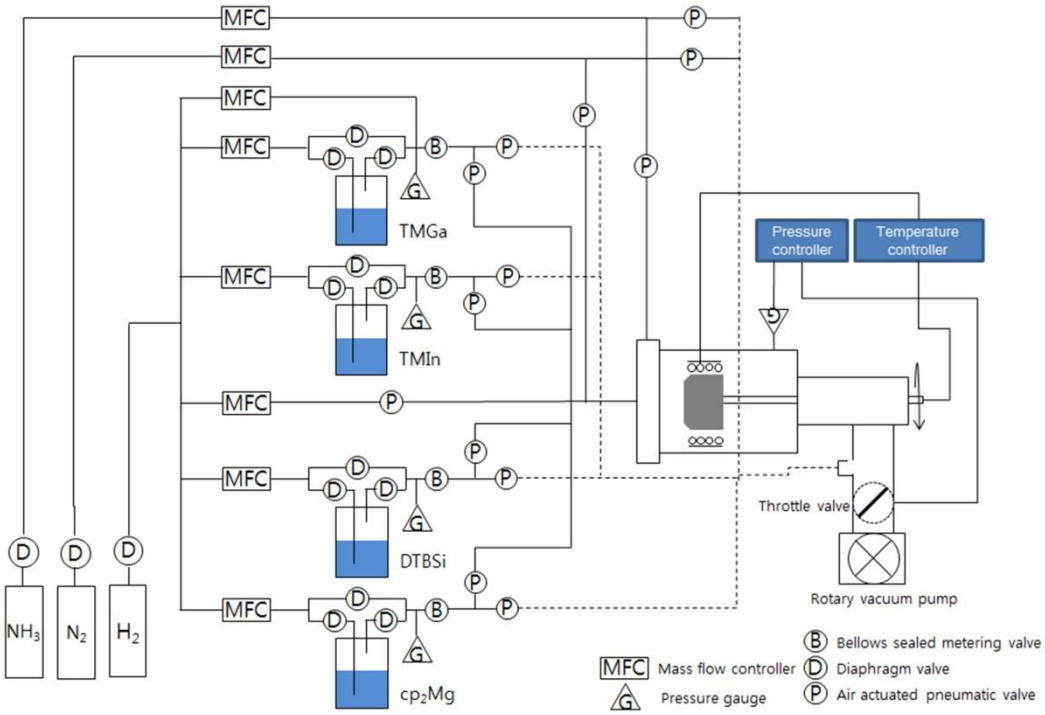

Fig. 3.1. Gas delivery system of nitride semiconductor MOCVD.

3.1.2. Growth chamber and substrate heating

Two kinds of reactor were used in the nitride semiconductor and ZnO MOCVD systems, as shown in Fig 3.2a and 3.3b, respectively. The chamber for nitride semiconductor is vertical type reactor made of SS with water jackets (SYSNEX 1×2" reactor). The ZnO chamber is also vertical type reactor and made of a fire polished tube quartz (material grade: GE-214), with 90-mm-diameter and 300-mm-length, and two 316-SS ultra-torr fitting flanges on both ends. GaN and ZnO were grown in these chamber using susceptor and induction heating system. The susceptor is made of SiC-coated graphite with a 2 inch wafer size pocket, and they were heated by a ratio frequency induction heater (Eltek, Inc., 20 and 30 kW for SYSNEX chambers and 15 kW for ZnO reactor). A high frequency copper coil was surrounded the susceptor with inter-distance of 10 mm, and temperature above 1200°C were obtained in the Sysnex chambers. The growth temperatures were controlled and measured by proportional-integral-derivative (PID) type temperature controller (Chino Co. KP1000) and thermocouples (Omega Co. K-type or R-type), respectively. Additionally, both Sysnex and ZnO chambers contain showerhead and susceptor rotation parts which improve the uniformity of growth rate or composition over the entire 2 inch wafer-scale substrate. The showerheads are connected to the gas delivery system with using O-ring sealed ultra-torr fitting. NH_3 gas lines of Sysnex chambers and O_2 gas line of ZnO chamber are separately connected to the chambers for preventing pre-reactions of nitride semiconductors and ZnO, respectively.

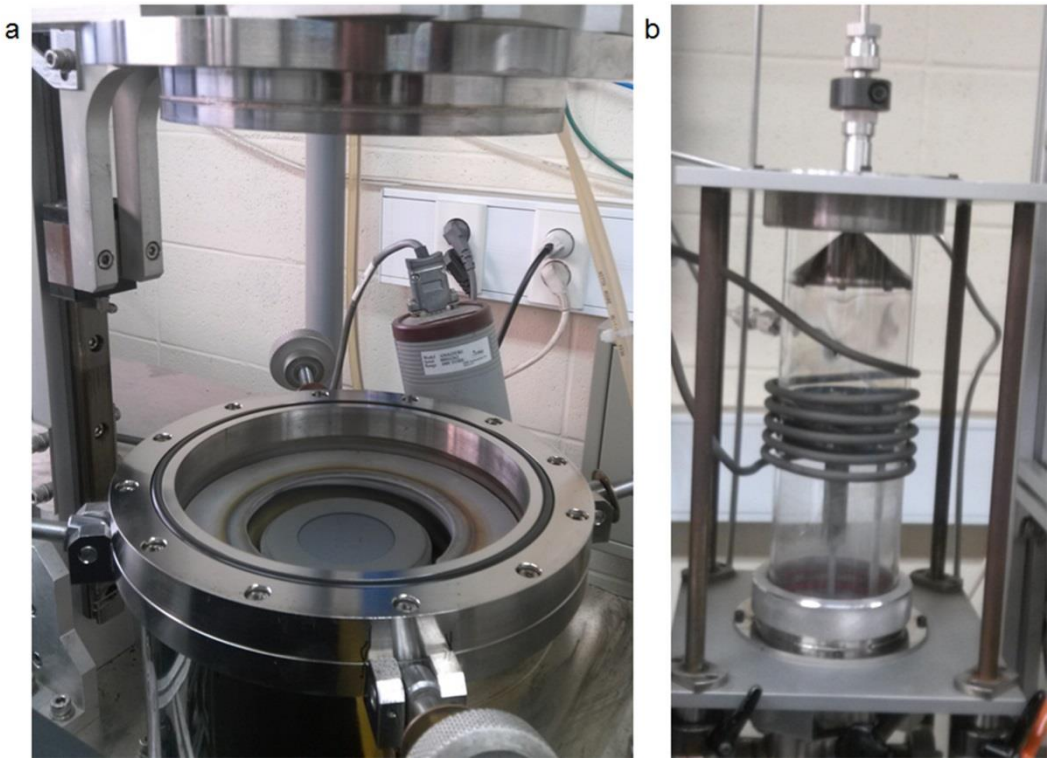

Fig. 3.2. Optical images of MOCVD chambers for (a) nitride semiconductors and (b) ZnO.

3.1.3. Low pressure pumping and exhaust system

The low pressure pumping systems consist of Baratron pressure gauge (MKS Co.), throttle valve (MKS Co. No. 253B), manual angle valve, and rotary pump (Edward Co. E2M28-chmical type for Sysnex chamber, PFEIRRER Vacuum Inc. DUO 10 for ZnO chamber). The reactor pressure was controlled using PID pressure controller (MKS Co. 651C) which is linked with the baratron gause and the throttle valve. Typical controllable pressure range was 1−1000 Torr. The exhaust gas and particles from rotary pump, such as unreacted gas, by-product from the growth chamber, and precursors bypass the chamber, are burnt then washed out in water using scrubber system (Tera Tech Co. NSHW400).

3.1.4. Gas, reactants, and dopants

For nitride semiconductor growths, high purity gas and metal-organic sources were used. H_2 (99.9999%) and N_2 (99.999%) were used as an ambient gas or carrier gas. NH_3 (99.9995%), trimethylgallium (TMGa), and trimethylindium (TMIn) were used as reactants. The *n*-type and *p*-type dopants of nitride semiconductors were ditertiarybutylsilane (DTBSi) and biscyclopentadienylmagnesium (MgCp or Cp_2Mg), respectively. For ZnO growths, diethylzinc (DEZn) and O_2 (99.9995%) were used as reactants, and high purity Ar (99.9995%) was used as an ambient and carrier gas.

Since the vapor pressures of metal-organic sources were changed by the source temperature, every metal-organic source, sealed in a SS bubbler, kept constant temperature using refrigerated and heating bath circulators (JEIO TECH

Co. RW-1025G). Typical bath temperatures were –15°C for TMGa, 21.5°C for TMIn, –20°C for DTBSi, 20°C for Cp_2Mg and MgCp, and –10 - –15°C for DEZn. All gases and metal-organic sources are summarized in Tables 3.1. and 3.2

Table 3.1. Gases, reactants, and dopants for nitride semiconductor MOCVD

Reactant	Dopant	Gas	Purity (%)	Vapor pressure	Company
TMGa			Electronic grade	$Log_{10}P = 8.07–1703/T$	Epichem
TMIn			Electronic grade	$Log_{10}P = 10.52–3014/T$	Epichem
NH_3			99.9995		Matheson Co.
	DTBSi		Epigrade	$Log_{10}P = 8.83–2321/T$	SAFC hightech
	Cp_2Mg		Electronic grade	$Log_{10}P = 28.14–2.18lnT–4198/T$	Epichem
	MgCp		Electronic grade	-	Epichem
		H_2	99.9999		
		N_2	99.999		

Table 3.2. Gas and reactants for ZnO MOCVD

Reactant	Gas	Purity (%)	Vapor pressure	Company
DEZn		Electronic grade	$Log_{10}P = 8.208–2109/T$	Epichem
O_2		99.9995		
	Ar	99.9995		

P: Pressure (Torr), T: Temperature (K)

3.2. Growth techniques

This section describes growth conditions and details of GaN films and 1D GaN nanostructures. Substrates of *c*-Al_2O_3 and graphene (mechanically exfoliated graphene layers from graphite powder and CVD graphene) were employed for the GaN layer growths.

3.2.1. GaN films on sapphire substrate

GaN films and nitride semiconductor heterostructures were grown epitaxially on *c*-Al_2O_3 for the preliminary research. High quality GaN films and GaN-based devices have been widely fabricated on lattice matched single crystal sapphire substrates, and many previous results would make easy to optimize the growth conditions. Accordingly, undoped and doped nitride semiconductors were firstly grown on *c*-Al_2O_3 in order to confirm our MOCVD system.

3.2.1.1. Un-doped and *n*-type doped GaN films

Epitaxial GaN films were grown on *c*-Al_2O_3 substrates using MOCVD. Before the GaN growth, *c*-Al_2O_3 substrates were cleaned by acetone and methanol sonication of 3 min and loaded in the growth chamber. The growth schema of the un-doped and *n*-type doped GaN films is shown in Fig 3.3. Firstly, the substrate was heated at 1050°C for 10 min with H_2 gas for the substrate surface cleaning. Then, the temperature decreased to 540°C to grow GaN buffer layer. Typical growth time and reactor pressure of a thin buffer layer were 60s and 200 Torr, respectively. NH_3 was employed to the reactor 30s before TMGa flow at the

buffer layer growth. GaN films were grown on GaN buffer layer coated *c*-Al_2O_3 using two-step temperature growth. Middle temperature GaN (MT-GaN) layer and high temperature GaN (HT-GaN) layer were grown at 1000 and 1060–1090°C, respectively. Reactor pressure maintained at 300 Torr during these growth step. Typical growth conditions for un-doped and *n*-type doped GaN films on *c*-Al_2O_3 are summarized in Table 3.3.

GaN films grown on *c*-Al_2O_3 exhibited flat and uniform surface morphology as shown in Fig. 3.4. The flat surface morphology was obtained at growth temperatures of 1060−1090°C. Hall mobility and carrier concentration of un-doped GaN films grown at optimum growth condition were 320 cm^2/Vs and $2.2\times10^{17}/cm^3$, respectively. Furthermore, both surface morphology and electrical characteristics of GaN films were almost identical over the entire 2 inch sapphire wafer.

Since GaN films with high mobility and low back carrier concentration are desirable for doping and device fabrication, growth conditions of un-doped GaN films were optimized using Hall measurements. Both Hall mobility and carrier concentration exhibited negative sign because un-doped GaN is normally *n*-type semiconductor. The effect of GaN buffer layers on electrical characteristics is shown in Fig. 3.5a. As the GaN buffer growth time was decreased from 150 to 60s, the Hall mobility increased from 107 to 320 cm^2/Vs and the carrier concentration decreased from 3.6×10^{17} to $2.2\times10^{17}/cm^3$.

Figures 3.5b and 3.5c show electrical characteristics of GaN films grown at various HT-GaN growth temperatures and growth pressures, respectively. Both Hall mobility and carrier concentrations of GaN films were increased with decreasing the growth temperature in the growth temperature of 1060−1090°C. Meanwhile, GaN films grown on *c*-Al_2O_3 substrates at various growth pressures exhibited optimum values in the Hall measurement results. Specifically, the GaN films grown at 300 Torr showed highest Hall mobility with lowest carrier concentrations.

The *n*-type GaN films were grown on un-doped GaN films using DTBSi as a dopant. The growth condition of *n*-type GaN layers, including growth temperature, pressure, and TMGa flow rates are same with those of HT-GaN layers. For the doping control of *n*-GaN layers, DTBSi was injected to the reactor by modulating time. Specifically, DTBSi flew into the reactor at *x* s and bypassed to the vent line at *10-x* s during the repeat cycle of 10s. As the *x* s increased, growth rate and carrier concentration increased, while Hall mobility and resistivity decreased. Additionally, the thickness of *n*-GaN layers was increased with the increasing injection time of the Si precursor. Electrical characteristics of un-doped and *n*-type doped GaN films are summarized in Table 3.4.

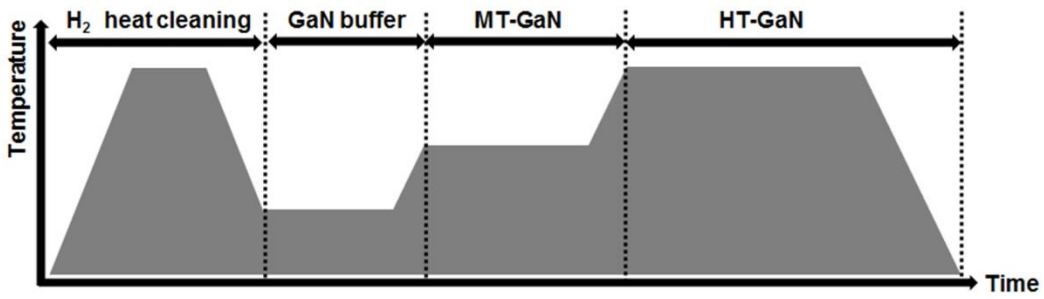

Fig. 3.3. Schematic diagram of GaN film growth on *c*-Al_2O_3.

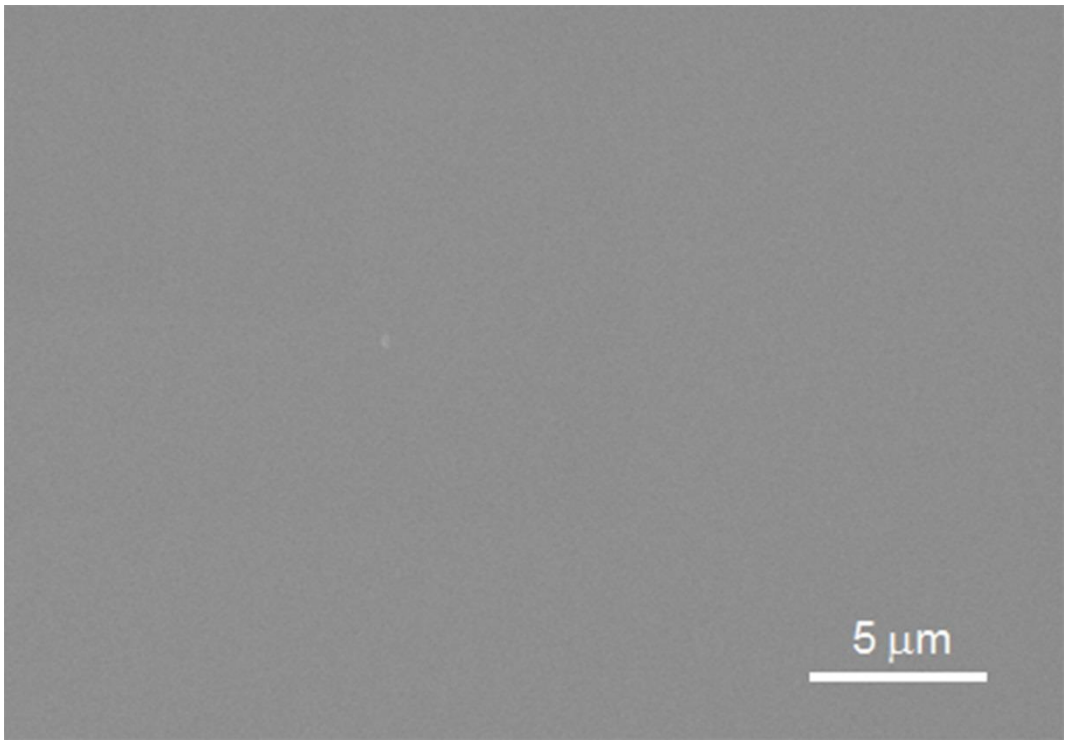

Fig. 3.4. Surface morphology of GaN films grown on *c*-Al_2O_3

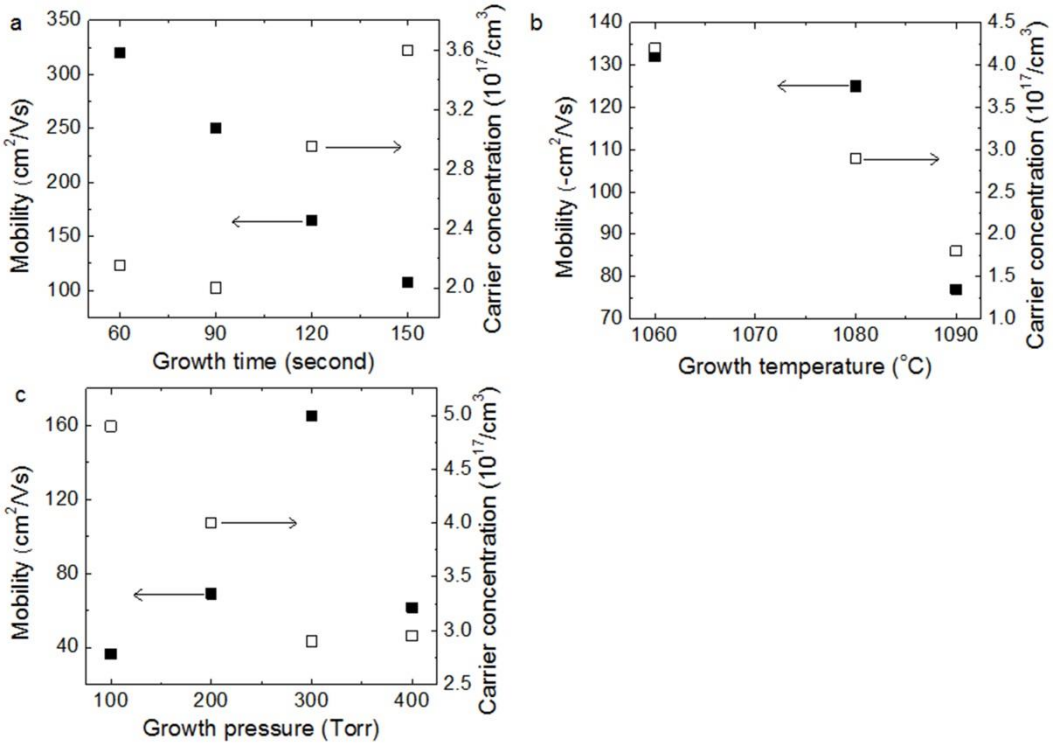

Fig. 3.5. Mobility (black square) and carrier concentration (white square) of un-doped GaN films grown on *c*-Al_2O_3 substrates. (a) Growth time of GaN buffer layer. (b) Growth temperature and (c) pressure of HT-GaN layers.

Table 3.3. Growth conditions for un-doped and *n*-type doped GaN films

	GaN buffer	MT-GaN	HT-GaN	*n*-GaN
Substrate Temperature (℃)	540	1000	1060–1090 (1080)	1060–1090 (1080)
Growth time	60–150 (60) s	5–15 (15) min	1–2 hr (2 hr)	1 hr
Reactor pressure (Torr)	200	100–400 (300)	100–400 (300)	100–400 (300)
H_2 flow rate (slm)	2	2	2	2
NH_3 flow rate (slm)	2	2	2	2
TMGa flow rate (sccm)	9	21	21	21
TMGa dilute flow rate (sccm)	21	9	9	9
TMGa line pressure (Torr)	400–450 (430)	400–450 (430)	400–450 (430)	400–450 (430)
DTBSi flow rate (sccm)				1
DTBSi dilute flow rate (sccm)				29
DTBSi line pressure (Torr)				1000–1100 (1050)

( ): Preferable conditions

Table 3.4. Electrical characteristics of un-doped and *n*-type doped GaN films

	u-GaN(*x*=0)	*n*-GaN (*x*=3)	*n*-GaN (*x*=5)
Growth rate (μm/hr)	1.3	2.3	5.2
Resistivity (Ω·cm)	8.6×10^{-2}	8.2×10^{-3}	4.1×10^{-3}
Hall mobility ($cm^2/V\cdot s$)	320	273	85
Carrier concentration ($/cm^3$)	2.2×10^{17}	1.3×10^{18}	7.6×10^{18}

3.2.1.2. Light-emitting diodes

For the LED structure, $In_xGa_{1-x}N$/GaN MQWs and *p*-type GaN layers were grown on *n*-type GaN thin films using nitride MOCVD. Typically, $In_xGa_{1-x}N$ QWs and QBs were grown at growth temperature of 760 and 850°C, respectively. Additionally, $In_xGa_{1-x}N$/GaN MQWs were grown with N_2 ambient gas to prevent degradation of the InGaN layers. Subsequently, an Mg-doped *p*-GaN layer was deposited on the top of the GaN quantum barrier layer at 1000-1080°C. The growth conditions of $In_xGa_{1-x}N$/GaN MQWs and *p*-type GaN layer are summarized in Table 3.5.

The growth conditions of GaN film LEDs were optimized by changing $In_xGa_{1-x}N$/GaN MQW numbers and *p*-type GaN growth temperatures. Figure 3.6a shows output powers of the LEDs grown at various QW numbers in the range of 0–8. When LEDs were fabricated without QW layers, the output power exhibited 10^4 times smaller than that of conventional GaN film LEDs (Samsung Co.). However, output power increased drastically from 1μW to 1mW as the QW number increased from 0 to 8. Electrical characteristics of the LEDs were investigated by measuring *I–V* curves as shown in Fig. 3.6b. All LEDs exhibited good *p–n* junction rectifying behavior. Furthermore, *I–V* curves of the LEDs grown with different QW numbers exhibited almost identical behavior although the slope slightly decreased with increasing QW numbers.

EL characteristics of LEDs grown at various *p*-GaN temperatures were investigated, as shown in Fig. 3.6c. The maximum output power of the LEDs was

estimated to be 1.3 mW, where the thin film LEDs were grown with the *p*-GaN growth temperature of 1040°C. Meanwhile, the thin film LED grown at p-GaN growth temperature of 1000°C showed drastic decrease in its output power presumably because of poor quality of the *p*-GaN layer, while the LEDs exhibited similar output powers in the range of 0.7–1.3 mW at the growth temperatures of 1020–1080°C. Additionally, dominant EL peak positions of the 20-mA-driven LEDs were investigated, as shown in Fig. 3.6d. As the *p*-GaN growth temperatures increased, the EL peaks slightly shifted from 412 to 404 nm. This blue shift may result from the inter-diffusion of indium and gallium in $In_xGa_{1-x}N$/GaN MQWs at high growth temperatures.[34, 35]

Table.3.5. Growth conditions for $In_xGa_{1-x}N$/GaN MQWs and *p*-type GaN

	GaN QB	$In_xGa_{1-x}N$ QW	*p*-GaN
Substrate Temperature (℃)	850	750–810 (760)	1000–1080
Growth time	185s	100s	30–60 min
Reactor pressure (Torr)	300	300	100
H_2 flow rate (slm)			2
N_2 flow rate (slm)	2	2	
NH_3 flow rate (slm)	3	3	2
TMGa flow rate (sccm)	4.2	1.1	9–21 (13)
TMGa dilute flow rate (sccm)	25.8	28.9	9–21 (17)
TMGa line pressure (Torr)	400–450 (430)	400–450 (430)	400–450 (430)
TMIn flow rate (sccm)		35	
TMIn line pressure (Torr)		400–450 (430)	
Cp_2Mg flow rate (sccm)			100
Cp_2Mg line pressure (Torr)			450

( ): Preferable conditions

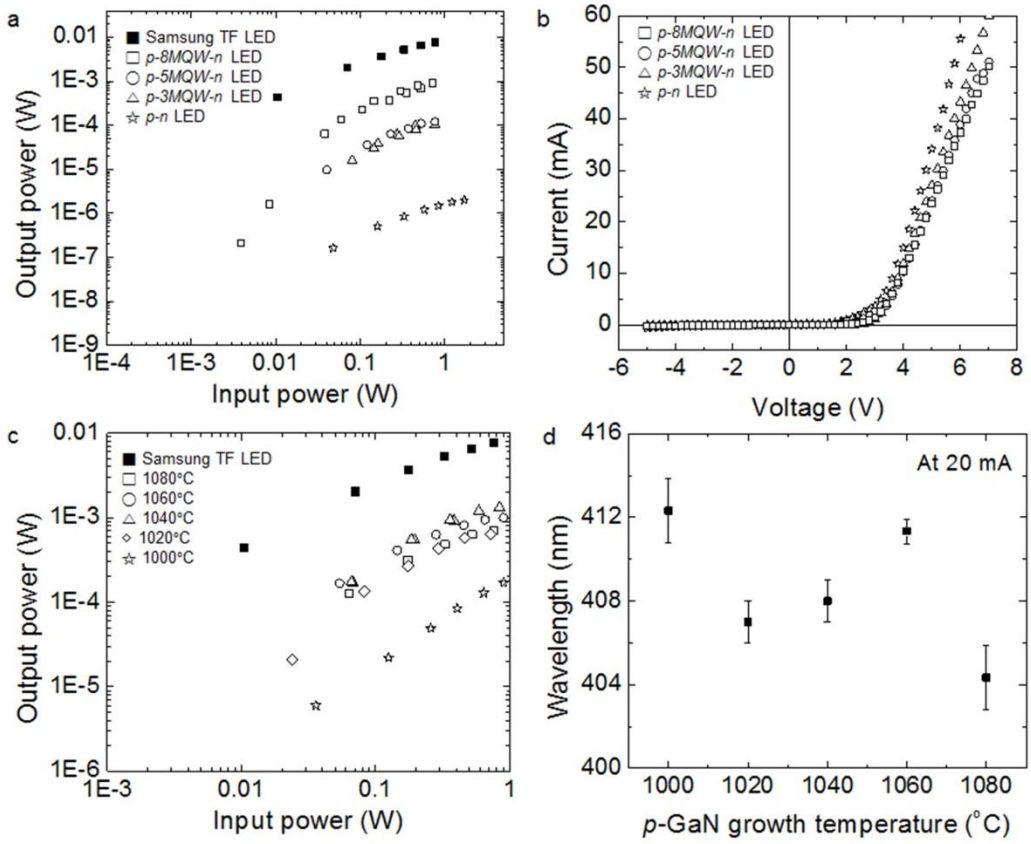

Fig. 3.6. (a) Output powers and (b) *I–V* curves of LEDs fabricated at various QW numbers of 0 (white star), 3 (white triangle), 5 (white circle), and 8 (white square). (c) Output power and (d) dominant EL peak positions of LEDs grown at various *p*-GaN growth temperatures of 1080 (white square), 1060 (white circle), 1040 (white triangle), 1020 (white diamond), and 1000°C (white star). Dark squares in Figs. 3.6a and 3.6c represent conventional GaN thin film LEDs. All EL and electrical characteristics were measured at room temperature.

3.2.2. GaN films on graphene

Graphene films, as a growth substrate of inorganic semiconductors, have many advantages over typical single crystalline growth substrates for device applications, such as transferability and flexibility. Nevertheless, the challenges of growing high quality inorganic semiconductors on graphene had remained unresolved. Meanwhile, this dissertation introduced a method to grow high quality epitaxial GaN films on graphene substrate, including mechanically exfoliated graphene layers and CVD graphene films.

3.2.2.1. GaN films on mechanical exfoliated graphene layers

High quality epitaxial GaN layers were grown on graphene layers using ZnO nanowall intermediate layer. Graphene layers were mechanically exfoliated from single crystalline graphite powder using a simple Scotch tape method and transferred onto rigid substrates. The typical size of graphene layers was 1−2000 μm. Then, O_2 plasma treatment was performed on the graphene layers to grow high density ZnO nanowalls. During the plasma treatment, O_2 partial pressure and applied current kept 100 mTorr and 50 mA, respectively. Subsequently, ZnO nanowalls were grown on the O_2 plasma treated graphene layers using catalyst-free MOCVD. The growth temperature and pressure of the reactor maintained at 550–650℃ and at 0.3–6 Torr, respectively. Flow rates of DEZn and O_2 were 20 sccm and 100 sccm, respectively. The experimental conditions for O_2 plasma treatment and ZnO nanowall growths are described in Table 3.6.

GaN thin films were grown on ZnO-coated graphene layers using nitride MOCVD. Firstly, a thin GaN layer was grown at 540–600°C with N_2 ambient gas to prevent degradation of ZnO nanowalls and prohibit reactions between ZnO and GaN layers at a higher temperature. After the growth of GaN protecting layer, high quality GaN films were grown at 1080–1140°C. High purity H_2 was used as the ambient gas at this growth stage.

3.2.2.2. GaN films on CVD graphene films

The graphene films were synthesized on copper foil by CVD method and then transferred onto rigid substrates for the growth of GaN films. Since CVD graphene films are large-scale, the graphene films were coated on the entire substrate surface and exhibited uniform and homogenous morphology. Then, O_2 plasma treatment and ZnO nanowall growth were performed on the graphene films before the GaN film growths, similar the growth methods of epitaxial GaN layers grown on mechanically exfoliated graphene layers.

Three-step-growth was performed for the epitaxial growth GaN layers on CVD graphene films. In the first step, a thin GaN protecting layer was grown on the ZnO nanowall-coated graphene films at 540–600°C for 10 min with nitrogen as an ambient gas. In the second step, GaN layers were grown at temperatures of 1000–1060°C for 15 min with hydrogen ambient gas. Finally, flat and uniform surface morphologies of GaN films were obtained after growing GaN layers at 1120–1160°C for 60 min. In particular, the second growth step improved the lateral growth of GaN layers, while it was hard to obtain fully coalescent GaN film without the second growth step because of very thin layer of CVD graphene

films. It is well known that the graphene films are very reactive under the plasma exposure. For the reason, it is hard to expose plasma on the CVD graphene films for a long time, where the plasma exposure time strongly affected to the density of ZnO nanowall nucleation layers. Accordingly, when we use very thin graphene films for the GaN layer growths, such as CVD graphene films synthesized on Cu foil, the density of ZnO nucleation layers were much smaller than that prepared on a multi-layer graphene films. To overcome this problem, lateral growth of GaN layers was enhanced by using the second growth step. The growth conditions of GaN films on mechanically exfoliated graphene layers and on CVD graphene films are presented in Table 3.7.

3.2.2.3. Epitaxial lateral overgrown GaN films on CVD graphene dot arrays

GaN micro-films were selectively grown on CVD graphene dot arrays by means of epitaxial lateral overgrowth (ELOG). Prior to the ELOG GaN growth, large-scale CVD graphene films were transferred onto rigid substrates, such as W films or SiO_2 layer coated Si substrate, and the graphene films were patterned into graphene dot array using photolithography and O_2 plasma etching. Subsequently, ZnO nanowalls were grown on the graphene dots for the nucleation layer of GaN layer growths. For the growth of ELOG GaN layers, NH_3 was injected to the reactor at 3 s and bypassed to the vent line at 7s during the repeated cycle of 10s. The time modulation of NH_3 was the key parameter to enhance the lateral growth of GaN layers. The growth conditions of ELOG GaN layers are summarized in Table 3.8.

Table. 3.6. Experimental conditions for O_2 plasma treatment and ZnO nanowall growths

Process	Process conditions	On mechanically exfoliated graphene	On CVD graphene
O_2 plasma treatment	Power (W)	30–50	
	O_2 partial pressure (mTorr)	100–105	
	Time	1–60 (10) s	1–5 (3) s
ZnO nanowall growth	Substrate temperature (℃)	550–650 (600)	
	Growth time (min)	5–20 (10)	
	Reactor pressure (Torr)	< 6	
	Ar flow rate (sccm)	1500	
	O_2 flow rate (sccm)	100	
	DEZn flow rate (sccm)	20	
	DEZn dilute flow rate (sccm)	40	
	DEZn line pressure (Torr)	300–400 (320)	

( ): Preferable conditions

Table 3.7. Growth conditions for GaN films on ZnO nanowall-coated graphene films

Growth condition	On mechanically exfoliated graphene		On CVD graphene		
Growth step	I	II	I	II	III
Substrate Temperature (℃)	540−600	1080−1140	540−600	1000−1060	1120−1160
Growth time (min)	10	60	10	15	60
Reactor pressure (Torr)	200	100	200	100	100
N_2 flow rate (slm)	2		2		
H_2 flow rate (slm)		2		2	2
NH_3 flow rate (slm)	2	2	2	2	2
TMGa flow rate (sccm)	9	21	9	21	21
TMGa dilute flow rate (sccm)	21	9	21	9	9
TMGa line pressure (Torr)	400–450 (430)		400–450 (430)		

( ): Preferable conditions

Table 3.8. Growth conditions for ELOG GaN layers

	GaN protecting layer	ELOG GaN	
Substrate Temperature (℃)	540−600	1000−1100 (1060)	
Growth time (min)	10	171−512 cycles, 10s for 1 cycle	
Reactor pressure (Torr)	200	100	
N_2 flow rate (slm)	2		
H_2 flow rate (slm)		2	
TMGa flow rate (sccm)	9	21	
TMGa dilute flow rate (sccm)	21	9	
TMGa line pressure (Torr)	400–450 (430)	400–450 (430)	
NH_3 flow rate (sccm)	2	100−500 (100)	
NH_3 injection time for 1 cycle	10s to the reactor	7s to vent line	3s to reactor

( ): Preferable conditions

3.2.3. One dimensional GaN micro- and nanostructures on graphene films

In addition to GaN films, catalyst-free 1D GaN micro-rods were grown on CVD graphene films. Typically, CVD graphene films are semi-transparent multi-layer-graphene with electrical resistance of 600－800 Ω/□. Then, a 2-μm-thick GaN film was grown on the graphene substrates using a MOCVD in order to form intermediate layer for vertical aligned micro-rod growth. GaN micro-rods were grown at typical two-step temperatures of 750−850°C for 3 min and 950−1050°C for 30 min, following by substrate heating at 1100°C for 10 min with hydrogen. For GaN micro-rod growth, TMGa, DTBSi, and NH_3 employed as reactants and nitrogen was used as a carrier gas. During GaN micro-rod growth, typical flow rates of TMGa, DTBSi, and NH_3 were 15－30, 1－3, and 100－500 sccm, respectively. The pressure of the reactor chamber maintained at 300 Torr with mixture gas of hydrogen and nitrogen. The small V/III ratio and the use of Si precursor were the key parameters to grow GaN micro-rods. Typical growth conditions for vertical aligned GaN micro-rods on CVD graphene films are summarized in Table 3.9.

Table 3.9. Growth conditions for 1D GaN micro-rods on CVD graphene films

Growth step	GaN buffer layer		GaN micro-rod		
	I	II	I	II	III
Substrate Temperature (℃)	540	1000–1060	1100	750−900(850)	950−1050(1000)
Growth time (min)	10	15	10	1–5 (3)	10–60 (30)
Reactor pressure (Torr)	200	100	300	300	300
N_2 flow rate (slm)	2			0.2	0.2
H_2 flow rate (slm)		2	2	0.8	0.8
NH_3 flow rate (slm)	2	2		100–500 (300)	100–500 (300)
TMGa flow rate (sccm)	9	9		15–30 (21)	15–30 (21)
TMGa dilute flow rate (sccm)	21	21		0–15 (9)	0–15 (9)
TMGa line pressure (Torr)	400–450 (430)			400–450 (430)	400–450 (430)
DTBSi flow rate (sccm)		1			1–3 (3)
DTBSi dilute flow rate (sccm)		29			29–27 (27)
DTBSi line pressure (Torr)		1000–1100 (1050)			1000–1100 (1050)
DTBSi injections		Time modulation			Continuous flow

( ): Preferable conditions

3.3. Material characterization

3.3.1. Structural characterization

Surface morphology was investigated using JEOL scanning electron microscopy (SEM), Carl Zeiss or TESCAN field-emission SEMs (FE-SEMs). Typical acceleration voltage and magnification were 10–20 kW and 30–1,000,000, respectively.

The crystal structure and growth orientations were investigated using PANalytical X'pert PRO X-ray diffraction (XRD) with Ni-filtered Cu K_α radiation. The θ–2θ scan, rocking curves, and azimuthal (ϕ) scans were performed. Additionally, microstructural characteristics were investigated using high-resolution transmission electron microscopy (HR-TEM). The TEM sampling and measurement were carried out by Hyobin Yoo and Kunsoo Kim under Prof. M. Kim in Department of Material Science and Engineering at SNU. The cross-sectional and plan-view TEM images, HT-TEM image, and fast Fourier transform image were obtained for the defect studies in GaN films or structural analysis of GaN nanostructures.

3.3.2. Optical characterization

Optical characteristics of GaN microstructures and nanostructures grown on graphene films were investigated using photoluminescence (PL) spectroscopy system, as shown schematically in Fig. 3.7. A continuous He-Cd laser (325 nm) and a pulsed Nd:YAG laser (355 nm) were employed as optical excitation sources.

For power dependent PL measurements, typical pulse width and repetition rate of Nd:YAG laser kept 6 ns and 10 Hz, respectively. The PL emissions from the samples were focused into the spectrometer, consisted of monochrometer (Dongwoo Optron Co. DM320i) and charge coupled device (CCD, Andor Inc. DUO401A). A computer program (Andor iDus) was employed to control the spectrometer and to record PL spectrum. The resolution of the monochromator was 0.5 nm. For low temperature PL study, A cryostat and a helium displex cooling system (EBARA technologiew InC., 531-120) were used for the sample cooling. The sample temperature was controlled by a temperature controller (Lake Shore Instruments Inc., No. 331s) and the temperature range was 11–300 K.

Micro-PL measurements were also performed to investigate optical characteristics of individual GaN microstructures. The laser beam was focused to the samples with a using objective lens, and the PL emissions were collected by the same objective lens. The typical spot size of He-Cd laser and Nd:YAG laser were 3 and 10 μm, respectively. Additionally, laser spot positions were controlled with 2 μm distance by stage controller. In this system, samples can be cooled down to 80 K for low temperature PL using mini cryostat and liquid nitrogen cooling system (Linkam Scientific Ins.).

In addition to PL spectroscopy, optical characteristics of individual GaN microstructures were investigated using cathodoluminescence (CL) spectroscopy. A Gatan MonoCL4 was employed to measure CL from the samples. Typically, CL spectrum and images were obtained at room temperature and low temperature of 80 K with 1 nm resolution.

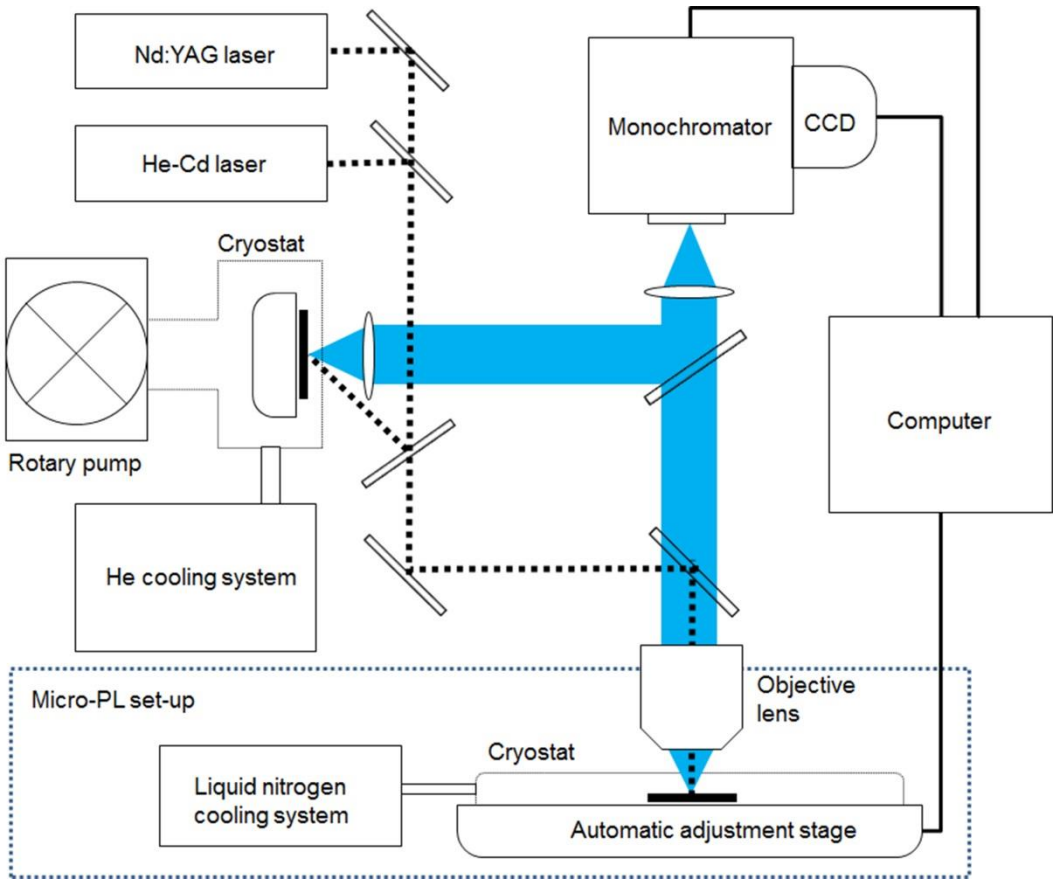

Fig. 3.7. Schematic of the PL measurement system.

3.3.3. Device characterization

3.3.3.1. Light emitting diodes

The LED characteristics were investigated using an EL measurement system, as shown schematically in Fig. 3.8. The optical microscopy (Carl Zeiss Co. Axoskop 2 MAT) was used for the contact probing and EL emission collecting. A Keithley 2400 was used for the *I–V* curve measurements as well as electrical source meter, which could apply voltages or currents to LEDs. To obtain EL spectrum of the LED, the EL emissions was passed through the optical microscopy and measured by a CCD (Andor InC. DU401A) with a monochromator ((Dongwoo Optron Co. DM150i). The resolution and the typical scan range of the EL spectrum were 1 nm and 360–700 nm, respectively. In addition to EL spectra, output powers of the LEDs were directly measured by power meter.

3.3.3.2. Photovoltaic devices

Photovoltaic devices were characterized using the LED characterization set-up, including optical microscopy, *I–V* curve measurement system, and power meter. Additionally, Xe lamp was employed as a source for the photovoltaic devices. To measure photovoltaic characteristics, lights from the Xe lamp passed through the optical microscopy and were focused on the photovoltaic devices. Since I fabricated GaN-based photovoltaic devices, 440 nm band pass filter was used for the exposure of short-wavelength-lights. Typical output powers of the Xe lamp with the band pass filters were 1─2 mW at wavelength of 400 nm.

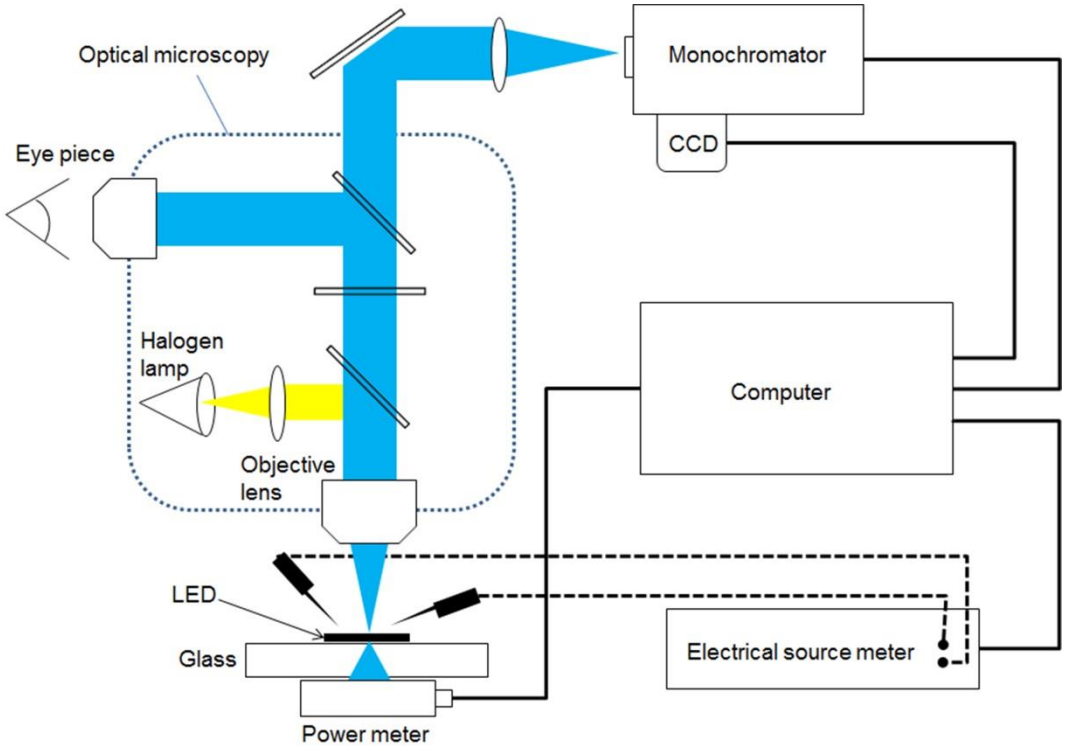

Fig. 3.8. Schematic of the LED characterization system.

Epitaxial growth and characterization of GaN films grown on graphene films

4

4.1. Introduction

This chapter describes the heteroepitaxial growth of flat and uniform GaN thin films on various graphene substrates, including mechanically exfoliated graphene layers and CVD graphene films. Although MOCVD of GaN thin films have been well developed on *c*-Al_2O_3 substrates, it is difficult to obtain high quality epitaxial GaN films on graphene films using typical film growth conditions. This result is because of lack of chemical reactivity of graphene films. Since the graphene surface is relatively free from the dangling bonds, it was difficult to make many nucleation sites for GaN film growth. To overcome this problem, ZnO nanostructures were employed as a nucleation layer for the epitaxial GaN film growth on graphene layers.[2, 36] Due to the nanoepitaxy, ZnO nanowalls can be easily grown on graphene films with high density and good epitaxial relationships. Furthermore, the same crystal structure and almost identical lattice constants of ZnO and GaN allow the heteroepitaxial growth of GaN layers on ZnO-coated graphene films.

Using this growth method, high quality GaN films can be grown on various graphene substrates of mechanically exfoliated graphene layers and large-scale CVD graphene films, which were synthesized on Cu and Ni foils. However, due to differences in crystal orientations of various graphene substrates, single crystal GaN films were grown on mechanically exfoliated graphene layers, while GaN films grown on CVD graphene films exhibited random in-plane orientations. The structural and optical characteristics of the epitaxial films grown on various graphene films are also discussed in this chapter.

4.2. Epitaxial growth of GaN thin films on graphene films

4.2.1. Growth methods

The basic strategy for epitaxial growth of GaN films on graphene layers is shown schematically in Fig. 4.1a. A mirror-smooth, epitaxial GaN thin film could not be grown on pristine graphene layers, presumably due to the lack of chemical reactivity. GaN islands can be grown readily along the naturally formed step-edges, while GaN nucleation would not occur on the basal plane of pristine graphene. Accordingly, the first step is to create many step-edges on the graphene surface by oxygen plasma treatment, which can act as nucleation sites. Oxygen plasma treatment can make graphene rough.[28] However, although the oxygen-plasma treatment increased the GaN island density, GaN films grown on oxygen plasma treated graphene layers exhibited rough and irregular surfaces, similar to the previous report on GaN films that were grown on graphite substrates.[37, 38] The

film crystallinity or morphology did not improve even the typical use of a low-temperature GaN buffer layer.

Thus, high-density ZnO nanowalls were grown on oxygen-plasma-treated graphene layers as an intermediate layer for GaN growth. Figures 4.1c shows SEM image of high-density, epitaxial ZnO nanowalls grown on plasma treated graphene layers. As previously reported,[18] ZnO nanowalls are grown along naturally formed graphene step-edges, and accordingly, step-edges generated by oxygen plasma lead to the formation of high-density ZnO nanowalls. Because of the same crystal structure and small lattice misfits with GaN, moreover, epitaxial GaN films grow on the nanowalls by lateral overgrowth. Although the lateral overgrowth depended on the nanowalls density, the SEM image in Fig. 4.1d shows the flat surface morphology of the GaN films. The high-density ZnO nanowalls play a critical role in the heteroepitaxial growth of GaN films on graphene layers.

As mentioned above, it was hard to obtain high quality GaN films on graphene layers using a typical GaN film growth conditions. Figure 4.2a shows SEM images of GaN layers grown on pristine graphene layers using typical GaN buffer layers. On using low-temperature GaN buffer layer, GaN islands can be grown readily along the naturally formed step-edges of graphene layers. To increase GaN nucleation sites, many step-edges were artificially created by oxygen plasma etching. Figure 4.2b shows GaN films were grown on the entire surface of oxygen plasma treated graphene layer because the oxygen plasma treatment increased the GaN island density. However, the GaN films exhibited

random growth orientations, and their surfaces were rough and irregular. The results indicate that even the typical use of a low-temperature GaN buffer layer did not improve the film morphology or crystallinity of GaN films grown on graphene layers. These difficulties may result from the lack of chemical reactivity of graphene surfaces, as shown schematically in Fig. 4.2c. Typical GaN growth substrates, such as *c*-Al_2O_3, have many dangling bonds on the substrate surfaces which make easy for high density nucleation. Meanwhile, without any step edges or point defects, graphene layers are relatively free from the dangling bonds, and makes hard for GaN nucleation.

For the growth of high quality GaN films on graphene layers, ZnO nanowalls were employed as an intermediate layer. Heteroepitaxial GaN layers can be coated on ZnO nanowalls because both GaN and ZnO have a wurtzite crystal structure with small lattice misfits that are within 2%. As previously reported, the clean interface between GaN and ZnO layers were confirmed using high-resolution TEM.[39, 40] In this study, epitaxial relations of ZnO nanowalls and graphene were further investigated using TEM. Figure 4.3a shows cross-sectional TEM image of ZnO nanostructures grown vertically on graphene layers. The selective area electron diffraction (SAED) patterns were obtained from each ZnO nanostructures and graphene layers. As shown in Figs. 4.3b and 4.3c, SAED patterns clearly show that the (0002) and $(11\bar{2}0)$ planes of ZnO are parallel to those of the graphene layers [i.e., ZnO(0002)$\|$C(0002) and ZnO$(11\bar{2}0)\|$C$(11\bar{2}0)$]. The in-plane and *c*-axis alignment of ZnO nanostructures and graphene layers

indicates that ZnO nanowalls were grown on graphene layers with epitaxial relationships.

Additionally, the surface morphologies of GaN layers grown with different ZnO nanowall densities were investigated because the ZnO intermediate layers played a critical role for the growth of high quality GaN film on graphene. Figure 4.4a shows SEM images of high density ZnO nanowalls and flat GaN film grown on the high density ZnO nanowalls. However, when the density of the ZnO nanowalls was too low for complete coalescence of GaN micro-pyramids (top of Fig. 4.4b), GaN films exhibited a rough surface morphology with hexagonal pyramidal facets (bottom of Fig. 4.4b). This result clearly indicates that lateral overgrowth of GaN on ZnO nanowalls plays a critical role in forming high quality GaN films with very smooth surface morphology.

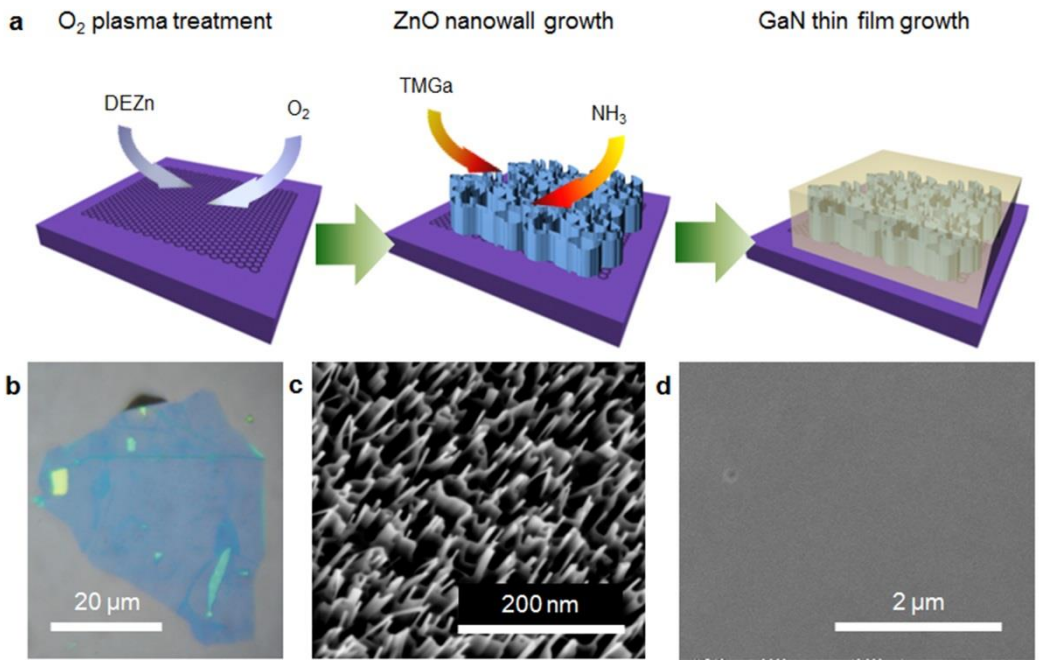

Fig. 4.1. (a) Schematic illustrations of fabrication process for epitaxial GaN thin films on graphene films. (b) Optical microscopic image of oxygen-plasma-treated graphene layers. SEM images of (c) ZnO nanowalls grown on plasma-treated graphene layers and (d) GaN thin film grown on ZnO nanowalls-coated graphene layers.

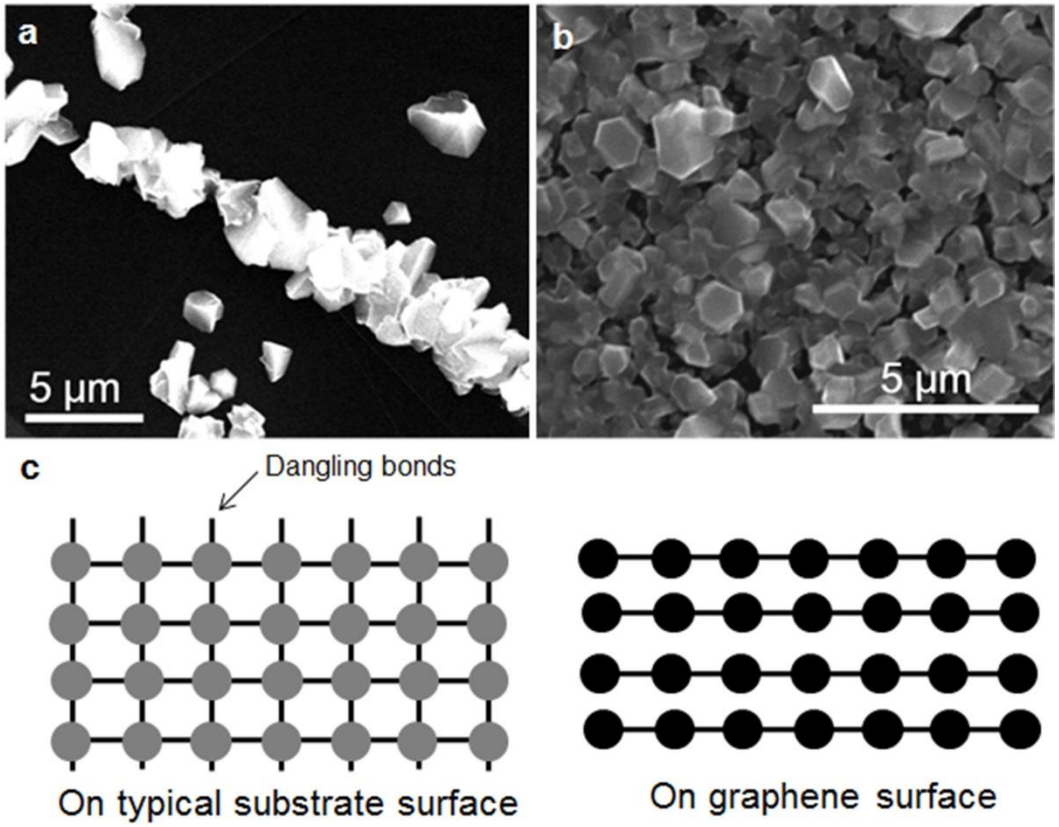

Fig. 4.2. SEM images of GaN layers directly grown on pristine graphene layers (a) without any treatment and (b) after oxygen-plasma treatment. (c) Schematics of typical substrates with dangling bonds (left image) and graphene substrates (right image).

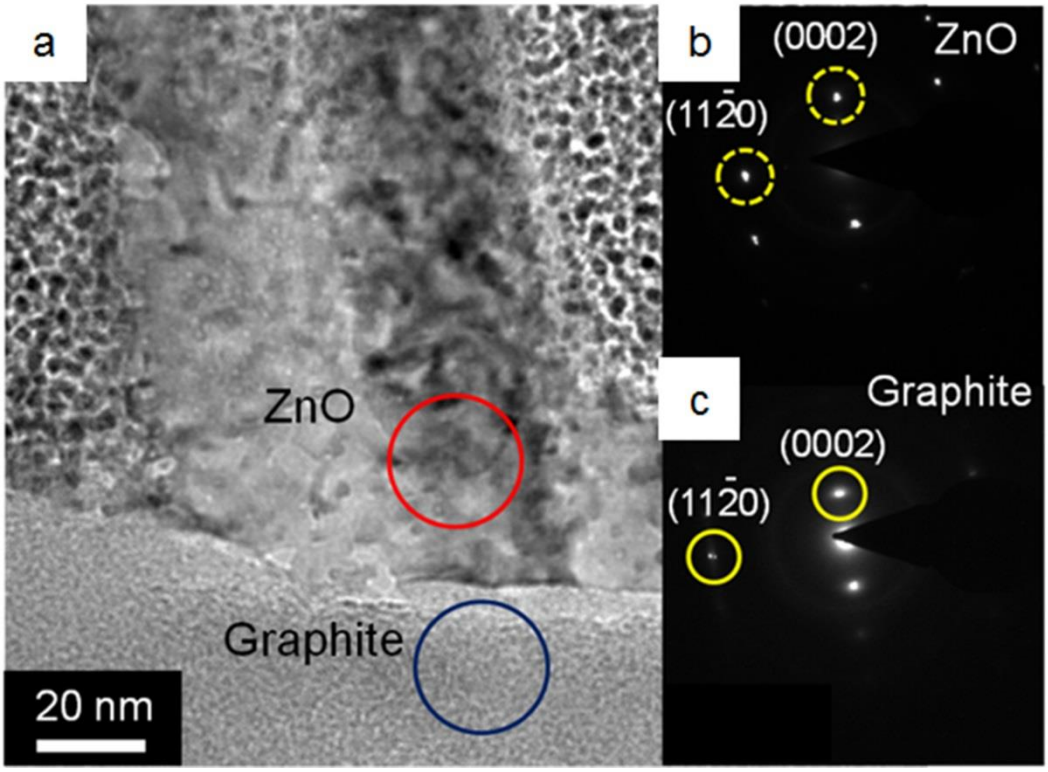

Fig. 4.3. (a) Cross-sectional TEM image of ZnO nanostructures grown on graphene layers and corresponding SAED patterns for (b) ZnO and (c) graphene layers. The SAED patterns were obtained from two areas: one from ZnO just above the interface (red circle), and the other from graphite (blue circle).

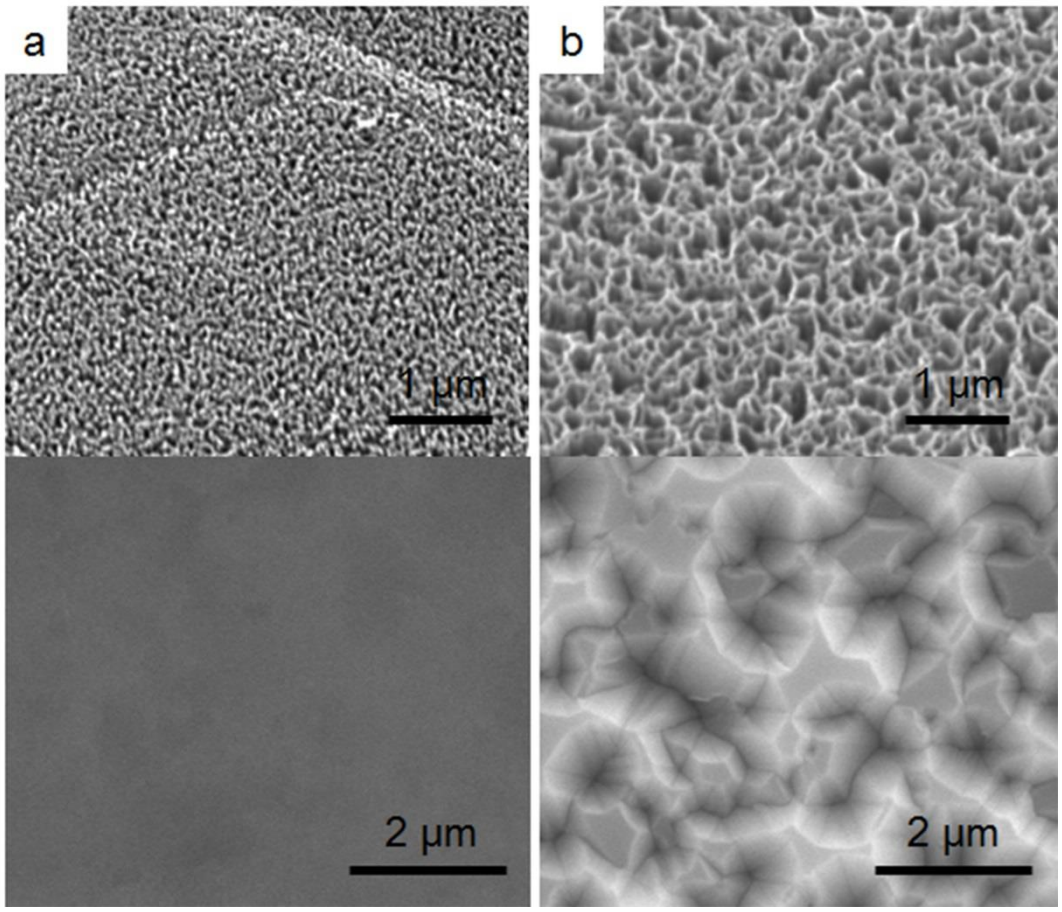

Fig. 4.4. SEM images of (a) high-density and (b) low-density ZnO nanowalls (top images) and corresponding GaN films (bottom images) grown on the nanowalls.

4.2.2. Surface morphologies of GaN films grown on mechanically exfoliated graphene layers and on chemical vapor deposited graphene films.

The heteroepitaxial growth of GaN films on graphene films were firstly demonstrate on mechanically exfoliated graphene layers because of the easy preparation methods of the graphene substrates. Moreover, this GaN film/graphene hybrid heterostructures would open up significant opportunities to fabricate various electronic and optoelectronic devices for commercial use by using large-scale graphene films. For this reason, GaN films were grown on large-scale CVD graphene films synthesized on Cu and Ni foils using the same growth methods. Figure 4.5a shows the GaN films were grown mechanically exfoliated graphene layers. The smooth and flat GaN films were grown over the entire graphene layers. Pits or cracks were rarely observed from the GaN films on mechanically exfoliated graphene layers. Similar to this result, GaN films were grown on CVD graphene films synthesized on Cu and Ni foils with flat surface morphologies, as shown in Figs. 4.5b and 4.5c, respectively. However, GaN films grown on CVD graphene films, which were synthesized on Cu foil, exhibited cracks on GaN films surfaces. The crack free area was approximately ten to hundreds of μm^2. Additionally, GaN films grown on CVD graphene films, which were synthesized on Ni foil, showed an assembly of few-μm^2-size thin films.

The morphology difference in GaN films grown on mechanically exfoliated graphene films and on CVD graphene films are presumably due to the graphene crystallinity. As determined by XRD, mechanically exfoliated graphene layers were single crystalline. However, according to previous reports of CVD

graphene films, typical CVD graphene films exhibited random in-plane orientations with graphene grain size bellow tens of μm.[19-21] Therefore, one of the reasons of cracks of the GaN films grown on CVD graphene films might be due to the epitaxial growth of GaN films on graphene films with random in-plane orientations. The structural characteristics of GaN films grown on various graphene films will be further discussed in Section 4.3.

The surface morphologies of GaN films grown on CVD graphene films were further investigated using electron back scattering diffraction (EBSD). Prior to the GaN films growths, CVD graphene films were synthesized on Cu foil with different growth conditions, which resulted in the different graphene grain size. The ZnO nanowall seed layers and the GaN films were grown on these CVD graphene films simultaneously using MOCVDs. Figures 4.6a and 4.6d show 70˚-tilted FE-SEM images of GaN films grown on the CVD graphene films, clearly exhibiting large differences in their surface roughness. Even though GaN films grown on CVD graphene films showed rough surface morphologies, the normal direction of EBSD inverse pole figure map indicated that the GaN films were well-ordered along c-axis, as shown in Fig. 4.6b. However, the rough GaN films had large and dense color contrasts in the transverse direction of EBSD inverse pole figure map, as shown in Fig. 4.6c.The large color contrast stands for GaN film grains with large-angle difference. Meanwhile, there were no significant differences in the normal direction and the transverse direction of EBSD inverse pole figure maps of the flat GaN films, as shown in Figs. 4.6e and 4.6f, respectively. This result strongly suggested that CVD graphene films strongly

affected to the surface morphologies and the grain size of GaN films. Additionally, cracks of the GaN films were observed in SEM image in Fig. 4.6d. However, as shown in Fig. 4.6f, I could not observed large-angle grain boundaries at GaN thin films with crack, strongly suggesting that large-angle grain boundaries were not significantly affected to crack formations. In this case, thermal expansion coefficient mismatches with GaN layers and the graphene supporting substrates underlying the graphene films may result in the crack problems. This issue will be discussed in Chap. 6 (see fabrication of GaN micro-disk arrays).

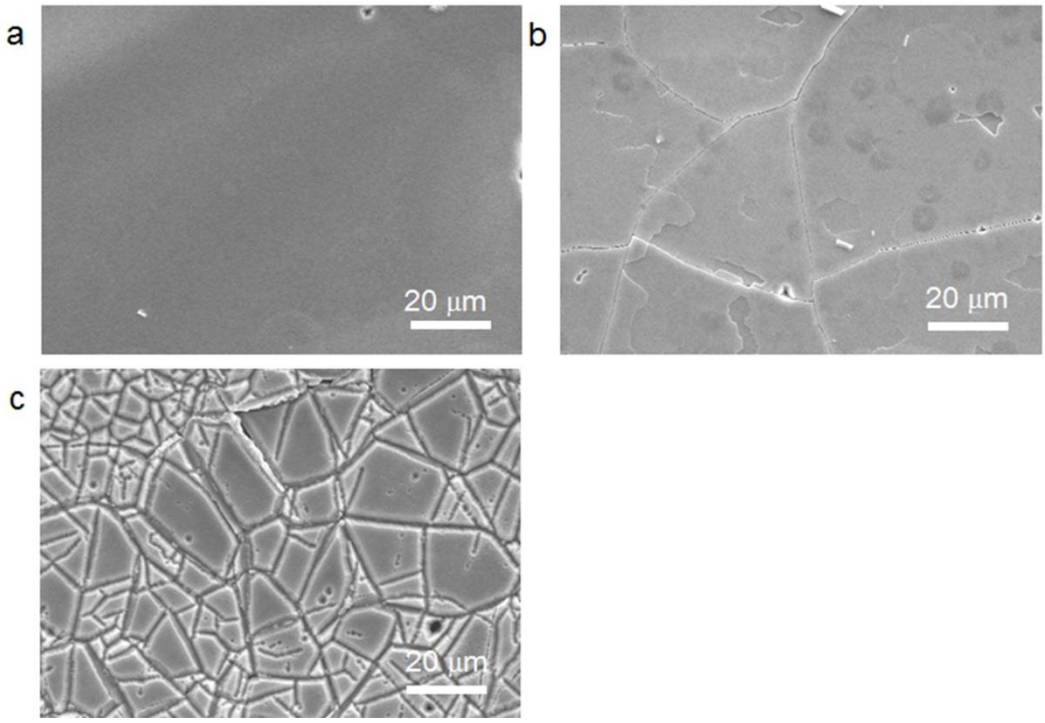

Fig. 4.5. Surface morphologies of GaN thin films grown on (a) mechanically exfoliated graphene layers, (b) CVD graphene films synthesized on Cu foil, and (c) CVD graphene films synthesized on Ni foil.

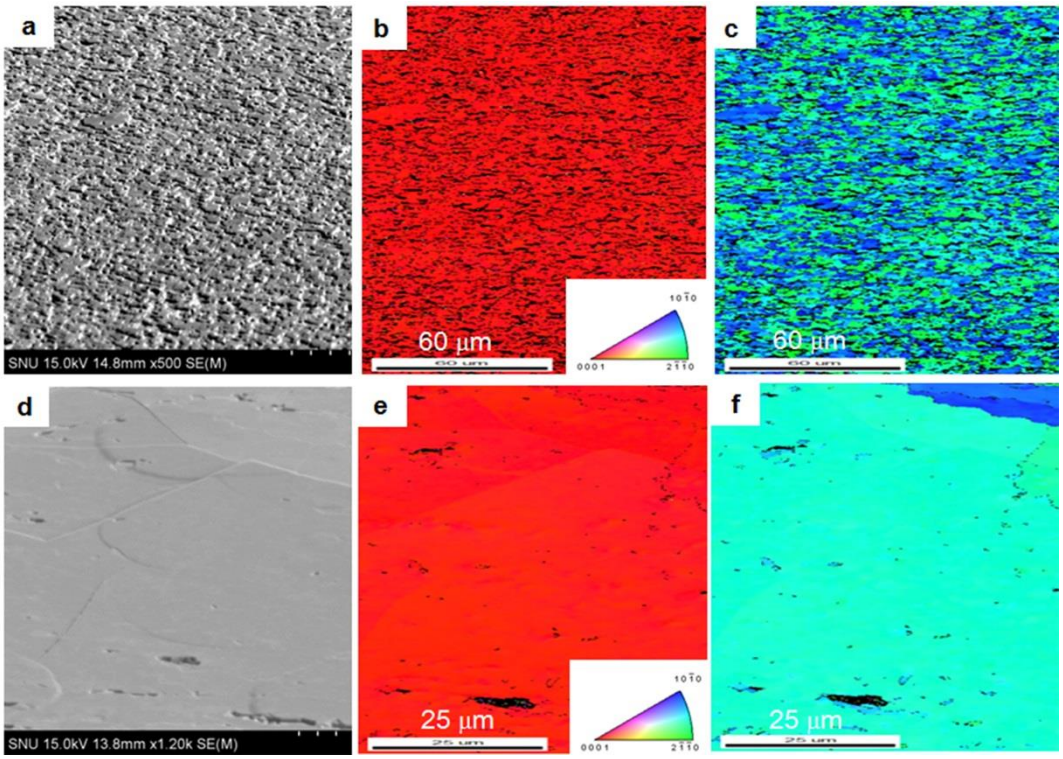

Fig. 4.6. GaN films grown on CVD graphene films, which were synthesized at different graphene growth conditions. 70°-tilted FE-SEM images of (a) rough and (d) flat GaN films grown on CVD graphene films. (b) The normal direction and the (c) transverse direction of EBSD inverse pole figure maps of Fig. 4.6a. (e) The normal direction and (f) the transverse direction of EBSD inverse pole figure maps of Fig. 4.6d.

4.3. Structural characteristics.

Structural analysis of GaN films grown on mechanically exfoliated graphene layers was performed using TEM. As shown in Fig. 4.7a, the low-magnification TEM image shows that GaN films were grown on graphene layers without significant microstructural defects such as voids or cracks. Additionally, threading dislocations were clearly shown, similar to those of the GaN layers grown on single crystal sapphire or silicon substrates. The threading dislocation density was low $10^9/cm^2$, which was comparable to those of GaN films on silicon substrates and slightly higher than those of GaN films on sapphire substrates.[41] Figure 4.7b shows the high-resolution TEM image of GaN films, exhibiting a well-ordered crystal lattice array. The lattice spacing between the adjacent planes was 0.52 nm, corresponding to the *d*-spacing of GaN(0001) planes. Furthermore, the electron diffraction pattern exhibits a regular spot array as shown in the inset of Fig. 4.7b. These TEM results suggest that GaN film were grown on graphene layers with high structural quality.

The crystal structure and growth orientation of GaN thin films on ZnO-coated graphene films were further investigated using XRD. Figure 4.8a shows a typical θ–2θ scan result of GaN thin films grown on mechanically exfoliated graphene layers, CVD graphene films synthesized on Cu foil, and CVD graphene films synthesized on Ni foil. The 2θ peaks of the thin films were observed at 34.58° and 72.90°, which correspond to the (0002) and (0004) diffraction peaks of wurtzite GaN, respectively. Besides the *c*-plane XRD peaks of GaN and graphite, no other peaks were observed in the measured range of 20–80°, indicating that the

films were grown with a preferred *c*-axis normal to the graphite substrates. Furthermore, XRD rocking curves could also be measured because the GaN films were highly oriented in the *c*-axis direction. As shown in Fig. 4.8b, the FWHM value of the XRD rocking curves was as small as 0.8° for GaN film grown on CVD graphene films synthesized on Cu foil, indicating good *c*-axis orientation of the GaN film. We also obtained the rocking curves of the GaN films grown on mechanically exfoliated graphene layers. Since FWHM value of rocking curve of mechanically exfoliated graphene was 3–6°, rocking curve of GaN films grown on the mechanically exfoliated graphene layers exhibited broader FWHM value of 6–8°.

We also investigated the in-plane orientation of the GaN films by measuring azimuthal (ϕ) scans of the GaN(112) diffraction. As shown in Figure 4.8c, three different peaks displaying 20° shifts and six-fold symmetry (black solid line) were observed for the GaN films grown using a CVD graphene film. This result indicated that the GaN grains in the thin film had large grain angle boundaries and preferred in-plane orientations. Similar in-plane orientations for CVD graphene films synthesized on Cu foil have previously been reported,[19, 20] suggesting that the in-plane orientation of GaN results from using the CVD graphene film. Only one set of peaks possessing six-fold symmetry was observed for the ϕ-scan (red solid line) of GaN films grown on an exfoliated graphene layer, indicating that the GaN films were single crystals without large-angle grain boundaries, similar to previous reports.

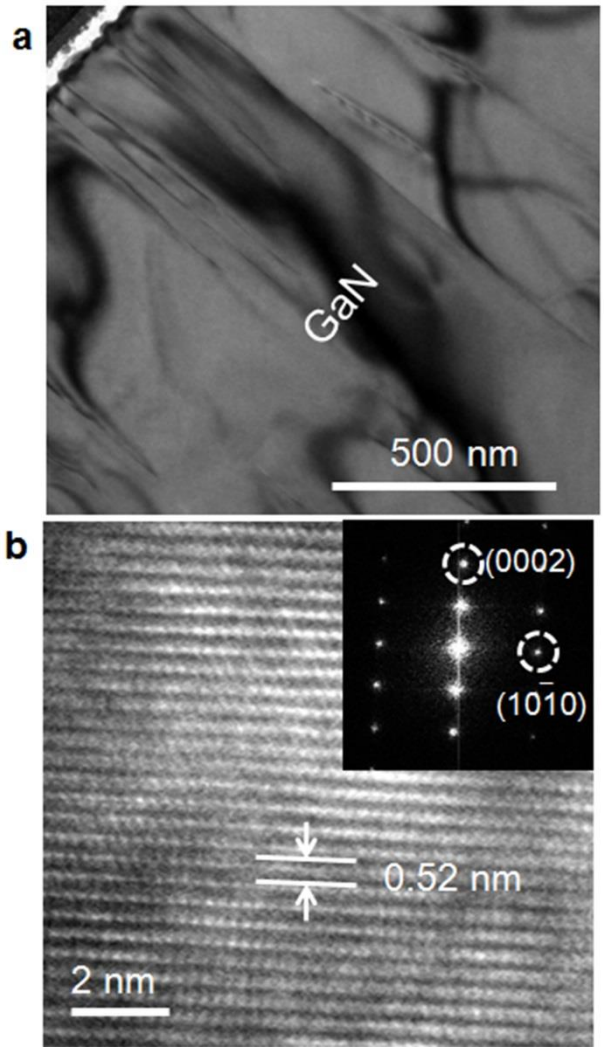

Fig. 4.7. (a) Low-magnification and (b) high-resolution TEM images of GaN films grown on mechanically exfoliated graphene layers. The inset of Fig. 4.7b shows diffraction patterns of the GaN films.

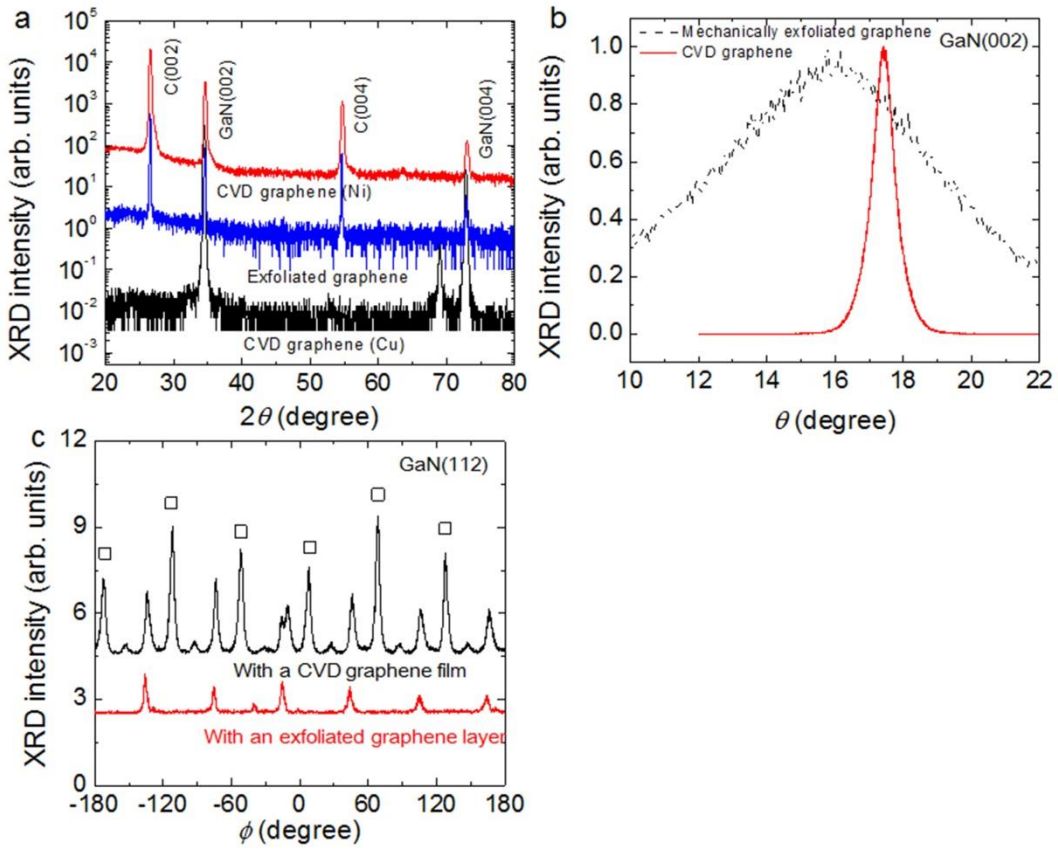

Fig. 4.8. XRD results of GaN thin films grown on mechanically exfoliated graphene layers and on CVD graphene films. (a) θ–2θ scans. (b) Rocking curves. (c) ϕ-scans.

4.4. Optical characteristics.

Optical characteristics of GaN films grown on graphene films were investigated using PL spectroscopy. Figures 4.9a and 4.9b show room temperature PL spectra of GaN thin films grown on mechanically exfoliated graphene layers and on CVD graphene films synthesized on Cu foil, respectively. A continuous-wave He-Cd laser was used as the optical excitation source. For GaN film grown on mechanically exfoliated graphene layers, the dominant PL emission peak was at 3.40 eV which correspond to near-band-edge (NBE) emission presumably associated with excitons, and a very weak deep level emission at 2.2 eV. This strong excitonic emission with the extremely low deep level emission indicates the high optical quality of the GaN films on graphene layers. In addition, PL peaks with strong NBE emission with weak deep level emission can be also obtained from the GaN films grown on CVD graphene films. However, the deep level emission/NBE emission ratio was slightly higher than those of GaN films grown mechanically exfoliated graphene layers.

Figure 4.10a shows temperature dependent PL spectra of GaN films on mechanically exfoliated graphene layers in the range of 20–210 K. The dominant PL emission peak was observed at 3.467 eV for low temperature PL spectrum of 20 K, which is attributed to excitons. Additional PL peaks were observed at 3.269 and 3.190 eV, which were attributed to donor-acceptor pair (DAP) recombination and its longitudinal optical-phonon replica emission, respectively. With increasing temperature, the DAP emission exhibited at blue shift, and finally quenched and vanished at the high temperature of 210 K.[42] Furthermore, there was no emission

peak associated with carbon impurities around 2.8 eV in the low-temperature PL spectra. This strongly suggests that carbon atoms in graphene layers were not incorporated into GaN films during the growth.[43]

Since low-temperature PL spectroscopy which is a very sensitive method to probe defect formation and impurity incorporation, optical characteristics of GaN films grown on CVD graphene films were also investigated using low-temperature PL spectroscopy. For the defect study, GaN films were grown on CVD graphene films synthesized on Cu foil at various temperatures in the range of 1120 to 1150°C, which GaN film showed similar growth morphologies. As shown in Fig. 4.10b, the PL spectra measured at 11 K exhibited the dominant emission peak at 3.468 eV which is attributed to neutral donor-bound excitons. Additionally, DAP recombination peak and its longitudinal optical-phonon replica emission peak were observed at 3.266 and 3.174 eV, respectively.[43] The dominant peak emission intensities increased with growth temperature from 1120 to 1140°C. For the GaN films grown at 1150°C, an additional PL peak was observed at 3.419 eV, attributed to excitons strongly bound to structural defects. The intensity of the DAP peak increased significantly and was stronger than those due to excitonic emission. This dependence of the PL spectra on growth temperature strongly suggests that defects, presumably originating from incorporation of oxygen in the SiO_2 substrates or carbon in the CVD graphene,[44] may be formed in GaN thin films during high-temperature growth.

In addition to PL spectra using a continuous He-Cd layer, a pulsed Nd:YAG laser was employed for the power-dependent PL measurements. For low

excitation power with the pulsed Nd:YAG laser below a threshold value (I_{th}) of 0.6 MW/cm^2, the broad NBE emission peak was observed at 3.40 eV from the GaN films grown on mechanically exfoliated graphene layers, similar to that measured using a He-Cd laser, as shown in Fig. 4.11a. Additionally a shoulder peak was seen at 3.34 eV. The integrated intensity increased linearly with the pumping power, indicating that the observed peak originated from the spontaneous emission. However, a very sharp and strong PL emission at 3.29 eV predominanted that evolved from the low-energy shoulder of the spontaneous emission for excitation power above I_{th}. Furthermore, the integrated PL intensity increased superlinearly with the pumping power, providing evidence of the stimulated emission. The threshold pumping power of 0.6 MW/cm^2, estimated from the inset in Fig. 4.11a, is similar to the previously reported values of 0.56 to 0.70 MW/cm^2 for GaN thin films on sapphire, Si, and SiC substrates.[45-47]

Figure 4.11b shows the power-dependent PL spectra of GaN films grown on CVD graphene films measured at room temperature. At low excitation laser power, below the I_{th} of the optical pumping power, the GaN thin films exhibited a dominant PL peak at 3.40 eV due to spontaneous emission. For excitation powers above the I_{th}, the GaN films exhibited a strong and sharp PL peak at 3.33 eV rising from the shoulder of the dominant peak. The integrated PL intensities of the GaN films increased superlinearly with the pumping power above the I_{th}, consistent with stimulated emission (inset of Fig. 4.11b). The I_{th} of the GaN films grown on the graphene-coated amorphous substrates was 0.6–0.7 MW/cm^2,

comparable to values for GaN films grown on mechanically exfoliated graphene layers.[2]

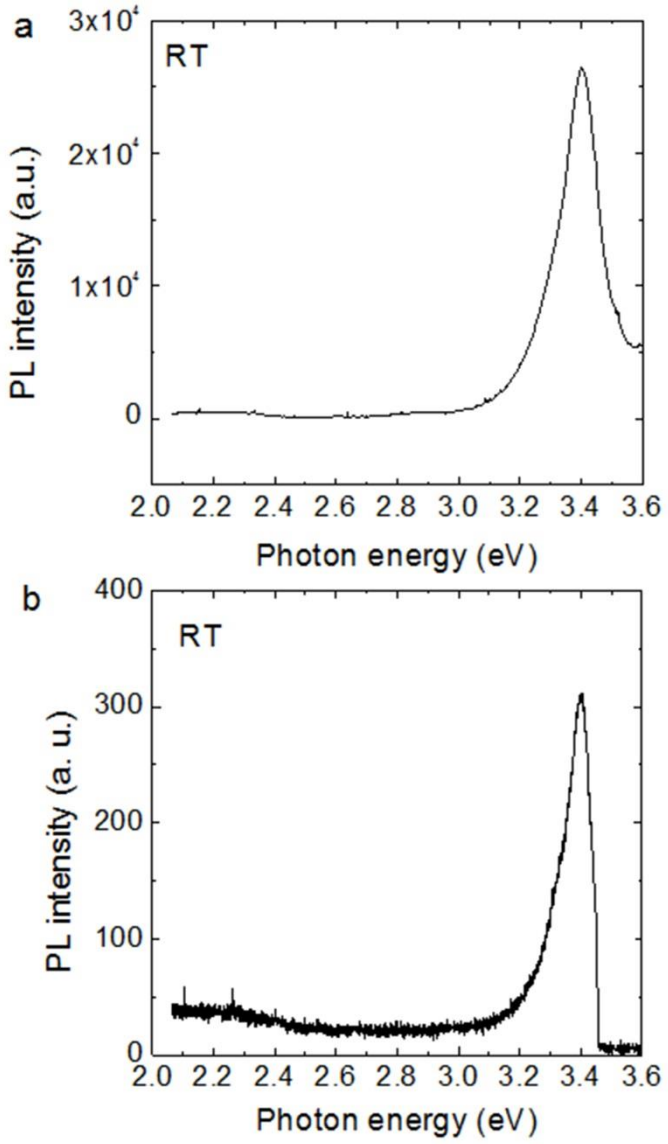

Fig. 4.9. Room-temperature PL spectra of GaN thin films grown (a) on mechanically exfoliated graphene layers and on (b) CVD graphene films synthesized on Cu foil.

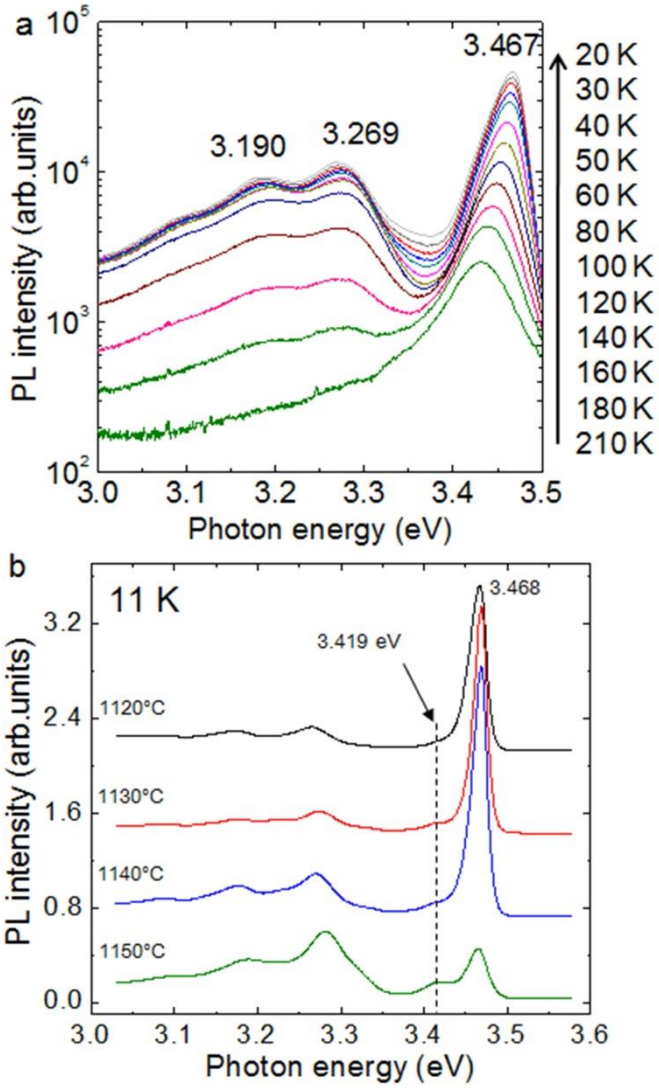

Fig. 4.10. (a) Temperature-dependent PL spectra of GaN thin films grown on mechanically exfoliated graphene layers in the range of 20–210 K. (b) Low-temperature PL spectra of GaN films grown on CVD graphene films synthesized on Cu foil at various temperatures between 1120 and 1150°C.

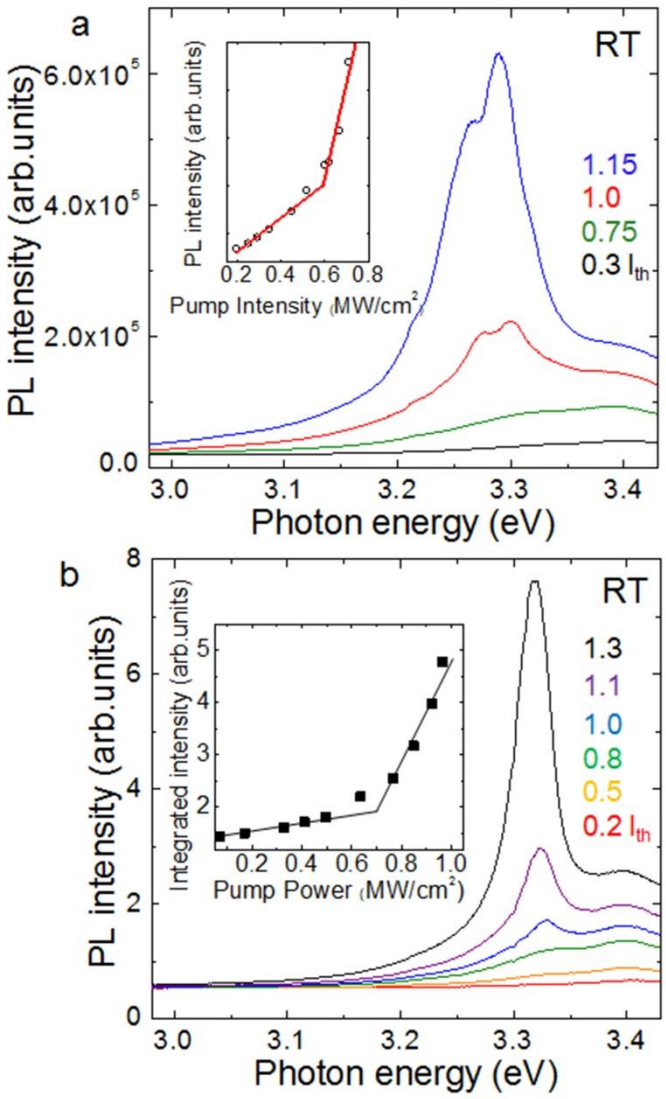

Fig. 4.11. Power-dependent PL spectra of GaN films grown on (a) mechanically exfoliated graphene layers and (b) on CVD graphene films at room temperature. The insets show integrated EL intensities as a function of pump power density.

4.5. Summary

This chapter describes an interesting finding of epitaxial growth of GaN films on graphene layers. Three-dimensional (3D) bulk single-crystal GaN films were grown on a 2D layered graphene sheets. In this case, 1D ZnO nanowalls were grown on graphene first and GaN epitaxial layers were then overgrown on the ZnO intermediate layer. This 2D-1D-3D approach can open up new epitaxial growth possibilities for material systems having problems of nucleation or lattice mismatch. Moreover, high quality GaN films can be obtained on various graphene substrates, including mechanically exfoliated graphene layers and CVD graphene films. The GaN thin films showed high *c*-axis alignment and high crystallinity as determined by XRD and TEM. In particular, the GaN films exhibited high optical characteristics at room temperature, such as stimulated emissions and strong NBE emission with a weak deep level emission.

Growth and characterization of one dimensional GaN micro- and nanorods on graphene films

5

5.1. Introduction

GaN nanostructures and microstructures have recently attracted much attention for light emitting devices because of their interesting characteristics, such as variable-color light emission, high density integration, and high material quality.[48-53] Moreover, when combined by flexible substrates such as graphene, excellent tolerance for mechanical deformation of these microstructures enable the fabrication of flexible and stretchable devices. Nevertheless, the key criteria for building reliable GaN microstructure LEDs on flexible substrates have rarely been studied, such as maintaining high crystallinity, control over doping, formation of heterostructures and quantum structures, and vertically aligned growth onto the underlying substrates. Here, the growth and characterization of GaN micro-rods on graphene films are described. In particular, the vertical growths of GaN micro-rods on graphene films were investigated as well as structural and optical characteristics.

5.2. Growth methods of GaN micro-rods on graphene films

5.2.1. Growth methods and general morphology

The GaN micro-rods were grown on graphene films by MOCVD, as shown in Fig. 5.1a. To prepare the graphene substrates, graphene films were synthesized on copper foil using chemical vapor deposition (CVD), and transferred onto supporting substrates of amorphous SiO_2-coated Si (SiO_2/Si) substrates. Then, a 2-μm-thick GaN buffer layer was grown to improve the vertical alignment of the micro-rods. GaN micro-rods were grown on graphene films using a two-step temperatures of 750−850°C for 3 min and 950−1050°C for 30 min, followed by substrate heating at 1100°C for 10 min with hydrogen. As shown in Fig. 5.1b, GaN micro-rods were grown over the entire graphene film, with a uniform areal density of 10^7 cm^{-2}, and were hexagonal. The length and aspect ratio of GaN micro-rods depended on the growth time. GaN micro-rods grown for 30 min exhibited a diameter of 1.0±0.3 μm and a length of 7.5±1.0 μm, as shown in Fig. 5.1c.

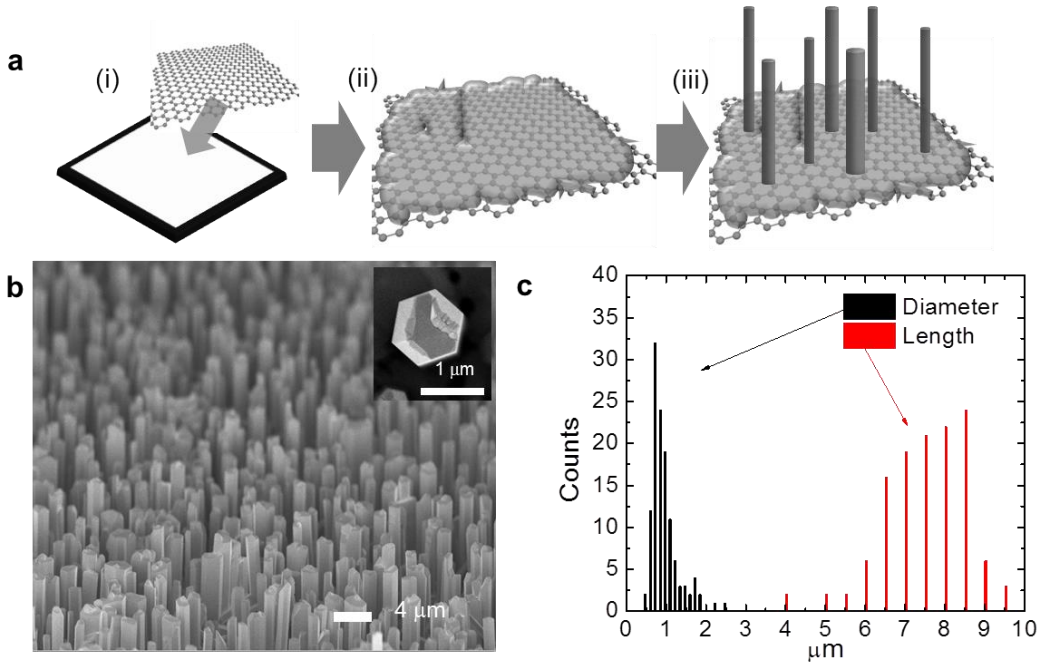

Fig. 5.1. (a) Schematic illustration of CVD-grown graphene transfer (i), GaN buffer layer growth (ii), and GaN micro-rod growth (iii). (b) 60˚-tilt-view FE-SEM image of GaN micro-rods grown on graphene films. The inset of (b) shows a plan-view of the GaN micro-rod. (c) Histogram of diameter and length of the GaN micro-rods.

5.2.2. Effects of growth temperature

As briefly described in section 5.2.1., GaN micro-rods were grown on graphene films using two-step growth temperatures, which are nucleation process and micro-rod growth process. GaN micro-rods with high aspect ratio can be obtained on sapphire substrates or on graphene films in the range of growth temperature of 1050-900˚C, while rough films were grown at growth temperatures below 850˚C. Additionally, since the nucleation process is important to grow inorganic semiconductors on graphene films, GaN micro-rods were grown on graphene films at various nucleation temperatures. In this run, the growth temperature of GaN micro-rods were kept 1000˚C.

Figure 5.2s shows GaN micro-rods grown CVD graphene films at high nucleation temperature of 1000˚C. The GaN microstructures were rarely grown on the graphene films presumably due to few nucleation sites. Although some of GaN microstructures exhibited rod morphology, many irregular GaN microstructures were observed from the FE-SEM image. However, the surface morphology of GaN microstructures grown on graphene films showed drastic changes when the nucleation temperature decreased to 900˚C, as shown in Fig. 5.2b. The GaN microstructures grown on graphene films exhibited rod surface morphology with high aspect ratio. Furthermore, the growth density significantly increased compared to those grown at nucleation temperature of 1000˚C. In addition, the growth density can be increased by decreasing the nucleation temperature to 800˚C, as shown in Fig. 5.3c. At the nucleation temperature of 800˚C, the GaN micro-rods showed similar surface morphology with those grown

with GaN micro-rods in Fig. 5.2b, while the GaN micro-rods showed high density growth, which can cover the whole surface of graphene substrates. This result suggested that 1D GaN microstructures and nanostructures can be grown on graphene films with high integration density, where the density is controllable by changing nucleation temperature. Meanwhile, the vertical growth of GaN micro-rods cannot be obtained by changing nucleation temperatures. The vertical growth of GaN micro-rods will be discussed in section 5.2.3.

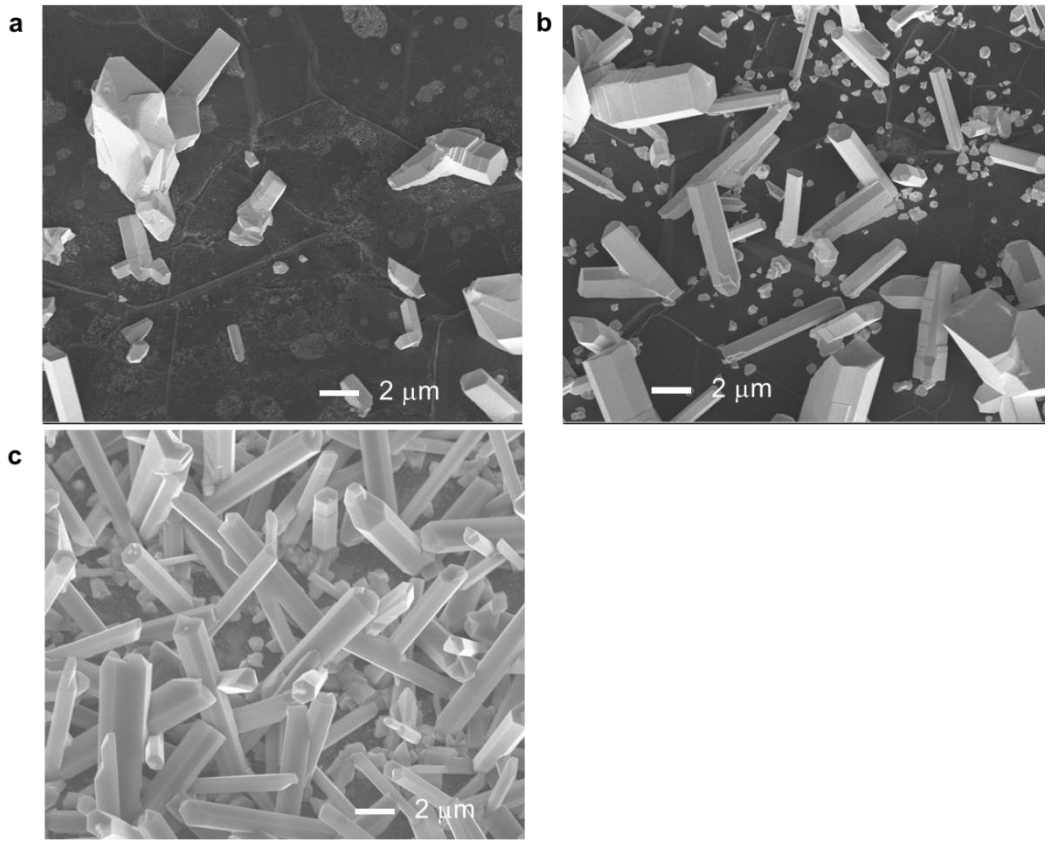

Fig. 5.2. GaN micro-rods grown on CVD graphene films at various nucleation temperatures of (a) 1000, (b) 900, and (c) 800˚C.

5.2.3. Vertical growth of GaN micro-rods on graphene films.

Vertically aligned growth of GaN micro-rods is desirable for light-emitting devices because it allows the fabrication of coaxial quantum-well structures, which exhibit useful optical properties, including color-tunable light emission and a high integration density. However, GaN micro-rods grown directly on pristine graphene without any surface treatment or additional buffer layer exhibited poor vertical alignment, with random growth directions, as shown in Fig. 5.3a. According to other previous research, vertical growth of nanostructures on CVD-grown graphene depends on the surface roughness of the graphene, and ledges or kinks in the graphene film act not only as nucleation sites but also result in random growth directions.[54] Thus, the use of high-quality single-layer-graphene is critical to obtain vertically aligned structures. Meanwhile, to improve the vertical alignment of the GaN micro-rods on the graphene, we grew a GaN buffer layer prior to the growth of the GaN micro-rods.

Figures 5.3b show a 30º tilted-view field-emission scanning electron microscopy (FE-SEM) images of the GaN micro-rods grown on graphene with a GaN buffer layer. The FE-SEM image clearly reveals surface morphologies of GaN buffer layer and GaN micro-rods. The vertical alignment of the GaN micro-rods was significantly improved compared with that of GaN micro-rods grown on pristine graphene, exhibiting excellent vertical alignment on the graphene using a GaN buffer layer. This result strongly suggested that the GaN buffer layer played a critical role for vertically aligned growth of GaN micro-rods on graphene films.

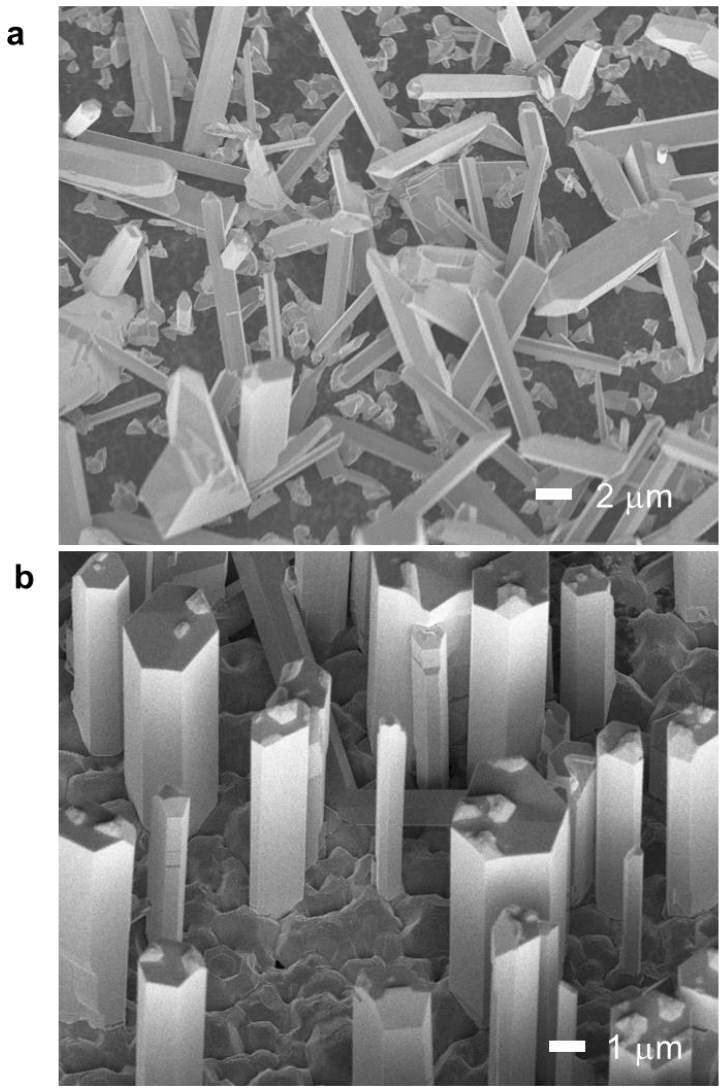

Fig. 5.3. FE-SEM images of GaN micro-rods grown on graphene films (a) without a GaN buffer layer, (b) with a GaN buffer layer.

5.3. Structural characteristics

The growth orientations and crystal structures of GaN micro-rods grown on graphene films was investigated by measuring XRD. Figure 5.4a shows θ–2θ scan results of GaN micro-rods grown on graphene with (the solid line) and without (the solid line with white circles) a GaN buffer layer. The range of angles was 20–80°. When the GaN micro-rods were grown on graphene with a buffer layer, only two wurtzite crystal peaks were observed, corresponding to GaN (002) and GaN (004) at 34.61° and 72.96°, respectively. (The additional peak at 69.18° is attributed to cubic Si(100) from the SiO_2/Si substrate.) However, additional peaks corresponding to GaN (100), GaN (101), GaN (102), GaN (110), and GaN (103) peaks were observed in the XRD spectra at 32.44°, 36.89°, 48.15°, 57.82°, and 63.47° from GaN micro-rods grown on graphene without a GaN buffer layer, respectively. Rocking curves of the GaN micro-rods grown on the buffer layer were also measured, as shown in Fig. 5.4b. The FWHM value of the GaN micro-rods was estimated to be 3°, which is consistent with the GaN buffer layer grown on graphene (2.5°). The SEM images and XRD data strongly suggested that the GaN micro-rods exhibited good vertical alignment, and were of sufficient quality for the fabrication of vertically aligned micro-rod optoelectronic devices.

The microstructural analyses of GaN micro-rods grown on graphene films were further performed using TEM. As shown in cross-sectional TEM image of Fig. 5.5a, GaN micro-rods were vertically grown on graphene films without any significant micro-structural defects. Furthermore, no metal clusters were observed on the micro-rod tips in contrast to GaN micro-rods or nanorods grown by

catalysis-assisted growth methods, indicating that the micro-rods were grown by a catalyst-free growth mechanism. The high-resolution TEM images in Figs. 5.5b and 5.5c showed highly ordered lattice structure of the GaN micro-rods. The lattice spacing between adjacent lattice planes was observed to be 0.519 nm, corresponding to the *d*-spacing of the GaN(001) plane. We observed very few extended crystal defects, such as dislocations and stacking faults, in high-resolution TEM image, indicating that these GaN micro-rods are highly crystalline. Figure 5.5d shows the diffraction patterns through the FFT of the HR-TEM image of Fig. 5.5c. The FFT image shows regular spot arrays with two diffraction spots making as right angle correspond to the GaN(002) and GaN(100) planes, indicating that GaN micro-rods are single crystalline.

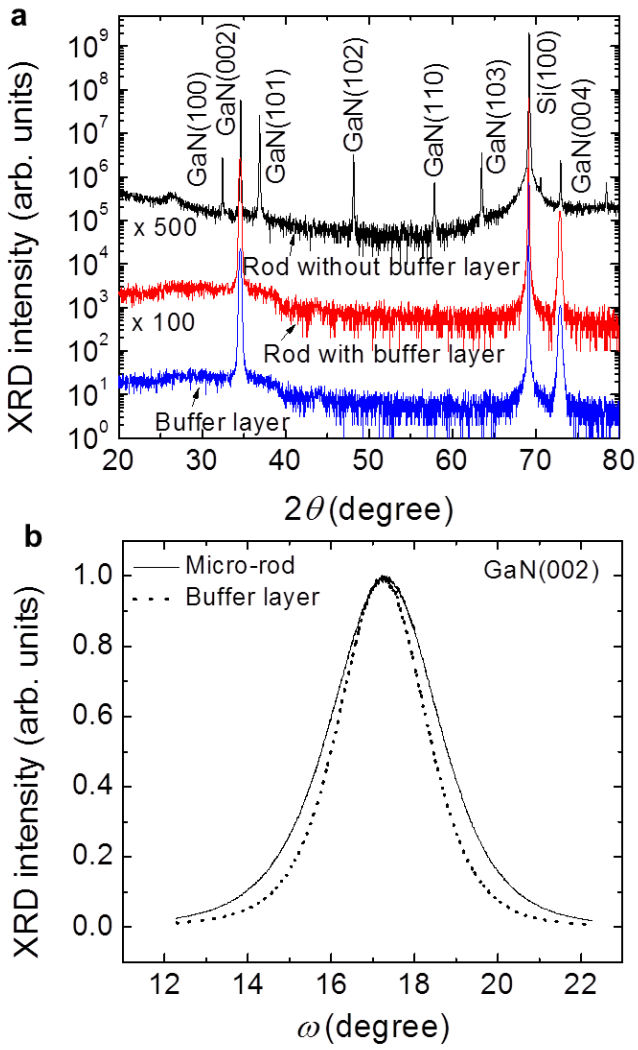

Fig. 5.4. (a) XRD θ–2θ scans of the GaN buffer layer grown on graphene films (blue solid line) and the GaN micro-rods grown on graphene films with (red solid line) and without GaN buffer layers (black solid line). (b) Rocking curves of GaN micro-rods (solid line) and GaN buffer layer (dotted line) grown on the graphene films.

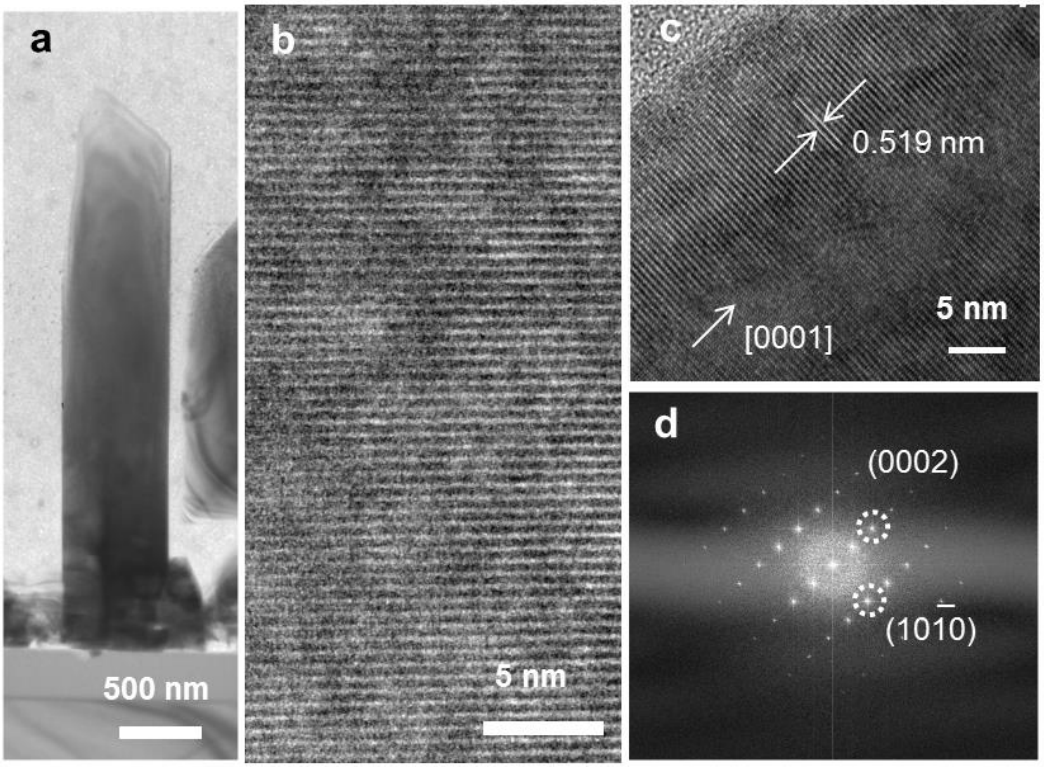

Fig. 5.5. Cross-sectional TEM of GaN micro-rods grown on graphene films. (a) Low-magnification image. (b, c) High-resolution TEM images. (d) FFT image of Fig. 5.5c.

5.4. Optical characteristics

To use GaN micro-rods grown on graphene films for optoelectronic devices, we investigated the optical characteristics of the GaN micro-rods using a pulsed Nd:YAG laser (355 nm) as an optical excitation source. Figure 5.6a shows room temperature PL spectra of the GaN micro-rods at various pump powers. At low excitation densities, the dominant PL peak was observed at 3.4 eV. As the excitation energy density increased, additional PL peaks appeared around the NBE emission, eventually becoming the dominant feature in the PL spectra. The inset of Fig. 5.6a shows a plot of the integrated PL intensity versus the excitation power density. As the pump power increased, the PL intensity increased linearly for low excitation powers; however, above a threshold of approximately 350 kW/cm^2, the slope of the PL intensity as a function of the pumping power drastically increased, becoming superlinear. This strong and sharp increase in the PL spectra is indicative of stimulated emission. The pump power threshold for stimulated emission of the GaN micro-rods grown on the graphene films was comparable to that of GaN nanorods grown on single-crystal sapphire substrates.[55]

The optical characteristics of individual GaN micro-rods grown on graphene films were further examined using micro-PL spectroscopy with a He-Cd laser (325 nm). As shown in Fig. 5.6b, typical room temperature PL spectra exhibit a strong NBE emission at 3.4 eV, with weak deep level emission at around 2.2 eV. The strong NBE emission and low deep level emission indicate that the GaN micro-rods were of high quality, comparable to that of GaN micro-rods and nano-rods grown on single-crystal sapphire and Si substrates.[30, 56, 57] Furthermore, the

PL spectra obtained at the top (region I), middle (region II), and bottom (region III) of the GaN micro-rods did not exhibit any significant variation in the peak position. This suggests that the strain in the GaN micro-rods was negligible, because strain results in a significant shift in the wavelength of the PL spectra.[58]

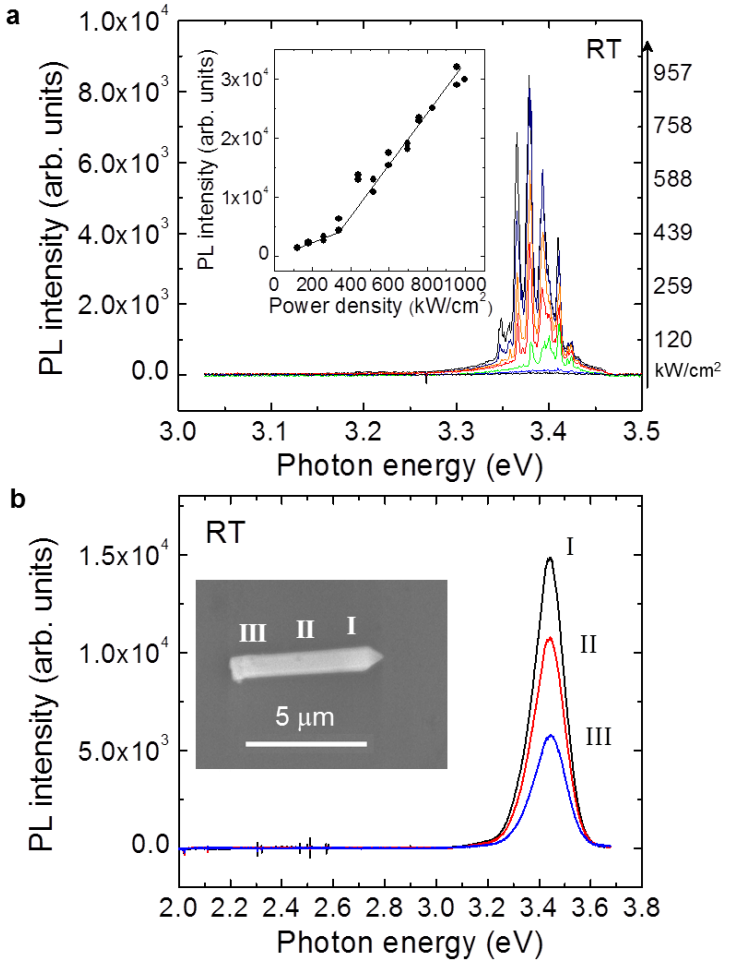

Fig. 5.6. Room-temperature PL spectra. (a) The power-dependent PL spectra of GaN micro-rod arrays vertically grown on graphene films. The inset shows the integrated PL intensity as a function of the pump power density. (b) PL spectra of the top (region I), middle (region II), and bottom part (region III) of an individual GaN micro-rod. The inset shows a corresponding SEM image of the micro-rod.

5.5. Summary

This chapter described the catalyst-free growth of vertically aligned 1D GaN micro-rods on large-area graphene films. Graphene films were grown on Cu foil by means of chemical vapor deposition, and used as the substrates for the growth of the GaN micro-rods, which were subsequently transferred onto SiO_2/Si substrates. Highly Si-doped, *n*-type GaN micro-rods were grown on the graphene films using MOCVD. The growth and vertical alignment of the GaN micro-rods, which is a critical factor for the fabrication of vertical structure nano- or micro-devices, were characterized using electron microscopy and X-ray diffraction. Moreover, the GaN micro-rods exhibited promising PL characteristics for optoelectronic device applications, including room-temperature stimulated emission. All these features show that GaN micro-rods grown on graphene films are desirable for fabricating 3D integrated devices.

Device applications of GaN/graphene hybrid heterostructures

6

6.1. Introduction

Hybrid heterostructures composed of high-quality inorganic semiconductors grown directly on atomic-scale layered sheets, such as graphene and boron nitride, offer a novel material system for transferable electronics and optoelectronics.[2, 3, 7, 59] While graphene has been considered to be an ideal supporting layer for the growth of inorganic materials because of its high thermal and mechanical stability and flexibility, inorganic semiconductor thin films exhibit excellent material characteristics, including a high carrier mobility, a radiative recombination rate, and long-term stability. Recently, large-size graphene films have become available, and hybrid heterostructures using these large-scale graphene films open up significant opportunities to fabricate various electronic and optoelectronic devices for commercial use. In this chapter, transferable and flexible LEDs were demonstrated with reliable operations using GaN microstructures and nanostructures grown on graphene films. Moreover, regular array of GaN microstructures, such as films and micro-disks, were fabricated on metal and SiO_2 substrates for large-scale device applications.

6.2. Transferable GaN thin film LEDs on graphene layers

This section describes on the fabrication of transferable GaN thin film LEDs using graphene layered sheets. Single-crystalline nitride epilayers were grown on graphene layers using high-density, vertically aligned ZnO nanowalls as an intermediate layer. The layered structure of a graphene substrate made it possible to transfer GaN-based LEDs onto foreign substrates such as glass, metal, or plastic very easily. The graphene layers were also used as an electrode for LEDs, exhibiting strong electroluminescent emissions even under room illumination. Furthermore, electrical and optical characteristics of the LEDs were not changed significantly after transfer onto foreign substrates.

6.2.1. Fabrication and transfer of LEDs grown on graphene layers

For the transferable device applications, LEDs were fabricated using GaN epitaxial films grown on graphene layers. The fabrication of GaN thin-film LEDs on graphene layers and their transfer onto foreign substrates are shown schematically in Fig. 6.1a. To fabricate LED structures, a *n*-GaN layer, three-period $In_xGa_{1-x}N$/GaN MQWs and a *p*-GaN layer were epitaxially grown on the ZnO-coated graphene layers. Following by LED growth, Ni/Au bi-layers were deposited on the top surface of *p*-GaN for *p*-type contact, and the metallic graphene layers underneath *n*-GaN and were used as a *n*-type contact. After fabricating the devices, thin film LEDs on the graphene layers were removed mechanically from the original substrate and transferred onto foreign substrates of metal, glass, and plastic.

Figure 6.1b shows optical microcopy images of as-fabricated and transferred LEDs, exhibiting very strong blue light emissions that could be seen with unaided eyes under normal room illumination. We also observed that light emission was fairly uniform over the area of 300 μm by 300 μm, presumably because of uniform current spreading and injection through the metallic graphene layers. Furthermore, the each substrate in Fig. 4.9b has remarkable benefits for LED applications. Metal substrate provide good thermal and electrical conductivity for high-power LEDs, whereas a glass or plastic substrate may allow inorganic LEDs to be fabricated as large-area, full-color LED displays in flexible or stretchable forms.

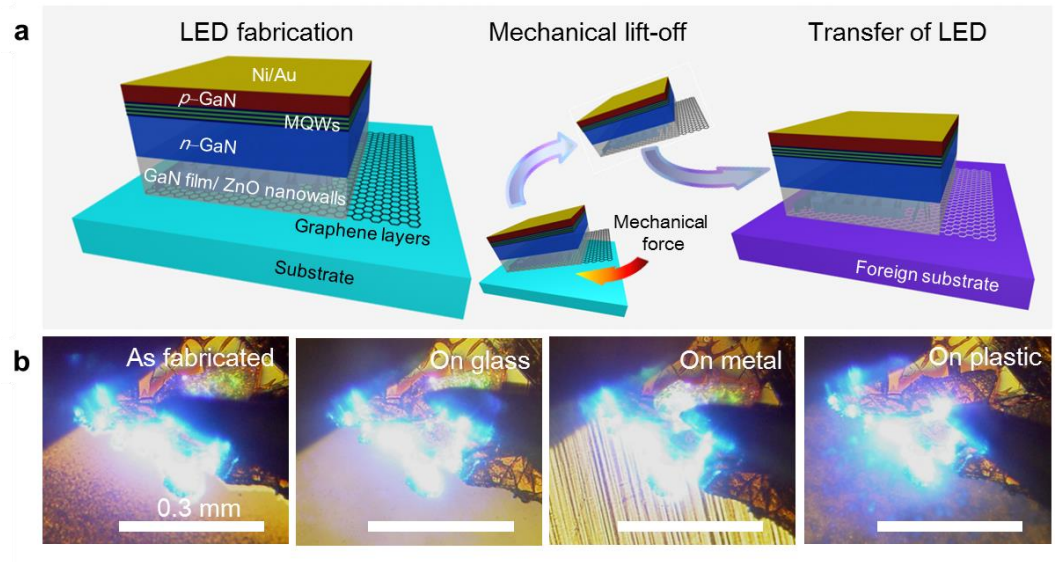

Fig. 6.1. (a) Schematic illustration of the fabrication and transfer processes for thin-film LEDs grown on graphene-layer substrates. (b) Optical images of light emissions from the as-fabricated LED on the original substrate and transferred LEDs on the foreign metal, glass, and plastic substrates.

6.2.2. EL and electrical characteristics

The EL characteristics of the LEDs transferred onto plastic were investigated using EL spectroscopy. Figure 6.2 shows the room temperature EL spectra and corresponding EL images of the LED at various applied current levels of 1.7, 3.2, 5.0, 6.4, and 8.1 mA. The EL spectra and LED light emission images show an increase of emission intensity with the applied current level increase. Additionally, as the applied current level increased from 1.7 to 8.1 mA, the dominant EL peak shifted slightly from 2.71 to 2.75 eV. This blue shift can be explained in terms of both a band filling effect of the localized energy states and a screening effect by the internal polarization electric field typically observed in LEDs with GaN/$In_{1-x}Ga_xN$ MQW structures grown on a polar surface of GaN(0001).[60]

In addition to the EL characteristics, the electrical characteristics of the LEDs transferred onto plastic were investigated by measuring their *I–V* characteristic curves. As shown in Fig. 6.3, the *I–V* characteristic curve exhibits a good rectifying behavior with a turn-on voltage of 4.5 V and a leakage current of 1×10^{-5} A at –4 V, similar to those of the as-fabricated LED. Moreover, above the turn-on voltages, both integrated EL intensity and currents increased simultaneously with the increasing applied bias voltages, indicating EL mechanism involves carrier transport though the *p–n* junction in the LEDs. However, compared with conventional GaN thin film LEDs prepared on sapphire substrates, the turn-on voltage was slightly higher presumably due to energy

barriers at the junctions between the three-material system of graphene, ZnO nanowalls, and GaN films.

LED devices on plastic can become hot due to the low thermal conduction of plastic. In this case, the EL peak position must show a red-shift with increasing current density. However, the EL emission peak position was blue-shifted with increasing current levels. Additionally, we also measured power-dependent EL spectra for LEDs transferred to glass, and metal substrates as shown in Fig. 6.4. None of the spectra showed red-shifts, indicating that no significant heating occurred at these current levels for LEDs fabricated on graphene layers. The blue-shift indicates that the device temperature was not high enough to cause the remarkable red-shift because the drive currents in these experiments were much lower than those used for conventional high-power LEDs. Moreover, we expect relatively better heat dissipation for the LEDs grown on graphene layers because graphene layers used as bottom electrodes have excellent thermal conductivity.

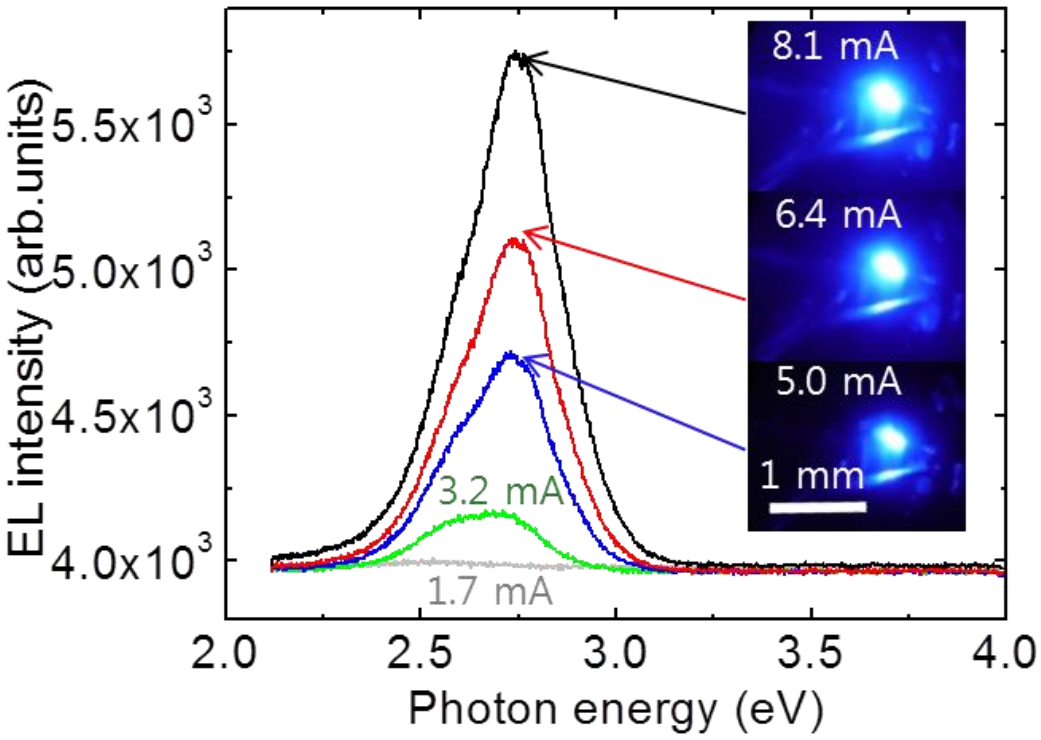

Fig. 6.2. Room-temperature EL spectra of the LED transferred onto a plastic substrate. Optical microscopy images show the light emission at different applied current levels of 5 to 8 mA.

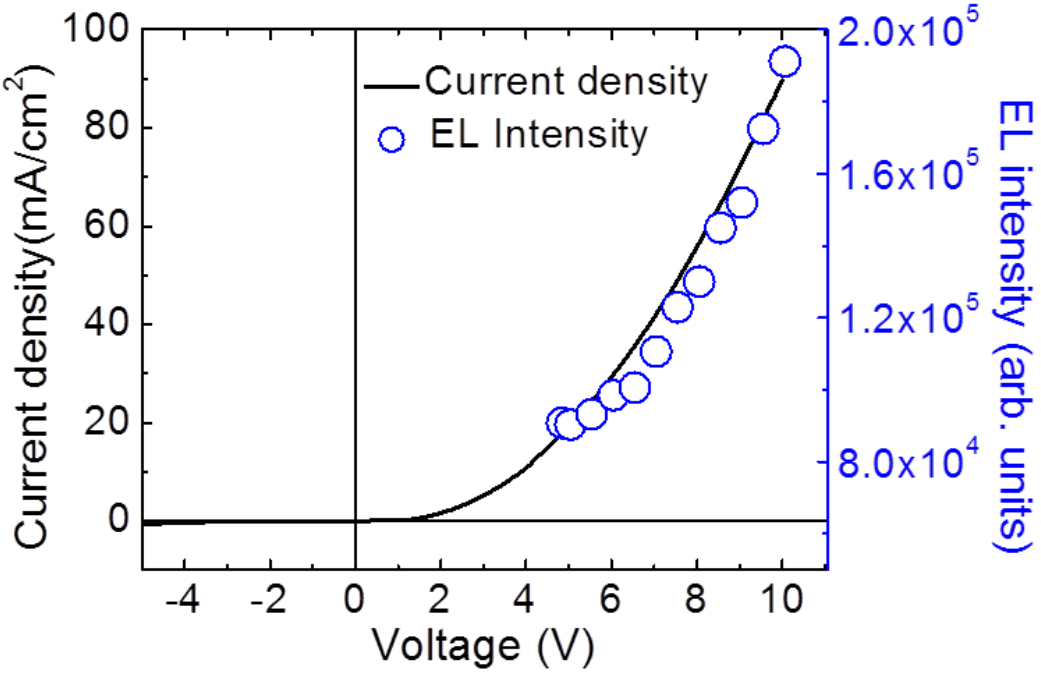

Fig. 6.3. Current density and integrated EL intensity as a function of the applied bias voltage of a representative LED on a plastic substrate. The solid line and open circle correspond to the current density and integrated EL intensity, respectively.

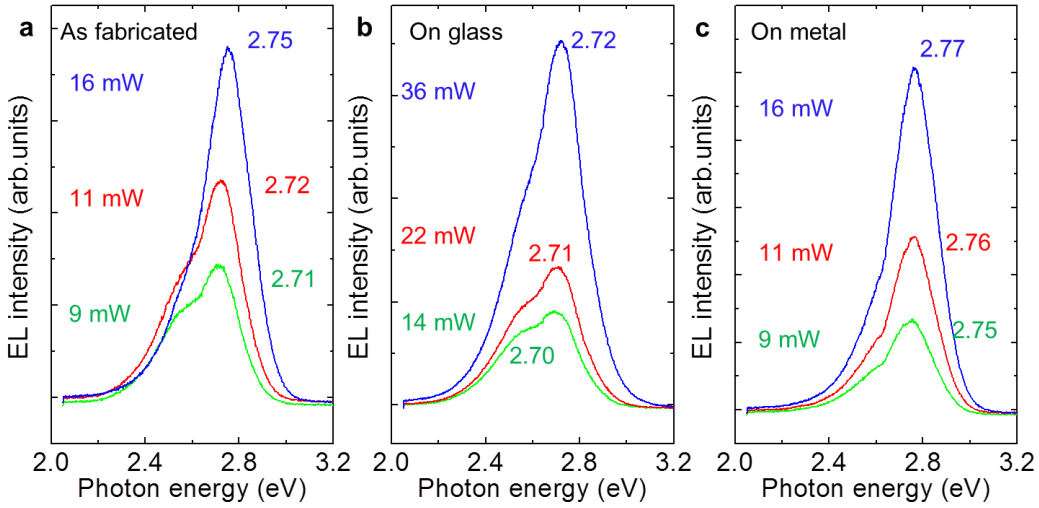

Fig. 6.4. Power-dependent EL spectra of as-fabricated LEDs and LEDs transferred onto glass and metal substrates.

6.3. GaN thin film LEDs fabricated on amorphous substrates

Optoelectronic devices fabricated on large-size substrates are of significant interest for applications to general illumination light sources, flat panel displays, and solar cells.[33, 61] For device applications, the growth of amorphous inorganic semiconductors and organic thin films on amorphous substrates has widely been studied.[62-64] However, the devices based on single-crystalline compound semiconductors such as GaN show much higher efficiencies, reliability, and long-term stability.[9, 65] Nevertheless, because high-quality, single-crystalline nitride films could be grown only on a lattice-matched single-crystal substrate, the use of amorphous substrates, such as fused silica, yielded poor thin film quality, including a rough surface morphology and a polycrystalline structure.[66] Thus, the obstacle to growing large high-quality nitride films on large-size amorphous substrates must be resolved in order to use inorganic LEDs in displays and flat light sources.[36, 67]

6.3.1. Thin film LEDs directly fabricated on amorphous silica substrates

We investigated the effect of using a CVD graphene film as an intermediate layer on the surface morphology of GaN films grown on amorphous substrates. As shown in Figure 6.5a, GaN films grown on a CVD graphene-coated amorphous SiO_2 substrate exhibited a flat and smooth morphology, presumably due to the heteroepitaxial relations between GaN on ZnO and ZnO on graphene. Meanwhile, a rough surface morphology with a few micron-sized irregular hillocks was observed for films directly grown on the SiO_2 substrates in the absence of a graphene film (Fig. 6.5b), indicating that the CVD graphene film

significantly affects the surface morphology of the GaN film. In addition, the surface roughness was reduced using a CVD graphene film: the root mean square surface roughness over a 5 μm × 5 μm area was 11 nm for GaN films grown using the graphene film, twenty times smaller than that for GaN films grown directly on the amorphous substrates.

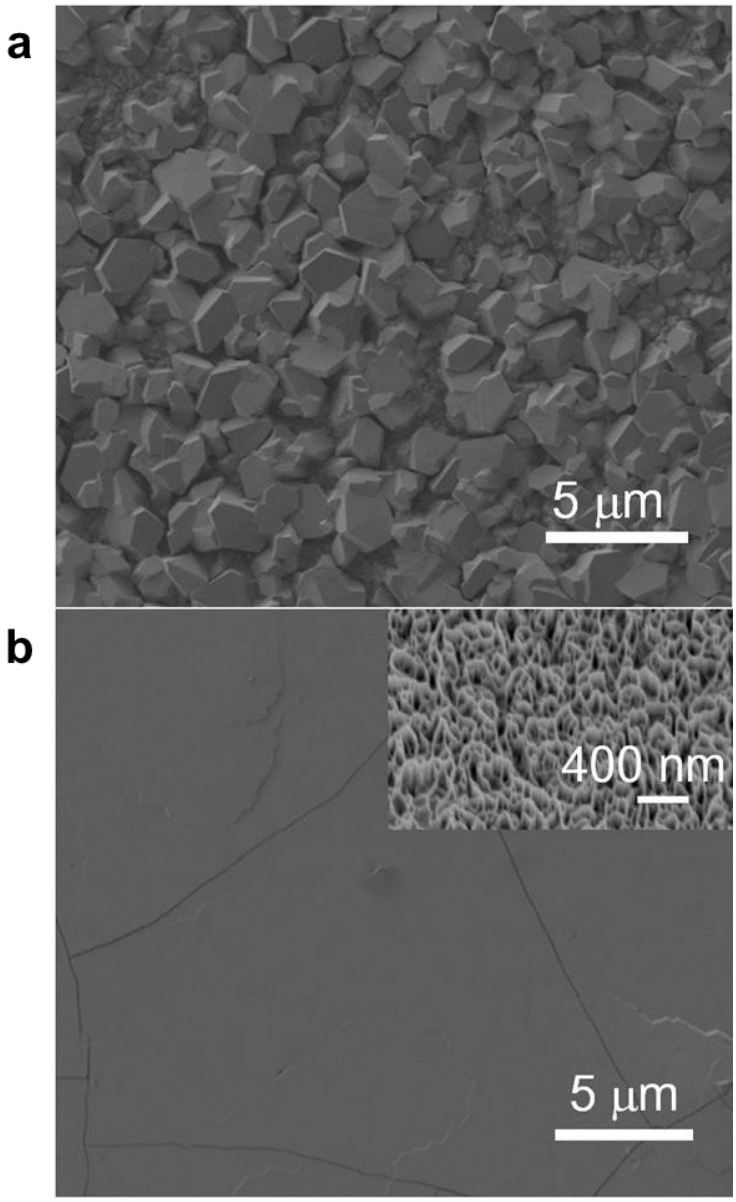

Fig. 6.5. GaN films grown on amorphous silica substrates (a) without and (b) with CVD graphene films as an intermediate layer.

6.3.2. LED fabrications

The LEDs were composed of an *n*-GaN layer, three-period $In_xGa_{1-x}N$/GaN MQWs, and a *p*-GaN layer (Fig. 6.6a). After growing the LED structures, lithography and BCl_3 reactive ion etching were used for the exposure of *n*-GaN layers. Ni/Au (with a thickness of 8/8 nm) and Ti/Au (20/20 nm) bilayers were deposited on the *p*- and *n*-GaN surfaces, respectively, and annealed in order to make ohmic contacts and reduce the contact resistance of the electrodes.

The GaN-based thin film LEDs fabricated on CVD graphene-coated amorphous SiO_2 substrates emitted strong blue light emissions that could be seen with unaided eyes under typical room illumination conditions (Fig. 6.6b). The light emission from the LED at a driving current of 3.1 mA was fairly uniformly distributed over the *p*-contact area of 70 × 70 μm^2. This result suggests that the hybrid heterostructure, composed of inorganic semiconductors directly grown on large scale graphene films, constitutes a new functional material system for developing unconventional inorganic optoelectronic devices in large scale forms, taking advantages of both inorganic semiconductors and graphene films.

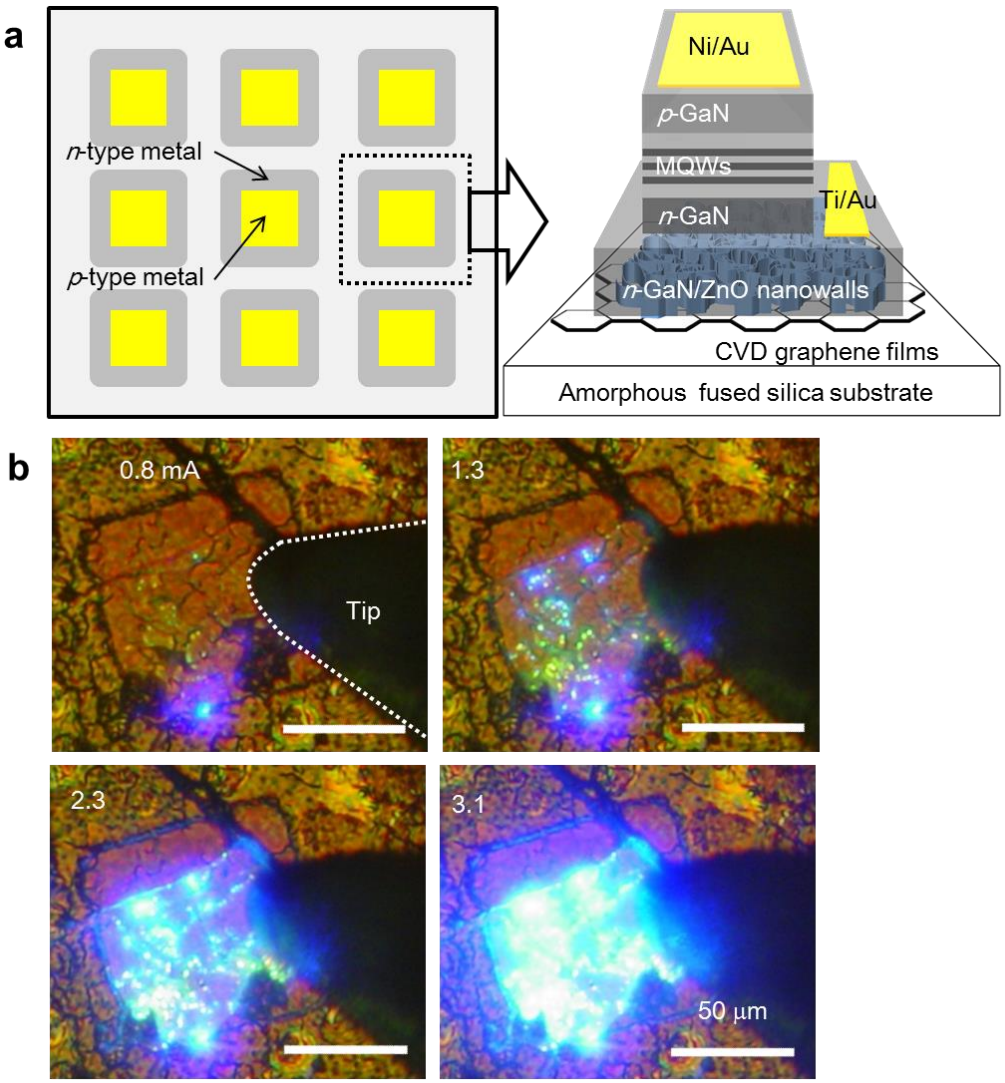

Fig. 6.6. Visible thin film LEDs fabricated on CVD graphene-coated amorphous SiO_2 substrates. (a) Schematics of an array (left) of LED pixels and one LED pixel (right) which is composed of *n*-GaN, MQWs, and *p*-GaN layers. (b) EL emission images of the LEDs under room illumination at different applied currents.

6.3.3. EL and electrical characteristics

We further investigated the EL characteristics of the LEDs fabricated on the CVD graphene-coated SiO_2 substrates. Room-temperature EL spectra and *I–V* characteristic curves of the LEDs were measured at various applied current levels (Fig. 6.7a). The EL intensity gradually increased without considerable EL peak shift as the applied current increased from 0.8 to 4.4 mA. Moreover, above the turn-on voltage of 6 V, both the current and the integrated EL intensity of the LEDs increased simultaneously upon increasing the applied bias voltage (inset of Fig. 6.7a). This indicates that the EL mechanism involves carrier transport through the *p–n* junctions in the LEDs. Furthermore, the emission color of the LEDs could be controlled by changing the growth temperature of $In_xGa_{1-x}N$ QW layers since the level of indium incorporated into the QW layers depended on the growth temperature.[68] As shown in Fig. 5.6b, blue (453 nm) and green (504 nm) EL images were obtained from the LEDs with the $In_xGa_{1-x}N$ layer grown at the 800 and 760°C, respectively.

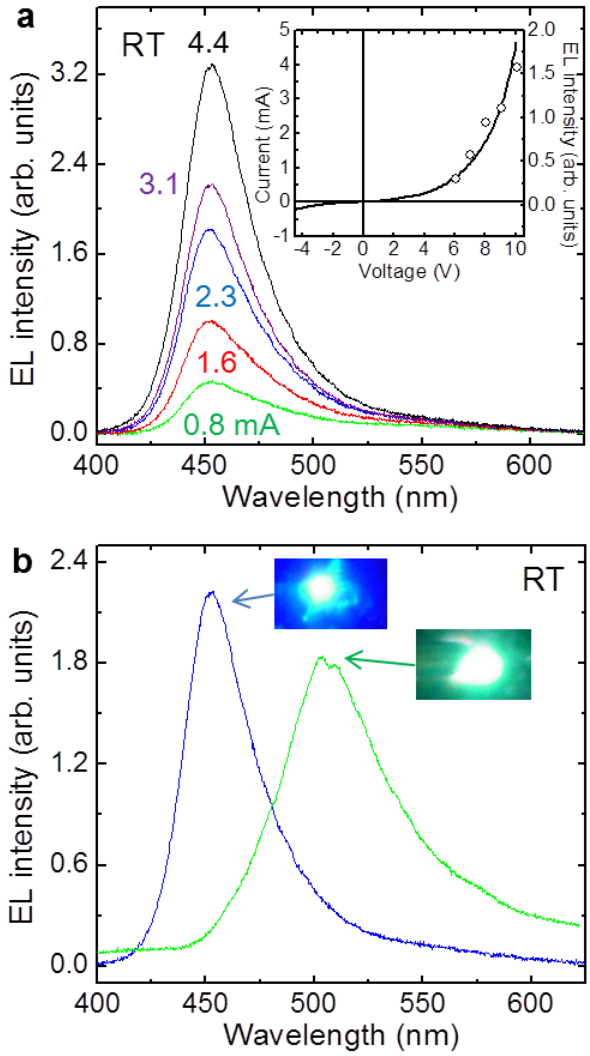

Fig. 6.7. Characteristics of GaN-based thin film LEDs fabricated on graphene-coated amorphous silica substrates. (a) Power-dependent EL spectra measured at room temperature. Inset of Fig. 5a shows the current and integrated EL intensity as a function of applied bias voltage. (b) Room temperature EL spectra and corresponding EL images of the LEDs made with $In_xGa_{1-x}N$ grown at 800°C and 760°C.

6.3.4. Output powers of LEDs fabricated on CVD graphene films

The GaN film LEDs were fabricated on CVD graphene films and on *c*-Al_2O_3 substrates to investigate the device performances. Single crystalline *c*-Al_2O_3 substrates are widely used for commercialized GaN-based LEDs, and comparing output powers of the LEDs fabricated on CVD graphene films with those fabricated on *c*-Al_2O_3 can provide a good method to investigate device performances based on GaN/graphene heterostructures. For the LED fabrication, Si-doped *n*-type GaN thin films were grown epitaxially both on CVD graphene films and on *c*-Al_2O_3 substrate; the GaN layers were grown on CVD graphene films using ZnO nanowall intermediate layer, while epitaxial GaN films on *c*-Al_2O_3 were obtained by typical GaN film growth technique. Then, $In_xGa_{1-x}N$/GaN multiple quantum wells and Mg-doped *p*-type GaN layers were deposited on the *n*-GaN thin films using conventional MOCVD system, which was carried out by Dr. Jeon in KOPTI. After growing the LED structures, the thin film LEDs were patterned into 200×200 μm^2 size LED arrays to compare light emission output powers from each LED chips. All LED fabrication processes, such as *p*-type activations and metal contact formations, were performed simultaneously for the measurements.

Figure 6.8a shows the light emission image from the LEDs fabricated on CVD graphene films. The light emission was very bright, and the strong emission can be seen clearly under the typical room illumination conditions. Further quantitative measurements of the LED performance were investigated by measuring output powers. Figure 6.8b shows output powers of LEDs fabricated

on CVD graphene films and on single crystal *c*-Al_2O_3 substrates as a function of input powers. The EL intensities of both LEDs were increased with increasing input powers. However, the maximum output power of the LEDs fabricated on CVD graphene exhibited 0.9 mW, which value was smaller than that of LEDs fabricated on *c*-Al_2O_3 substrates (4.7 mW). The relatively small LED output powers from the LEDs fabricated on CVD graphene films are presumably because of the large dislocation densities, which can largely affect to the LED efficiency. According to our results, the GaN films grown on single crystal graphene layers have shown dislocation density about 1-2 order larger than those grown on *c*-Al_2O_3 substrates. Furthermore, we used GaN films grown on CVD graphene films for the LED fabrication in this study, where many dislocations were observed along the large-angle grain boundaries of the GaN films.[69] Figure 6.8c shows optical microscopy image of thin film LEDs fabricated on CVD graphene films, clearly revealing the large-angle grain boundaries of the GaN films. Nevertheless, I believe that the relatively low device performance of the GaN LEDs fabricated on CVD graphene films can be overcome by optimizing processes of growths and device fabrications. For example, higher device performance is expected from inorganic semiconductor devices fabricated on graphene films. As recently reported, single crystal CVD graphene films with a 2-inch-wafer size are now become available.

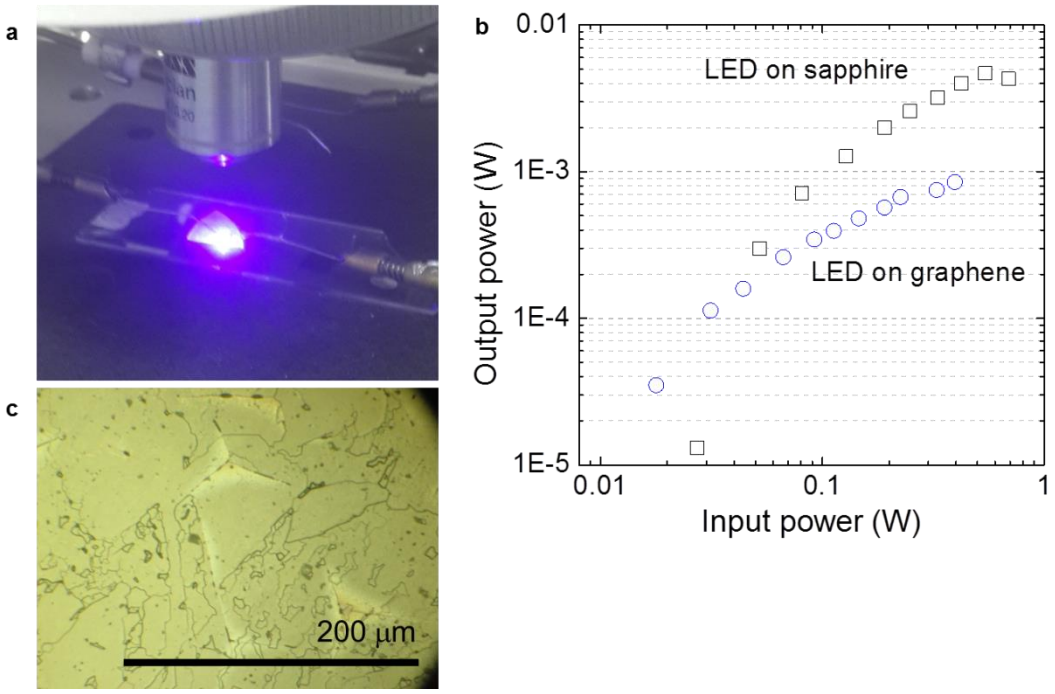

Fig. 6.8. (a) Light emission image of LEDs fabricated on CVD graphene films under room illumination condition. (b) Output powers of LEDs fabricated on CVD graphene films and on *c*-Al_2O_3 substrates as a function of input power. (c) Surface morphology of thin film LEDs fabricated on CVD graphene films. The random lines on the GaN films represent large-angle grain boundaries.

6.4. Flexible LEDs using GaN micro-rods grown on graphene films

The preparation of high-quality inorganic compound semiconductors on graphene substrates would represent a significant breakthrough in flexible and large-scale optoelectronic devices. As an example, flexible LEDs were fabricated by growing high-quality GaN micro-rods and coaxial quantum structures on graphene films, and then transferring these structures onto polymer substrates. The graphene films offer weak atomic bonding to the underlying substrate, as well as excellent mechanical flexibility, which can enable transfer of compound semiconductors to create flexible inorganic devices on polymer substrates. Furthermore, by meeting the key criteria for building reliable GaN microstructure LEDs on flexible substrates, such as maintaining high crystallinity, control over doping, formation of heterostructures and quantum structures, and vertically aligned growth onto the underlying substrates, reliable and flexible micro-rod LEDs were demonstrated.

6.4.1. Coaxial $In_xGa_{1-x}N$/GaN quantum well structures

For the LED structure, a MQW stack of 8 periods of $In_xGa_{1-x}N$/GaN heterostructures and a *p*-type GaN layer were coated coaxially on the *n*-type GaN micro-rods using MOCVD. As shown in Fig. 6.9a, the GaN micro-rod LEDs were vertically aligned on the graphene substrate following this coating process. The structural characteristics of these coaxial GaN micro-rod LEDs were further investigated using TEM. Scanning TEM images of the top and sidewalls of the GaN micro-rod LEDs are shown in Figs. 6.9b and 6.9c, respectively. The In_xGa_{1-}

$_x$N/GaN MQWs were formed at the top and sidewalls with abrupt interfaces, and the thicknesses of the $In_xGa_{1-x}N$ QWs at the top and sidewall were 8 and 4 nm, respectively. As determined by energy-dispersive X-ray spectroscopy, the x value for $In_xGa_{1-x}N$ was approximately 0.07. Additionally, room temperature cathodoluminescence (CL) spectra showed emissions at 439 nm and 414 nm for the top most QWs and sidewall QWs, respectively, indicating nonuniformities in thicknesses or composition of the QW heterostructures. Such results were observed in a previous report on multi-faceted nanostructure and microstructure LEDs.[49, 50, 52]

We further investigated the sidewall QWs from the top region (region I) to the bottom region (region II), as shown in Figs. 6.10a and 6.10b. As determined by energy-dispersive X-ray spectroscopy (EDX), the x values for $In_xGa_{1-x}N$ at region I and II were 0.08 and 0.06, respectively. This result indicates that the x values decrease toward the bottom. And due to the high resistivity of *p*-GaN layers, higher current densities can access the sidewall QWs at region II, which can result in the blue shifts of EL emission.

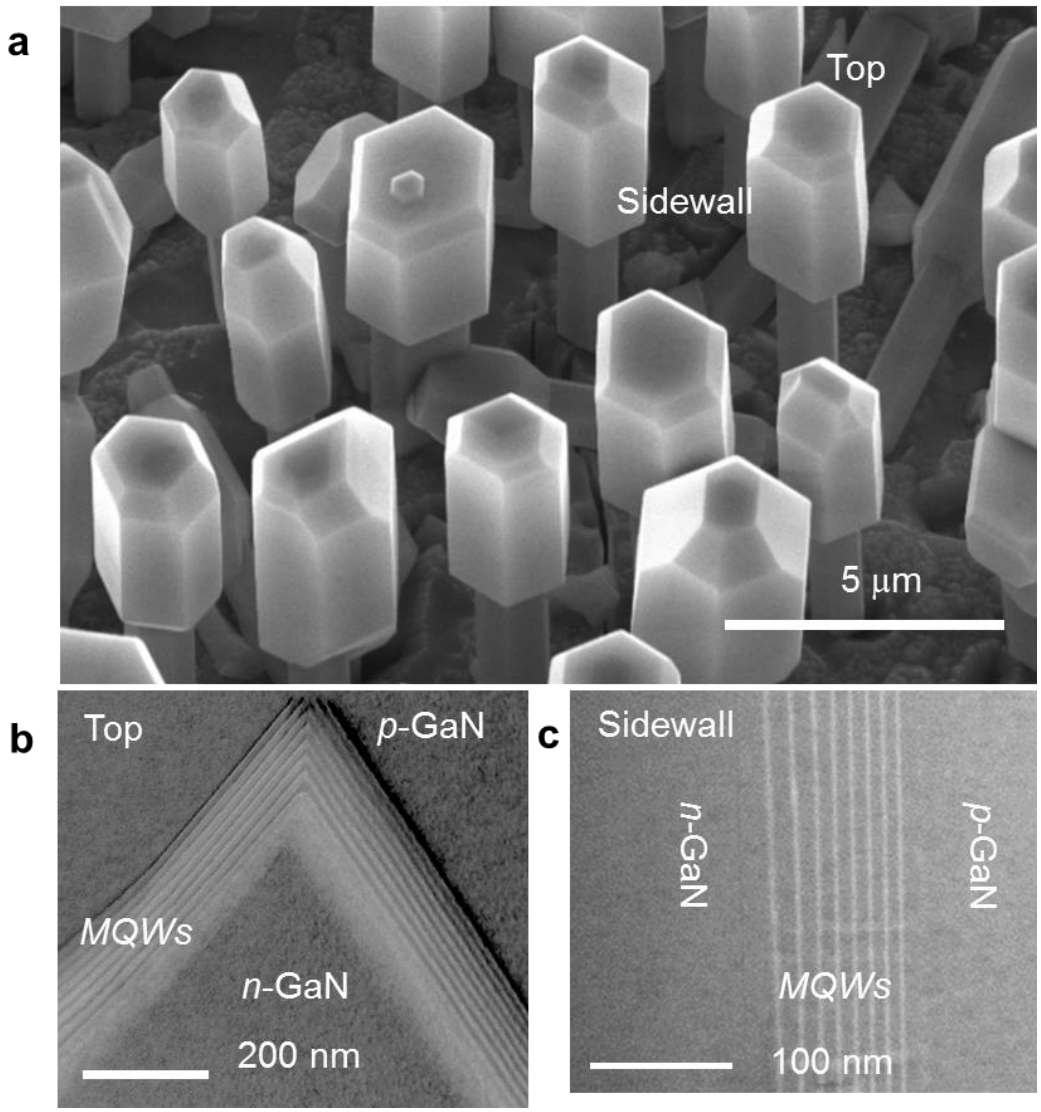

Fig. 6.9. (a) FE-SEM image of coaxial GaN micro-rod LEDs on graphene. Scanning TEM images of (b) the top and (c) the sidewall of the MQW layers on the micro-rod LED.

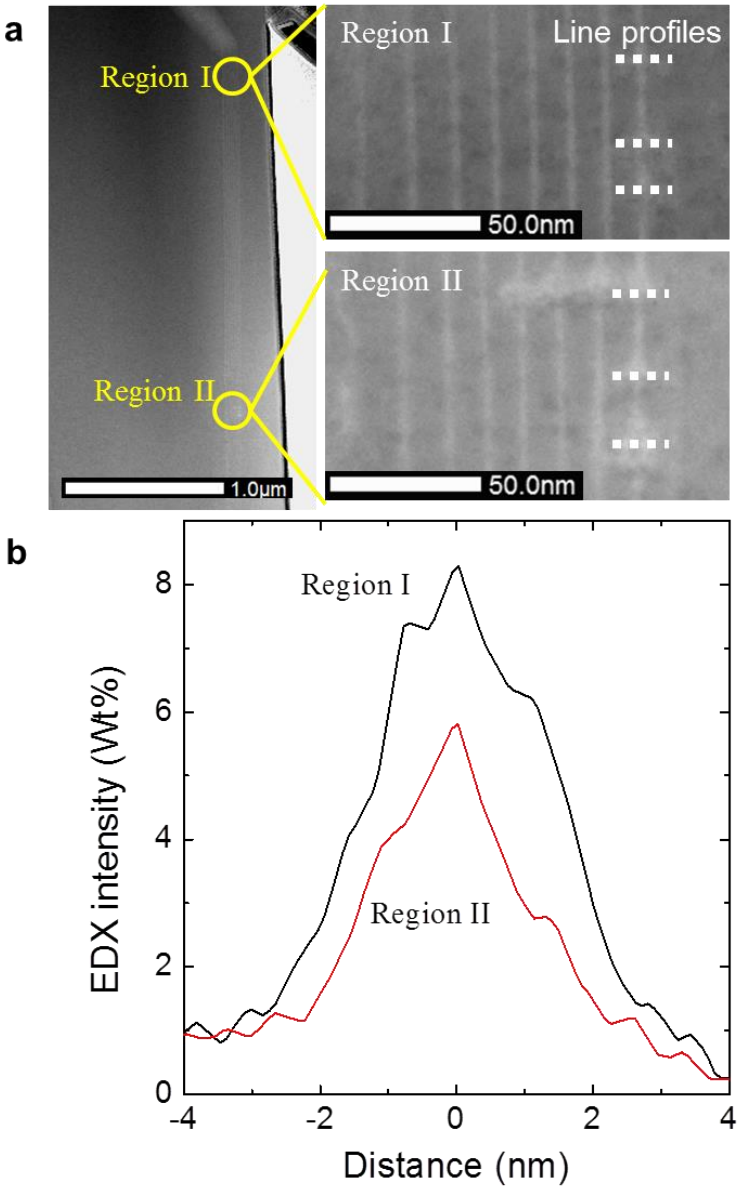

Fig. 6.10. (a) STEM images of sidewall QWs at different regions of I and II and (b) the corresponding average EDX line profiles of indium composition.

6.4.2. Flexible LED fabrications

The fabrication of the GaN micro-rod LEDs was completed by depositing metal contacts, and film transfer onto the polymer substrate, as shown schematically in Fig. 6.11. Following growth of the coaxial GaN micro-rod LEDs, the gaps in the micro-rod LEDs were filled using a polyimide insulating layer, and oxygen plasma etching was carried out to expose the top of the GaN micro-rod LEDs. A Ni/Au bi-layer was then deposited on *p*-type GaN and thermally annealed, resulting in Ohmic contacts. To form *n*-type GaN Ohmic contacts, the LEDs were removed from the SiO_2/Si substrate by wet etching the sacrificial SiO_2 layer of the substrate, where the GaN micro-LEDs were fabricated on CVD graphene coated SiO_2/Si substrates. A Ti/Au metal layer was then deposited on the bottom of the LEDs and an additional thick Ag layer was coated onto the Ti/Au layer to provide reliable current injection. The coaxial GaN micro-rod LEDs were then transferred onto the polyimide substrate.

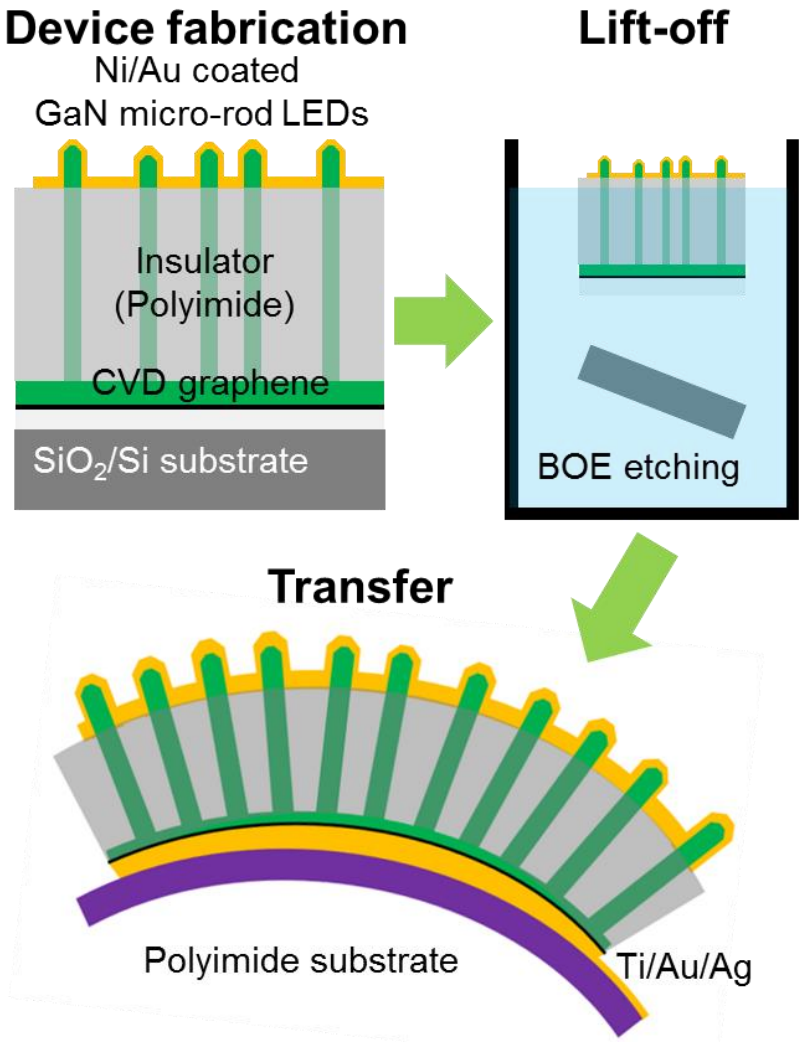

Fig. 6.11. Schematic illustration of the fabrication process for vertical structure micro-rod LEDs.

6.4.3. EL characteristics.

Figure 6.12a shows a magnified optical image of the optical emission from the micro-rod LEDs on the polymer substrate with an applied current of 10 mA. The contact area of the LED device was 50×50 μm^2. Individual light spots from the micro-rod LEDs can be observed clearly. Furthermore, the LED emitted strong blue light, which could be observed using the naked eye under normal interior lighting conditions. Additionally, we observed green and orange light emissions from some micro-rod LEDs at an applied current of 6 mA, which changed to blue as the current increased up to 10 mA. Because the *n*-type GaN micro-rods and the $In_xGa_{1-x}N$/GaN QW heterostructures exhibited extremely weak deep-level PL and CL emissions, respectively, the emission of green or orange light is presumably attributable to yellow emission from the *p*-type GaN layer. However, we believe the yellow emission can be reduced by optimizing the growth condition.[70]

The EL characteristics of the GaN micro-rod LEDs were further investigated by measuring power-dependent EL spectra. Figure 6.12b shows room-temperature EL spectra at applied currents in the range 2.6–10 mA. With a current of 2.6 mA, the dominant EL emission was observed at 437 nm, with a broad low-energy shoulder at 590 nm. The EL peaks at 437 and 590 nm presumably originate from the $In_xGa_{1-x}N$/GaN QWs and deep-levels of the *p*-type GaN layer, respectively. As the current was increased to 10 mA, the EL intensity gradually increased, and the dominant EL peak shifted from 437 nm to 407 nm. The inhomogeneities in indium composition or thickness of the QWs along the

micro-rod LEDs may contribute to the large blue shift, which result is also consistent with the TEM result.[50, 52]

We investigated room temperature cathodoluminescence (CL) spectroscopy of $In_xGa_{1-x}N$/GaN MQW coated GaN micro-rods in order to come to a better understanding on the origin of the EL emission. As shown in Fig. 6.13, dominant CL peaks from the top most region (polar QWs), sidewall of the top region (semipolar QWs), and sidewall of the micro-rod body (nonpolar QWs) were observed at 439, 424, and 414 nm, respectively. These results match closely the dominant EL peaks. We also observed broad CL peaks at 552-562 nm from the *p*-GaN layer surrounding the micro-rod, corresponding to deep-level states in the *p*-GaN. From this, we are able to attribute the yellow emission observed in the EL spectrum to low-quality p-GaN layers while the blue emission is attributed to the QWs. The results also imply that the growth condition for *p*-GaN can be further optimized.

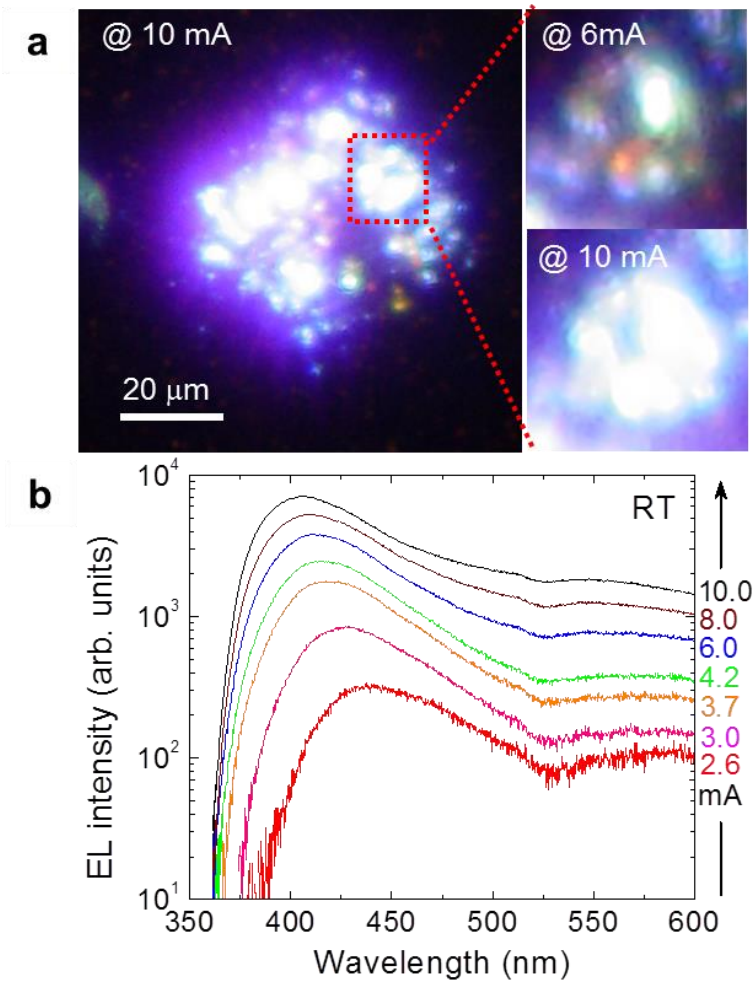

Fig. 6.12. (a) Magnified optical images of light emission from the micro-rod LED. (b) Power-dependent EL spectra at room temperature.

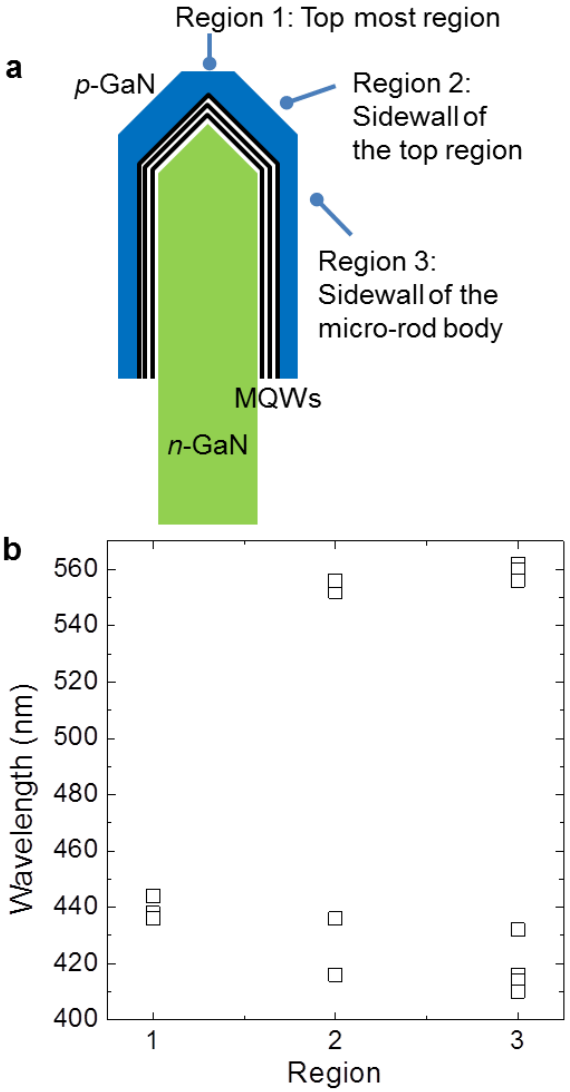

Fig. 6.13. (a) Schematics of the GaN micro-rod LEDs. (b) CL peaks from the top most region (region 1), sidewall of the top region (region 2), and sidewall of the micro-rod body (region 3). The CL peaks at 552-562 nm were observed from the *p*-GaN layer surrounding the micro-rod.

6.4.4. Flexibility under bending conditions.

We investigated the flexibility and reliability of the GaN micro-rod LEDs fabricated on large-area graphene films. Figure 6.14a shows the EL spectra with bending radii of ∞, 6, and 4 mm. When the 20-mm-wide substrate was bent to a radius of curvature of 6 mm, the EL intensity was not observed to degrade, and the dominant EL peak wavelength did not change. For a radius of curvature of 4 mm, however, the EL intensity markedly decreased, indicating that the GaN micro-rod LEDs became damaged by the mechanical deformation. The reliability of the LEDs was investigated by measuring the EL characteristics following repeated bending cycles. Figure 6.14b shows a plot of integrated EL intensity and wavelength of the dominant EL peak as a function of the number of cycles. Following 10 bending cycles, a slight degradation of the EL intensity was observed. Nevertheless, neither the wavelength of the dominant EL peak nor the integrated EL intensity exhibited significant changes following 1000 bending cycles.

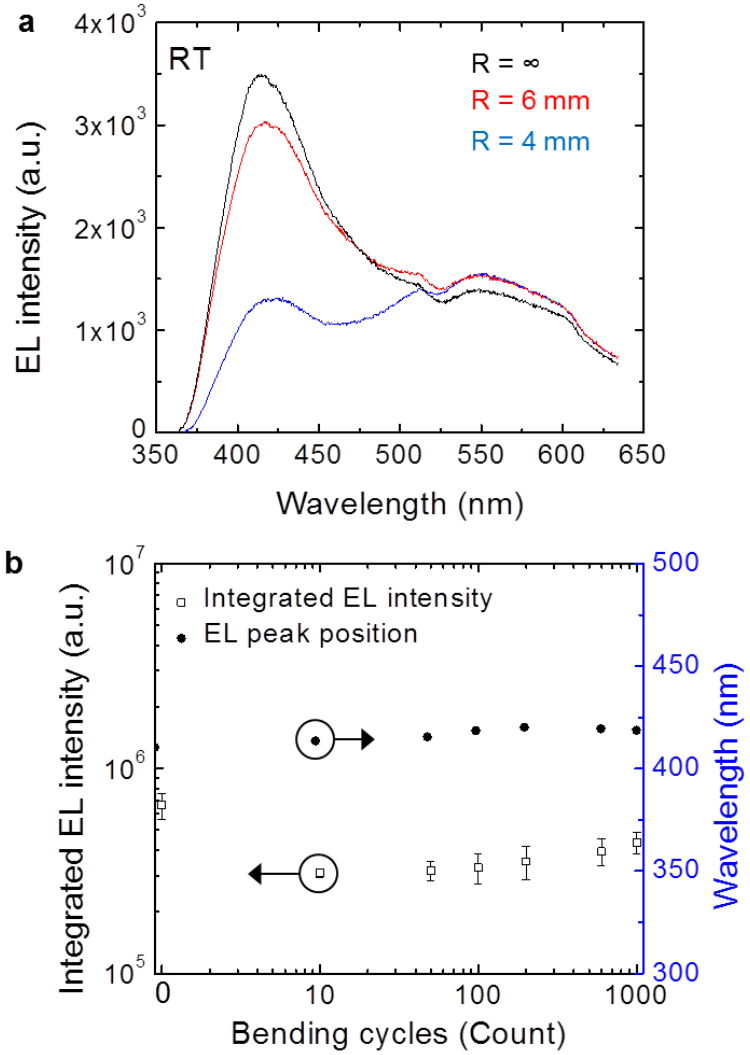

Fig. 6.14. Flexible coaxial GaN micro-rod LEDs. (a) EL spectra at bending radii of ∞, 6, and 4 mm. (b) The integrated EL intensities (white squares) and dominant EL peak wavelength (black squares) as a function of the number of bending cycles. All EL spectra were obtained with a current of 8 mA.

6.5. GaN/graphene heterostructure array

Methods to fabricate large-scale and flexible inorganic optoelectronic devices have recently attracted much attention for use in wearable display, solar cell, and biomedical devices.[3, 71-74] Central to achieving high performance and long term stability with the devices is realizing high quality crystalline semiconductors. Typically, the crystallinity is optimized by growing the semiconductor film on single crystalline growth substrates that share negligible lattice mismatch with the film. However, this process gives rise to two major obstacles in achieving inorganic flexible devices. One is the high cost of the growth substrate associated with the single crystallinity, which imposes an economic limitation and the scalability of the film. The second is the difficulty to meet the flexibility demands because of the rigidity and brittleness inherent in the single crystalline film. Accordingly, preparing high quality inorganic semiconductors on large-scale and low-cost substrates would be one of the important challenges to be resolved.

To overcome these problems, growth of semiconductor films on intermediate layers composed of 2D layered materials such as graphene has been proposed and demonstrated as a promising solution.[2, 7] Graphene films can provide many advantages for inorganic semiconductor device applications because of their excellent electrical, optical, and mechanical properties as well as large-scalability. Graphene films are particularly well-suited for growing II-VI or III-V semiconductors, the workhorse for optoelectronics, due to their good lattice match with wurtzite crystals. Because an epitaxial relation is not required between

substrate and graphene, any arbitrary substrate can be used as a support for the graphene, including large-size and low-cost metal or amorphous substrates. Furthermore, since the films grown on graphene can be easily transferred to other foreign substrates, all costly substrate restrictions can be completely lifted.

One consequence of the substrate-independence is that flexibility requirements can be met by transferring or growing films onto flexible or elastic plastic substrates. However, homogeneity in performance throughout inorganic thin films is usually not guaranteed because of the mismatch in thermal expansion coefficient between graphene and supporting substrate, where cracking and tearing in the inorganic thin films can arise. In this case, heavy stress and strain imposed by extreme bending conditions can be de-concentrated by growing the semiconductor into an array of small units, usually in the form of micro- and nanostructures. In this section, we fabricated GaN microstructure LEDs on micron-sized graphene patterns instead of a homogeneous film. The reduced dimension of the graphene enables stress and strain to be accommodated, ensuring high performance and excellent flexibility from the microstructure LEDs.

6.5.1. Transferable GaN thin film LED arrays

6.5.1.1. Device fabrications

Figure 6.15a shows schematic illustrations of LED arrays grown on patterned CVD graphene films. For the growth of LED arrays, CVD graphene films were patterned using photolithography and O_2 plasma etching. Firstly, large-scale CVD graphene films were transferred onto entire surface of amorphous SiO_2/Si substrate. Then, 100×100-μm^2-size and 1-μm-thick photo resist (AZ 5214) arrays were prepared on the graphene films using photolithography. Subsequently, O_2 plasma treatment was performed on the pattered photo resist arrays for the selective etching of CVD graphene films. Typical power and exposure time of O_2 plasma treatment were 50 W and 2 min, respectively. Following by graphene etching, the photo resist residue was removed from the graphene films by acetone with 10s sonication. Figure 6.15b shows CVD graphene film arrays prepared on SiO_2/Si substrates, exhibiting good selectivity and no observable damages. After preparing CVD graphene film arrays, *n*-GaN thin films were heteroepitaxially grown on the CVD graphene patterns using ZnO nanowall intermediate layer. Following by *n*-GaN layer growth, three-period $In_xGa_{1-x}N$/GaN MQWs and a *p*-GaN layer were grown on the thin film arrays to fabricate LEDs. The as-grown LEDs on the patterned CVD graphene film array exhibited uniform and regular LED arrays with good selectivity as shown in Fig. 6.15c.

Figure 6.16a shows schematic illustration of thin film LED arrays transferred onto copper foil. For the LED fabrication, Ni/Au bi-layer was deposited on the *p*-GaN layer and thermally annealed to form ohmic contacts. Then, polyimide (PI) layer was coated on the LED arrays for the supporting layer and LEDs were removed from the as-grown SiO_2/Si substrates by chemical etching of SiO_2 sacrificial layer of the substrate. As shown in Fig. 6.16b, the entire LED arrays can be released from the substrate by BOE etching. Finally, the LED arrays were transferred onto indium layer-coated copper foil, which indium layer served as a *n*-GaN ohmic contact as well as adhesive material between LEDs and copper foil. Figure 6.16c shows the optical image of GaN thin film LED array transferred onto Cu foils. The LEDs exhibited regular array after the transfer process.

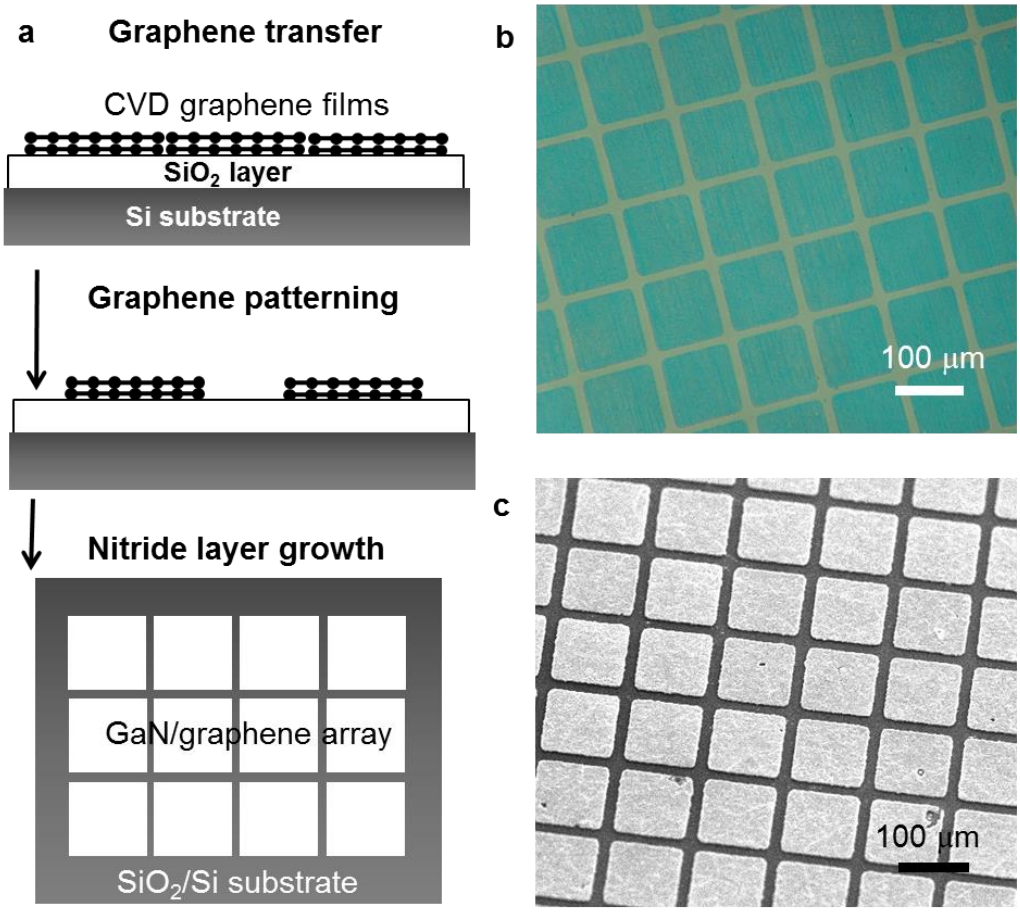

Fig. 6.15. Thin film LED arrays. (a) Schematic illustration of fabrication process of LED arrays on CVD graphene film. (b) Optical microscopy images of CVD graphene arrays. (c) SEM image of thin film LED arrays grown on patterned CVD graphene films.

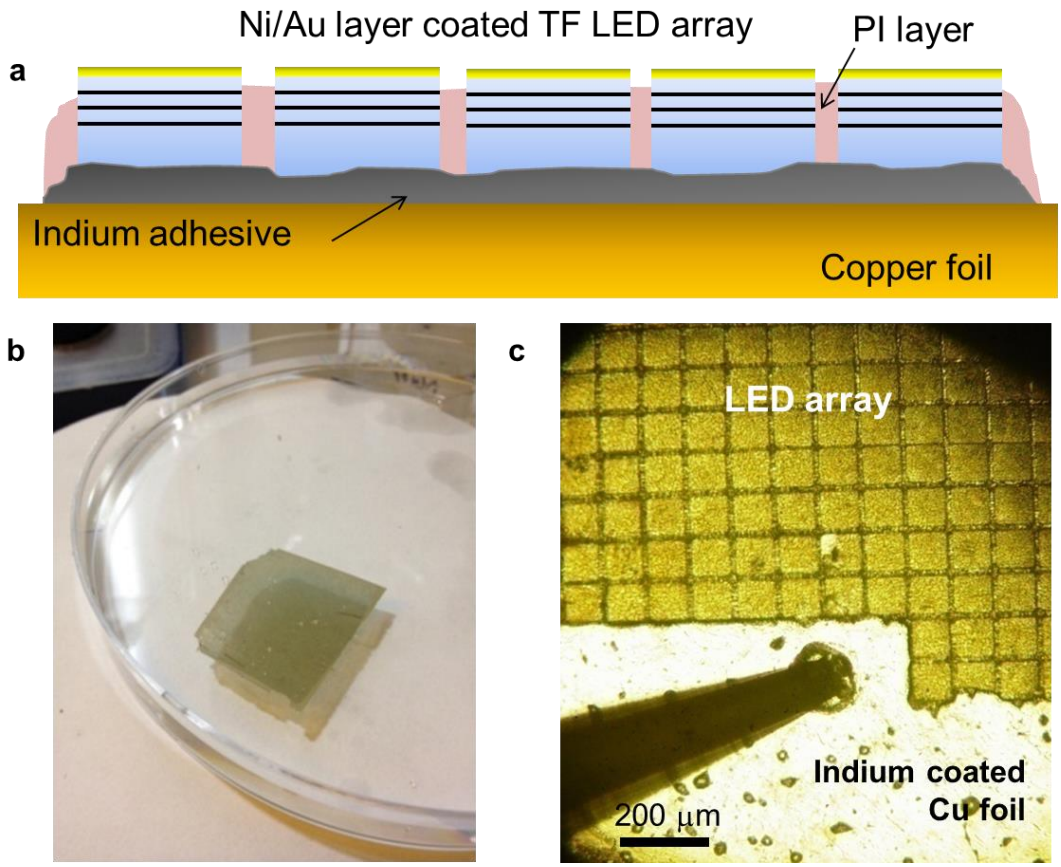

Fig. 6.16. Transferable LED array. (a) Schematic illustration of the LED structure. Photograph images of (b) polymer-coated LED arrays floating in the deionized water and (c) LED arrays transferred onto indium layer-coated copper foil.

6.5.1.2. EL and electrical characteristics

To investigate the reliable operation of individual GaN micro-LEDs, EL and electrical characteristics were investigated. Figure 6.17a shows optical images of the individual GaN LED chips at various positions. Each LEDs showed strong blue light emissions uniformly from the *p*-GaN metal contact area of 100×100 μm^2. This result suggested that the top and bottom contacts were electrically well connected to the LED device. Additionally, the individual GaN LED chips exhibited almost identical characteristics in their light emission area and intensities due to the regular and uniform surface morphologies.

The LED characteristics were further investigated by measuring room temperature EL spectra, as shown in Fig. 6.17b. The dominant EL peak was observed at 419 nm, which result was consistent with the blue light emission in Fig. 6.17a. Meanwhile, there was no yellow emission from the EL spectra. As the applied bias voltages increased, the EL intensity showed gradual increase without no significant EL peak shifts. Figure 6.16c shows an *I*–*V* characteristic curve of the individual GaN micro-LEDs. The *I*–*V* curve exhibited a typical rectifying behavior of *p*–*n* junction GaN LEDs.

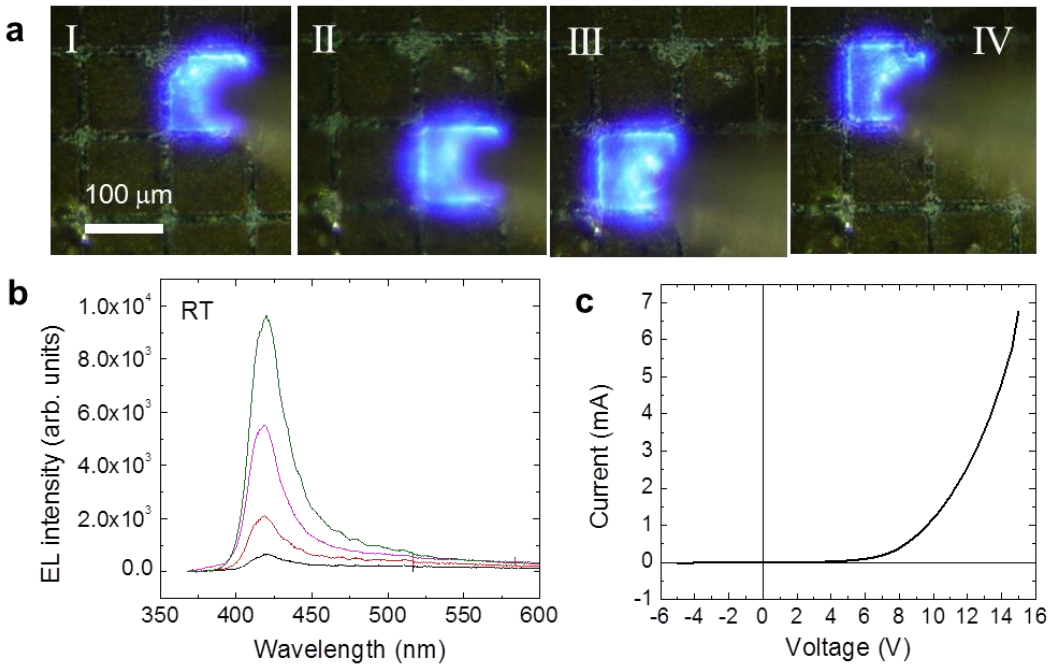

Fig. 6.17. (a) Light emission images of various individual LEDs. (b) Power dependent EL spectra at room temperature. (c) *I*–*V* characteristic curve.

6.5.2. GaN micro-disk arrays fabricated on graphene dot patterns.

6.5.2.1. Selective area growth of GaN micro-disks on graphene dot arrays

The sequential steps of preparing GaN microstructures on graphene dot patterns are shown schematically in Fig. 6.18a. For the substrate preparation, graphene films were synthesized on Cu foil by chemical vapor deposition, and then were transferred over the entire surface of the graphene supporting substrates. In this study, tungsten (W) film or amorphous SiO_2 layer coated Si substrates were used for the graphene supporting substrates, which substrates had no epitaxial relations to GaN or graphene, while they have high temperature tolerance for the GaN growths. Additionally, the graphene films were selectively etched in order to form the graphene dot array using photolithography and O_2 plasma exposure. Without graphene patterning, uniform GaN films were grown on the large-scale graphene films, similar to the previous report of GaN films grown on graphene-coated amorphous silica substrates.[36] However, although graphene can provide good epitaxial growth of GaN films, the GaN films grown on W films and SiO_2 layers with CVD graphene intermediate layers showed many cracks, and some of them were even peeled off from the substrates, as shown in Fig. 6.18b. This result is presumably due to the large stain and stress from thermal expansion coefficient mismatches between GaN layers and graphene supporting substrates of W or SiO_2 layers.

To avoid this problem, graphene films were patterned into micron size dot array, where the contact areas of the GaN/graphene/supporting-substrate

interfaces can be much reduced. Typical diameter and dot-to-dot distance of the graphene dots were 3.5 and 10 μm, respectively. Subsequently, GaN microstructures were selectively grown on the graphene dot array using a ZnO seed layer. The field emission scanning electron microscopy (FE-SEM) images in Fig. 6.18a shows ZnO nanowalls grown on graphene dot arrays. The ZnO nanostructures exhibited high density with uniform heights, and they grew only on graphene dots. Finally, hexagonal GaN micro-disks were grown on ZnO-coated graphene dot arrays, as shown in Fig. 6.18c, exhibiting good growth selectivity, regular surface morphology, and uniform heights and diameters. Furthermore, we could obtain regular GaN micro-disk arrays across the entire surface of graphene supporting substrates without any cracks or peeling off problems. Additionally, Fig. 6.18d shows that typical diameter of these micro-disks was 10 μm, which was about three times larger than that of graphene dots, indicating lateral growth of GaN micro-disks. The dimensions and the growth selectivity of GaN micro-disks could be controlled by changing growth conditions. Specifically, the diameter of micro-disks was increased with the longer growth time, while the growth selectivity was improved by decreasing NH_3 flow rates.

Figure 6.19 shows effects of growth temperature and NH_3 flow rates on the growth selectivity of GaN micro-disks on graphene dot arrays. At growth temperature of 1000˚C, it is clearly seen that GaN micro-disks were grown on graphene dot arrays with a hexagonal shape, as shown in Fig. 6.19a. However, rough GaN films were also coated on the W film surfaces, indicating the poor growth selectivity. The growth selectivity was improved by increasing the growth

temperatures. Figure 6.19b and 6.19c show GaN microstructure arrays grown on graphene dot patterns with growth temperatures of 1060 and 1100˚C, respectively. Compared to the result of the 1000˚C-grown GaN micro-disk arrays, GaN particles were rarely observed from the W films without graphene dot. However, GaN microstructure showed irregular surface morphology at growth temperature of 1100˚C. The growth selectivity depends on the growth temperature can be explained in terms of enhanced surface diffusion of GaN at high growth temperature, while the higher growth temperature also could result in the decomposition of GaN crystals which may cause the irregular surface morphology. In addition to the growth temperature, we grew GaN micro-disk arrays with a reduced NH_3 flow rates. Figure 6.19d shows GaN micro-disks grown with a NH_3 flow rate of 100 sccm, while GaN micro-disks grown with a 500 sccm NH_3 flow rate are shown in Fig. 6.19b. The diameter of GaN micro-disks in both cases did not show a significant change. However, by reducing the NH_3 flow rates, GaN micro-disk arrays with excellent growth selectivity were obtained.

The diameter of the GaN micro-disks can be controlled typically by increasing the growth time, since the micro-disks were grown by means of epitaixial lateral overgrowth (ELOG). After growing GaN micro-disks for 90 min, the GaN micro-disks exhibited a diameter of 10 μm (Fig. 6.19e), which was twice larger than those of 30-min-grown GaN micro-disks (Fig. 6.19d). Furthermore, coalescent GaN films can be obtained by increasing time over 120 min, where the coalescent GaN films showed no significant cracks or peeling off problems from the supporting W/Si substrates.

It is also notable that we obtained a regular GaN micro-disk array without using SiO_2 or Si_xN_{1-x} mask layers or additional epitaxial layers underlying the mask layers, which are typically used for the selective area growths of inorganic semiconductor microstructures or nanostructures. In particular, the epitaxial films underlying the mask layer is essential because these films provide strong growth selectivity compare to that of the mask layer.[75] Otherwise, the inorganic semiconductors would be grown randomly on the substrates due to the high density nucleation of catalyst-free growth mechanism.[26] For this reason, single crystal substrates have been required in bottom-up approach of fabricating regular device array although microstructures and nanostructures are relatively free from the substrate limitations. However, we demonstrated that the graphene dot array provides excellent growth selectivity. Accordingly, this result suggests an interesting feature of using inorganic semiconductor-graphene hybrid heterostructures for fabricating device arrays.

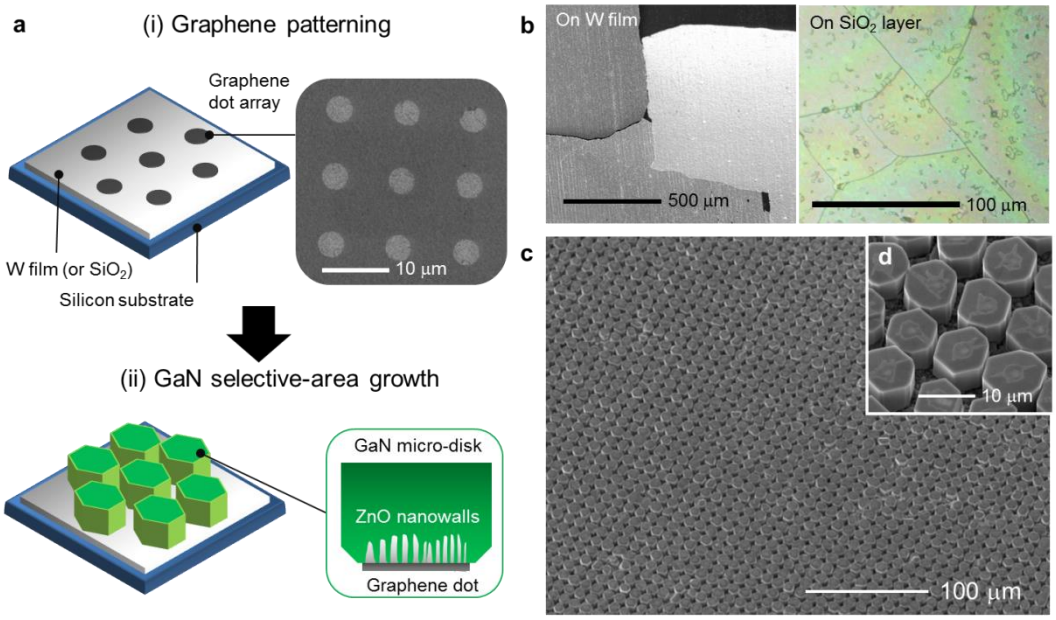

Fig. 6.18. Selective area growth of GaN micro-disk array on graphene dot patterns. (a) Schematic illustration of graphene dot array preparation on W/Si substrates and selective area growth of GaN micro-disks on the graphene dot array. The inset FE-SEM shows ZnO nanowall coated graphene dot array. (b) Surface morphologies of GaN films grown on graphene-coated W/Si and SiO_2/Si substrates without graphene patterning. (c) Low-magnification FE-SEM image of the GaN micro-disk/graphene dot heterostructure array fabricated on the entire surface of W/Si substrates. (d) Magnified FE-SEM image of the GaN micro-disk array.

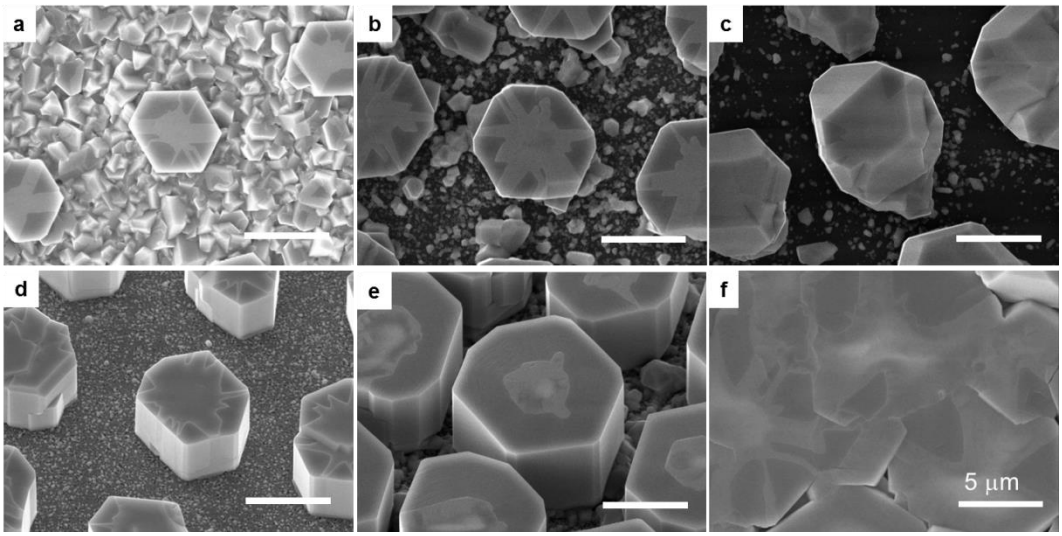

Fig. 6.19. GaN micro-disks grown on graphene dot arrays at various growth temperatures of (a) 1000, (b) 1060, and (c) 1100˚C. (d) GaN micro-disks with a reduced NH_3 flow rates from 500 to 100 sccm. GaN micro-disks with increasing growth time to (e) 90 min and (f) 120 min.

6.5.2.2. Electrical characteristics of GaN/graphene heterojunction.

The electrical characteristics of the GaN micro-disk/graphene were investigated using *I—V* measurements. Figure 6.20a shows a schematic of the vertical heterostructure, where Si-doped *n*-GaN micro-disks were grown on graphene-coated W films. Indium layer was deposited on the top of *n*-GaN micro-film arrays and then thermally annealed in order to form Ohmic contacts, while W film was used as the bottom contact. Additionally, thick indium layer was deposited on the W film for a reliable current injection. Figure 6.20b shows a linear *I—V* characteristic curve, indicating that GaN microstructure array is electrically well connected to the W films.

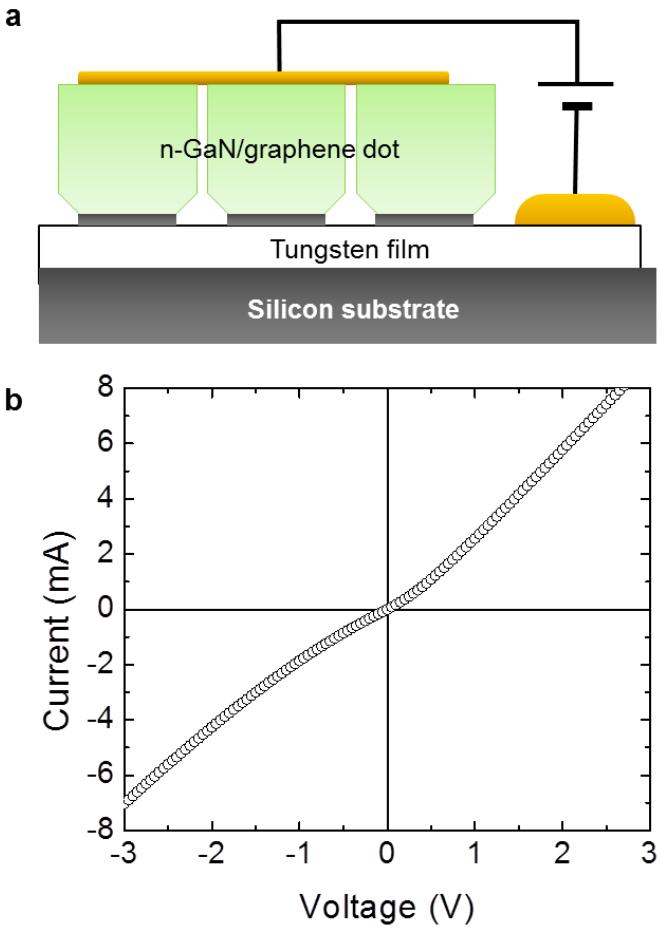

Fig. 6.20. Electrical characteristics of *n*-GaN/graphene heterojunctions. (a) Schematic illustration of metal contact formations. (b) *I*—*V* characteristic curve of the heterojunction structure.

6.5.2.3. Device fabrications

We further grew $In_xGa_{1-x}N$/GaN MQW layers and an Mg-doped *p*-GaN layer on the *n*-GaN micro-disk array to fabricate LEDs. Prior to the growth, the *n*-GaN layers were coated additionally on the micro-disks for the conformal coatings of the MQW and *p*-GaN layers. Figure 6.21a shows the additional *n*-GaN layer-coated micro-disks, exhibiting pyramidal shape on the top and smooth surfaces in the sidewalls. After that, three-periods of $In_xGa_{1-x}N$/GaN MQW layers were coated on both top and sidewalls of the three-dimensional *n*-GaN microstructure array. Finally, the *p*-GaN layer was deposited to form a micro-disk LEDs with flat top surfaces, as shown in Fig. 6.21b.

The reliable formation of $In_xGa_{1-x}N$ QW layers were examined using scanning transmission electron microscopy (STEM) after the TEM sample preparation of milling individual micro-disk LED by focused ion beam. Figure 6.21c shows the cross-sectional STEM images of $In_xGa_{1-x}N$ layers-embedded micro-disk LEDs. Three repeated bright and dark lines were clearly observed from the MQW regions, indicating that $In_xGa_{1-x}N$ quantum wells (bright lines) and GaN quantum barriers (dark lines) are formed in the micro-LEDs. Furthermore, the MQW layers had abrupt and clean interface, we could measure compositions and thicknesses of the $In_xGa_{1-x}N$ layers by line profiles of the indium contents using EDX.

Figure 6.21d shows EDX intensities of the indium contents and thicknesses of the QWs formed at different regions of I, II, III, IV and V, which

regions are corresponding to those in Fig. 3c. From these EDX results, the QWs formed at region I showed highest relative indium composition as well as the largest QW thickness of 7 nm. Additionally, various $In_xGa_{1-x}N$ layers were obtained from different QW regions, while they showed a downtrend both in their indium compositions and thicknesses from topmost to sidewalls. The formation of $In_xGa_{1-x}N$ layers with various composition and thickness can be explained by the anisotropic surface formation energies of GaN crystal planes, where similar results have reported previously from the multi-facetted GaN microstructures and nanostructures.

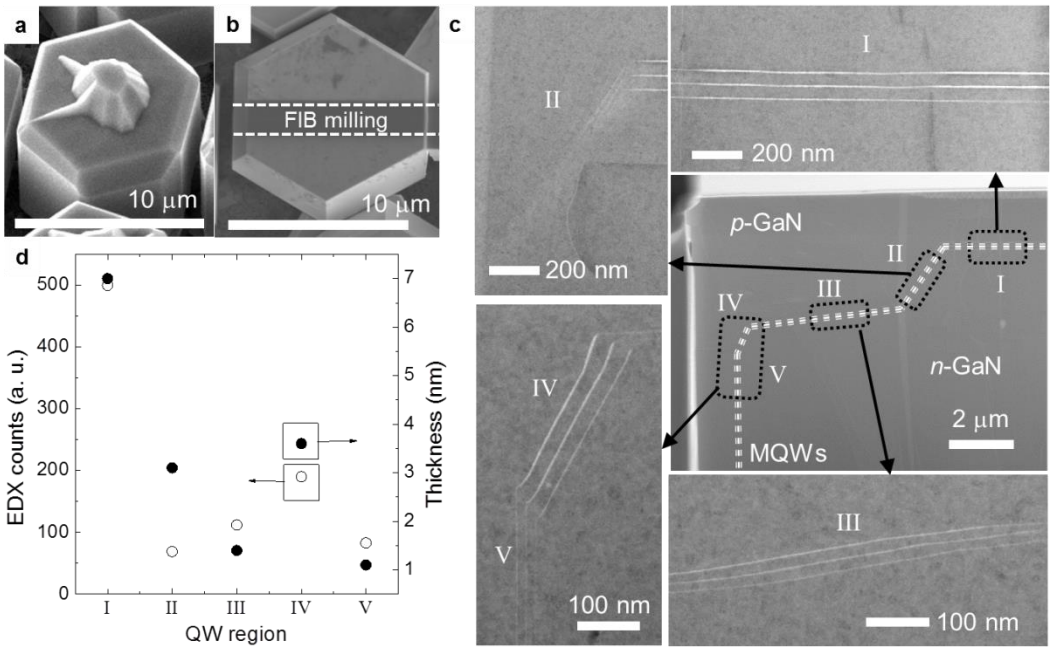

Fig. 6.21. (a) Additional *n*-GaN layer coated GaN micro-disk (b) GaN micro-LEDs after MQW layer and *p*-GaN layer coating. (c) Cross-sectional STEM images of the MQW embedded GaN micro-LED. (d) EDX intensities of the indium concentration and QW thickness at different MQW regions of I, II, III, IV, and V, which regions are same with those in Fig 6.21c.

To fabricate LEDs, *p*-GaN metal contacts were formed on the top region of as-grown GaN micro-disk LEDs by sequential steps of *p*-GaN activation, Ni/Au layer deposition, and polyimide layer filling process, as shown schematically in Fig. 6.22a. Specifically, very thin Ni/Au bilayers were deposited over the entire surface of *p*-GaN activated LEDs with a thickness of 5/5 nm. Then, they were thermally annealed at 500˚C for 5 min to make ohmic contacts with the *p*-GaN layers. Although the conformal coating of Ni/Au metal layers, we could not observe serious leakage current problems from the fabricated LEDs presumably because the heat treatment can make Ni/Au islands. Finally, the gaps between individual GaN micro-disk LEDs were filled with polyimide (PI) insulating layer. For the PI layer filling, the repeated PI layer coating was employed to submerge the GaN micro-LEDs. Then, the PI layer, coated GaN micro-LEDs, were thermally annealed with N_2 ambient gas for the PI layer curing. Subsequently, PI layers were partially etched by oxygen plasma treatment. As shown in FE-SEM image of Fig. 6.22a, the top region of Ni/Au bilayer coated GaN micro-LEDs were well exposed from the PI insulating layers, while the sidewalls of the GaN micro-LEDs were surrounded by the PI layers. Additionally, the GaN micro-LEDs exhibited uniform and regular surface morphologies after the growths of $In_xGa_{1-x}N$/GaN MQWs and *p*-GaN layer. Furthermore, the GaN micro-LEDs maintained their regular arrays for further device fabrication process because the PI layer could support the individual micro-LED chips into one piece.

The GaN micro-disk LEDs were firstly demonstrated on W films because the metal layer underlying the GaN/graphene heterostructures are already

electrically connected to the LEDs, and enabled us to fabricate LEDs with simple fabrication process. As shown schematically in Fig. 6.22b, additional Ni/Au (20/20 nm) metal contact pads were deposited on the PI layer coated GaN micro-disk LEDs with a contact area of 200×200 μm^2, while W films were used as the *n*-GaN metal contacts. The optical images in Fig. 6.22b shows the GaN micro-LEDs fabricated on W films. The blue light emissions were observed over the *p*-GaN metal contact pads with high yield and uniform distributions, strongly suggesting the reliable current injection through W films. Additionally, we could clearly observe the individual light spots from the LED array, indicating each micro-LED worked as a single light emitter.

Meanwhile, flexible GaN micro-LEDs can be fabricated using SiO_2/Si graphene supporting substrates, as shown in Fig. 6.22c. After *p*-GaN ohmic contact formations and PI layer filling, free-standing GaN micro-LEDs can be prepared by chemical etching of the SiO_2 sacrificial layer. To complete the metal contact fabrications, the array of GaN micro-LEDs was transferred onto Cu foil using Ag paste as an adhesive. Then, Ni/Au metal contact pads were formed on the GaN micro-LEDs similar to those fabricated on W films. However, the light emissions were observed only from the near region of probing tips, as shown in optical microscopy image in Fig. 6.22c. The embossing-like top surface of GaN micro-LEDs with PI surrounds and the deformable Cu foils underlying the micro-LEDs presumably resulted in this contact failure. For the reliable contact formations, we further fabricated flip-chip micro-LEDs because the PI layers showed more smooth and even surfaces with the bottom *n*-GaN layers compare to

those with top *p*-GaN layers. As shown in Fig. 6.22d, the uneven *p*-GaN surfaces were attached with Cu foil using Ag adhesive, and 20-nm-thickness of In and Au layers were subsequently deposited on the *n*-GaN surfaces. The optical microscopy image in Fig. 6.22d shows the flip-chip micro-LEDs transferred onto Cu foil, clearly revealing the blue light emissions over the entire area of In/Au metal contact pads.

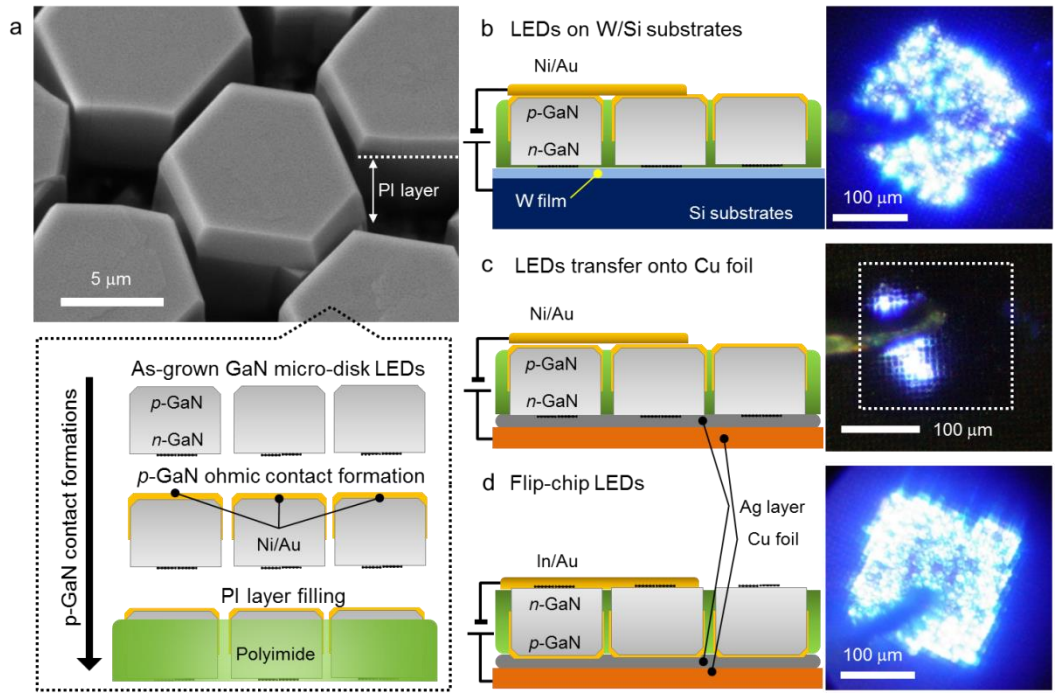

Fig. 6.22. (a) Schematic illustration of *p*-GaN contact formation (bottom image) and FE-SEM image of PI layer-coated GaN micro-disk LEDs (top image). Device schematics and light emission images of (b) GaN micro-disk LEDs fabricated on W films, (c) GaN micro-disk LEDs transferred onto Cu foils, and (d) flip-chip GaN micro-disk LEDs.

6.5.2.4. LED characteristics

By fabricating reliable metal contacts, we could further investigate the flexible functionalities and typical electroluminescence EL characteristics of the micro-LEDs transferred onto Cu foils. The micro-LEDs exhibited strong blue light emissions that could be seen under the typical room illumination condition, as shown in Fig. 6.23a. We fabricated many In/Au contact pads on the micro-LEDs, and they all showed similar light emission behavior presumably because the regular GaN micro-disk array allows us to fabricate individual micro-LEDs with uniform doping, band-gaps of MQWs, and volume of active layers.

We further obtained room temperature EL spectra of the GaN micro-LEDs transferred onto Cu foils at various applied bias voltages in the range of 4−9 V, as shown in Fig. 6.23b. At low applied bias voltage of 4 V, the dominant EL peak position was observed at 475 nm and the FWHM value of the EL spectrum was estimated to be 169 nm. However, as the applied bias voltage increase to 9 V, the EL spectra showed the peak shifts toward 446 nm with a largely decreased FWHM value of 48 nm. The observed large changes in EL peak positions and FWHM values are presumably due to the non-uniform indium compositions and thicknesses of the QW layers formed on the multi-faceted *n*-GaN microstructures, while the inhomogeneous QW layers have been commonly observed from GaN micro- or nanostructures.[50, 52]

In addition to changes in shapes and positions of the EL spectra, the EL intensities showed gradual increase with the applied bias voltages. Therefore, we

plotted integrated EL intensity and current as a function of applied bias voltages, as shown in Fig. 6.23d. The $I-V$ curve exhibited a typical rectifying behavior of GaN $p-n$ junction diodes. The leakage current and the turn-on voltage of the micro-LED arrays were 6×10^{-4} A at −5 V and 4 V, respectively. Furthermore, the integrated EL intensity increased simultaneously with the $I-V$ curve, which indicates the EL emissions are originated from the carrier transport though the $p-n$ junction and supports the reliable operation of the micro-LEDs.

Since we fabricated micro-LEDs with a small diameter about 10 μm, high degree of flexibility was to be expected even under extreme bending conditions. Figure 6.24a shows FE-SEM image of the GaN micro-LEDs wrapped on a 1-mm-diameter paper clip, where bending radius of GaN micro-LEDs was 0.6−0.8 mm. The micro-LEDs exhibited regular array without any mechanical deformations. Furthermore, it was hard to indicate the bending condition in the magnified FE-SEM image, as shown in the inset of Fig. 6.24a. This result clearly shows that the bending effects are negligible when the devices are fabricated in a form of microstructures or nanostructures.

EL and electrical characteristics of the micro-LED arrays were further investigated at various bending radius. Figure 6.24b shows room temperature EL spectra with bending radius of ∞, 11, 8, and 6 mm. When the micro-LEDs were firstly bended to 11-mm-radius, the EL intensity was slightly decreased. However, the EL spectra showed almost identical shape, intensity, and dominant EL peak position regardless of the bending radius from 11 to 6 mm. The inset of Fig. 6.24b also shows the reliable light emission of the GaN micro-LEDs at bending radius

of 6 nm. In addition, the $I-V$ curves showed no significant changes under these bending conditions, as shown in Fig. 6.24c. Meanwhile we could observe drastic decrease of forward current levels at bending radius of 5 mm. As confirmed the light emission images, some cracks were appeared on the In/Au contact pad, which resulted in small area of current injections and light emission area, as shown in Fig. 6.24d. Nevertheless, the uniform light emissions were observed from the crack-free metal contact pad.

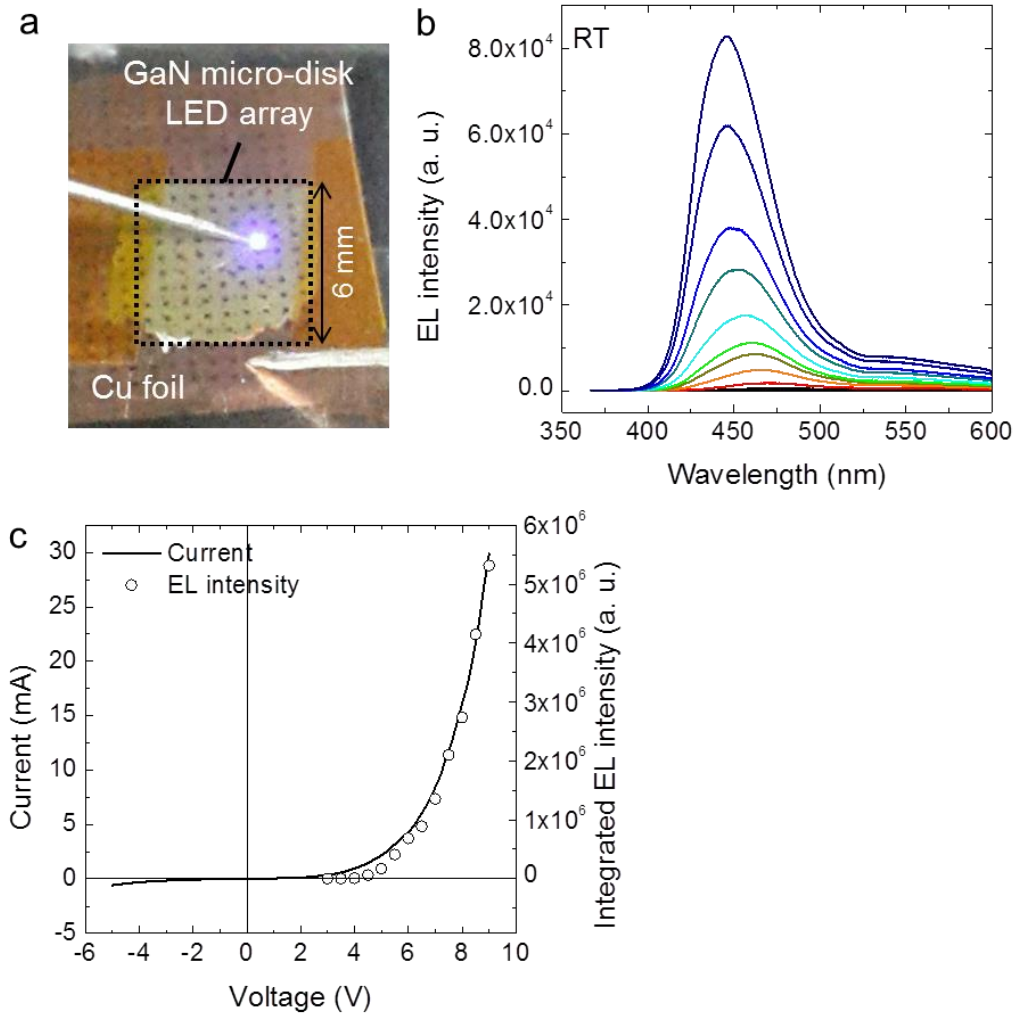

Fig. 6.23. (a) Light emission image of GaN micro-disk LEDs under typical room illumination condition. (b) Room temperature EL spectra. (c) Current and integrated EL spectra as a function of applied bias voltage.

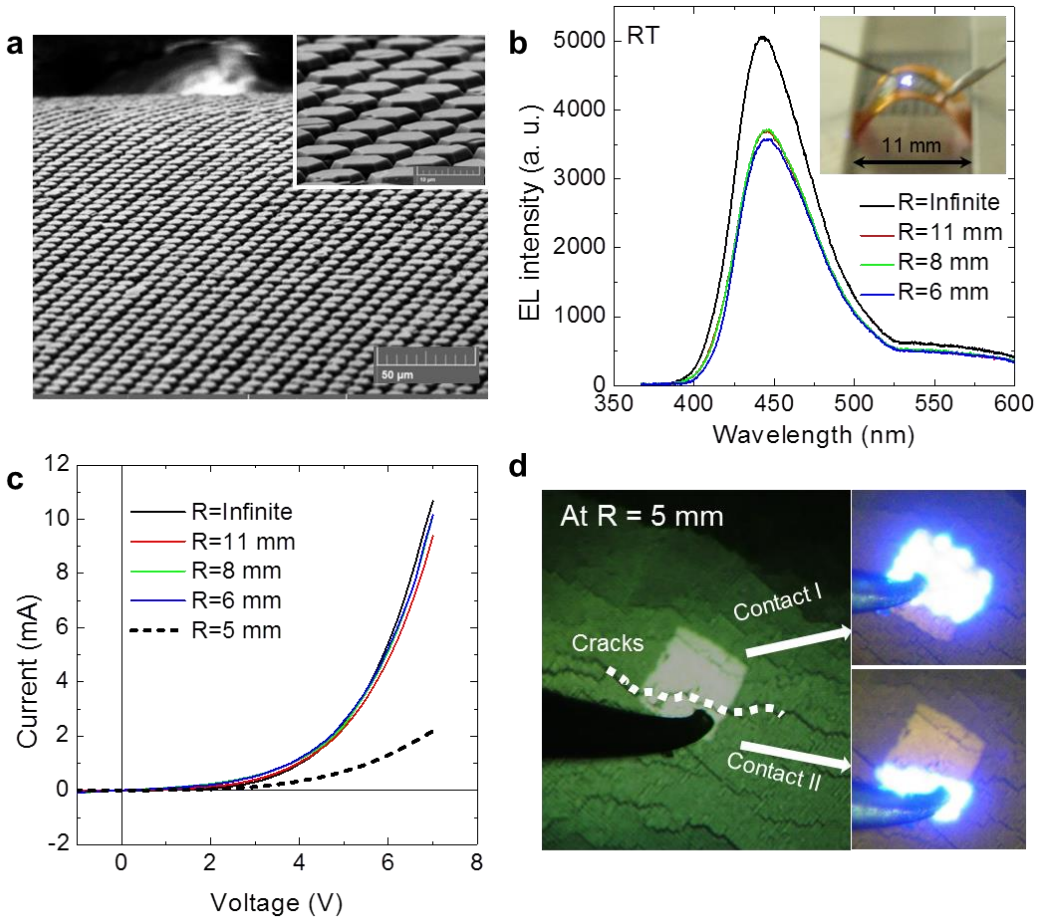

Fig. 6.24. (a) FE-SEM images of GaN micro-disk LEDs with bending radius of 0.6−0.8 mm. (b) EL spectra and (c) *I*−*V* curves of GaN micro-LEDs at various bending radius. (d) Light emission image of GaN micro-LEDs at bending radius of 5 mm.

6.5.2.5. Photovoltaic characteristics

Since LEDs and solar cell have similar device structure, photovoltaic characteristics of the micro LED arrays were additionally investigated using Xe lamp light source with band pass filter (440 nm). The power of Xe lamp with the band path filter was measured in the range of 0.9-1.2 mW at 400-nm-wavelength. Figure 6.25 shows $I-V$ characteristic curves of the GaN microstructure device arrays at dark and Xe lamp illumination conditions, clearly exhibiting current shifts at zero voltage. The short circuit current density and open circuit voltages were measured to be 0.1 mA/cm^2 and 0.2 V, respectively. This result suggested that inorganic semiconductor/graphene heterostructures can be utilized in photovoltaic devices, including solar cells and photo-detectors.

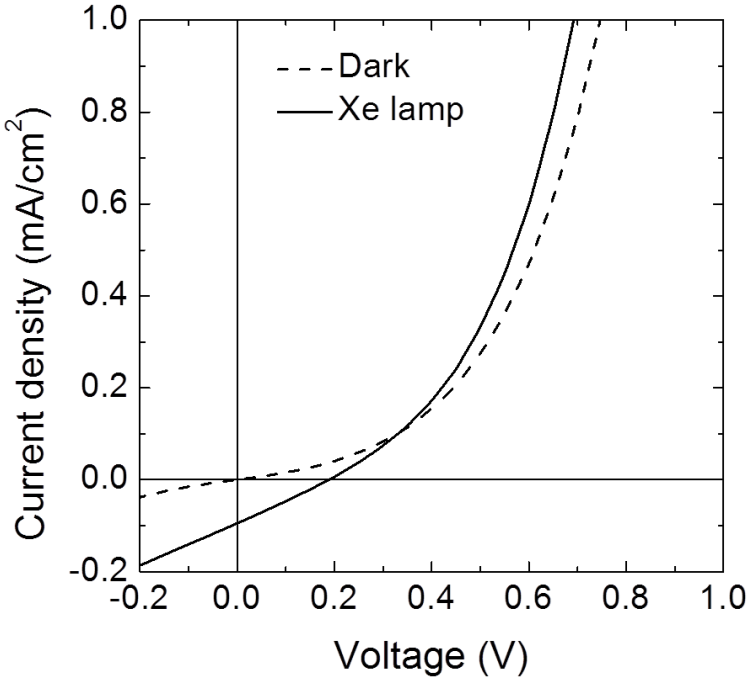

Fig. 6.25. *I*−*V* characteristic curves of the *p*−MQW−*n* junction GaN micro-disk array at dark (dashed line) and Xe lamp illumination (solid line) conditions.

6.6. Summery

The transfer of the materials and devices fabricated on graphene onto foreign substrates should provide advantages in integration and design of electronics and optoelectronic devices. In particular, the transferable fabrication route to achieve flexible inorganic semiconductor/graphene heterostructures on a plastic and metal substrate has numerous potential applications in flexible optoelectronic devices, and provides a method of integrating flexible substrates and inorganic semiconductor materials without much considering of the material compatibilities between semiconductors and the substrates. Furthermore, the simple technique used to obtain high-quality inorganic semiconductor thin films even on amorphous substrates makes it possible to fabricate LEDs on large-area noncrystalline solid substrates and to provide and manufacture large and cost-effective optoelectronic and electronic devices. More importantly, the selective area growth of GaN microstructures on graphene patterns now available for the fabrication of various GaN/graphene heterostructure optoelectronic devices in a form of array.

Concluding Remarks and Outlooks

7

7.1. Summary

The goal of this research was to provide a novel material system for transferable and flexible optoelectronic device applications using graphene films as an inorganic semiconductor growth substrate. High quality GaN films and 1D micro- and nanostructures were grown on graphene films by MOCVD, exhibiting high *c*-axis alignments and promising optical characteristics. In addition, GaN-based LEDs were fabricated on graphene films by satisfying the key criteria for building reliable LEDs, such as controls over doping, and fabrications of heterostructures and quantum structures. More importantly, transferability and flexibility of the inorganic devices are readily available, while the devices can be fabricated even on non-crystalline substrates by taking advantages of graphene films. The details of experiment achievements and findings are summarized as follow.

(1) Growths of GaN films on graphene films.

- ✓ High quality GaN films were grown epitaxially on graphene films. Because of the lack of chemical reactivity of pristine graphene surface, high density ZnO nanowalls were grown on plasma treated graphene

films and were used as a nucleation layer for the GaN growth. As a result flat and uniform GaN films can be obtained on graphene layers.

- ✓ Various graphene films, including mechanically exfoliated graphene layers and CVD graphene films, were employed for the fabrication of GaN film/graphene hybrid heterostructures. Although structural characteristics as well as growth morphologies were influenced by the graphene crystallinity, epitaxial GaN films were successfully grown even on large-scale graphene films over the area of 2 inch wafer with uniform surface morphology.

- ✓ The XRD and TEM results revealed that the GaN films were grown on graphene films with high *c*-axis orientation. The FWHM value of the XRD rocking curve was as small as 0.8˚. Meanwhile, GaN films grown on CVD graphene films showed random in-plane orientations, while single crystal GaN films were grown on mechanically exfoliated graphene layers.

- ✓ From the optical measurements of PL, room temperature stimulated emissions were observed, strongly suggesting that the GaN films grown on graphene films are of high optical quality. Moreover, there was no carbon related emissions from low-temperature PL spectra which allows us to control *n*-type and *p*-type doping for the optoelectronic device fabrication.

(2) Growths of 1D GaN micro-rods on graphene films.

- ✓ GaN micro-rods were grown on large-scale CVD graphene films using catalyst-free MOCVD. In particular, vertical growth of GaN micro-rods were investigated because the vertical alignment of the 1D structure is essential for high density device integration with easy and simple fabrication process. Although GaN micro-rods grown on pristine graphene films exhibited random growth direction, we could obtain vertically well aligned GaN micro-rods on graphene films using a GaN buffer layer. As determined by XRD rocking curve, FWHM value of the vertical GaN micro-rods was 3˚.

- ✓ TEM results showed that GaN micro-rods grown on graphene films are single crystalline with high crystallinity. In addition, strong NBE emissions with extremely low deep level emission were observed from the room temperature PL and CL spectra. Moreover, the GaN micro-rods showed stimulated emissions at room temperature.

(3) Optoelectronic device applications using GaN/graphene hybrid heterostructure

- ✓ For the optoelectronic device fabrications, heterostructures of *p*-GaN, $In_xGa_{1-x}N$/GaN MQWs, and *n*-GaN layers were coated on GaN films and 1D micro- and nanostructures. Since GaN grown on graphene films showed high crystallinity without carbon impurities, reliable LEDs, that showed strong EL emissions, were fabricated even on graphene films.

- ✓ Typically, GaN-based LEDs were fabricated on graphene films with the sequence of graphene transfer onto a supporting substrate, which

substrate has high stabilities under the GaN growth conditions, and growths of *p*-MQW-*n* heterostructures on the graphene films. It is notable that GaN layers were grown on graphene films with epitaxial relationships, while the supporting substrates do not required restrict compatibilities for the GaN growth. Accordingly, high quality GaN layers can be obtained on various supporting substrates, including *c*-Al_2O_3, Si(100) , W films, and amorphous silica substrates.

- ✓ Due to the interesting and powerful characteristics of graphene films, transferable and flexible LEDs were demonstrated using GaN/graphene hybrid heterostructures. The layered structure of graphene films makes it easy to lift off the LEDs from the supporting growth substrates and to transfer onto large-scale and flexible substrates of metal, glass, and plastic. In addition, the mechanical strength and flexibility of graphene films allows us to fabricate reliable LEDs under numerous bending conditions over 1000 cycle.

- ✓ Position controlled GaN/graphene microstructure arrays were fabricated without using growth mask, which is for the growth selectivity, or single crystal substrates, which is for the epitaxial growth. Since graphene films can be easily etched by plasma exposure, graphene dot arrays were fabricated on W films and SiO_2 layers with a simple fabrication process of photolithography and O_2 plasma etching. More importantly, GaN micro-films were selectively grown on graphene dot arrays, where graphene provides both epitaxial relations and growth selectivity on the

selective area growths. LEDs and photovoltaic devices were fabricated using the GaN/graphene heterostructure arrays and showed their reliable operation as an individual optoelectronic device.

7.2. Future works and prospects for GaN-based devices fabricated on graphene films

Hybrid heterostructures, which composed of inorganic semiconductor devices fabricated on graphene films, have many advantages for transferable and flexible device applications. As an example, this dissertation showed the epitaxial growth of GaN layers on graphene films and demonstrated the simple and easy process of fabricating reliable optoelectronic devices that exhibited transferability and flexibility. Moreover, the ability to prepare graphene in large-scale is very promising for the next generation large-scale optoelectronic device applications. Nevertheless, this field is still in the early stage and requires further progress to make high performance devices in large-scale. The details are as follow.

- ✓ Up to now, most of the transferable and flexible inorganic optoelectronic devices have been fabricated using thin film devices grown on single crystal substrates, where high performance devices are expected. For a comparison, LEDs were fabricated on *c*-Al_2O_3 and graphene films and their output powers were investigated. As a result, LEDs fabricated on graphene films showed 10−20 % light emission output powers compared to those fabricated on *c*-Al_2O_3 substrates. Due to the well-developed thin film technology on single crystal substrates, inorganic optoelectronic

devices are already commercially available. Meanwhile, a number of challenges remain in the fabrication of high efficiency optoelectronic devices fabricated on graphene films. However, I believe that these problems can be eventually solved by optimizing growth and process parameters for the device fabrications.

- ✓ Since GaN based optoelectronic devices were fabricated on CVD graphene films, which the large-size graphene films have become available over 30 inches, the hybrid heterostructures would open up diverse opportunities to fabricate various electronic and optoelectronic devices such as flexible and wearable LED displays in large-scale. Furthermore, graphene offers a hexagonal basal plane of atomic lattices, which enables to grow high-quality inorganic compound semiconductors without using expansive and size limited single crystal substrates. Additionally, MOCVD is a desirable growth technique for the hybrid heterostructure fabrication because of the feasibility of large-area growth as well as the relatively simple and accurate doping and thickness control. Typically, GaN films can be grown uniformly on 2-4 inch *c*-Al_2O_3 substrates by MOCVD. However, growth uniformity can be one of the major challenges for the large-area growth because typical MOCVDs have substrate bowing problems at high growth temperature, for example. Therefore, a modified MOCVD system or other large-area growth methods would be required for the large-area growth as large as graphene size.

References

1. S.-I. Park, Y. J. Xiong, R.-H. Kim, P. Elvikis, M. Meitl, D.-H. Kim, J. Wu, J. Yoon, C.-J. Yu, Z. J. Liu, Y. G. Huang, K.-C. Hwang, P. Ferreira, X. Li, K. Choquette, J. A. Rogers, *Science* **325**, 977 (2009).
2. K. Chung, C.-H. Lee, G.-C. Yi, *Science* **330**, 655 (2010).
3. C.-H. Lee, Y.-J. Kim, Y. J. Hong, S.-R. Jeon, S. Bae, B. H. Hong, G.-C. Yi, *Adv. Mater.* **23**, 4614 (2011).
4. T. I. Kim, J. G. McCall, Y. H. Jung, X. Huang, E. R. Siuda, Y. H. Li, J. Z. Song, Y. M. Song, H. A. Pao, R. H. Kim, C. F. Lu, S. D. Lee, I. S. Song, G. Shin, R. Al-Hasani, S. Kim, M. P. Tan, Y. G. Huang, F. G. Omenetto, J. A. Rogers, M. R. Bruchas, *Science* **340**, 211 (2013).
5. W. S. Wong, T. Sands, N. W. Cheung, M. Kneissl, D. P. Bour, P. Mei, L. T. Romano, N. M. Johnson, *Appl. Phys. Lett.* **75**, 1360 (1999).
6. K. J. Lee, J. Lee, H. D. Hwang, Z. J. Reitmeier, R. F. Davis, J. A. Rogers, R. G. Nuzzo, *Small* **1**, 1164 (2005).
7. Y. Kobayashi, K. Kumakura, T. Akasaka, T. Makimoto, *Nature* **484**, 223 (2012).
8. S. Nakamura, T. Mukai, M. Senoh, *Appl. Phys. Lett.* **64**, 1687 (1994).
9. F. A. Ponce, D. P. Bour, *Nature* **386**, 351 (1997).
10. S. Nakamura, S. Pearton, G. Fasol, *The Blue Laser Diode: The Complete Story*. (Springer-Verlag Berlin, 2000).

11. D. P. Bour, N. M. Nickel, C. G. Van de Walle, M. S. Kneissl, B. S. Krusor, P. Mei, N. M. Johnson, *Appl. Phys. Lett.* **76**, 2182 (2000).
12. W. S. Wong, T. Sands, N. W. Cheung, *Appl. Phys. Lett.* **72**, 599 (1998).
13. S. Bae, H. Kim, Y. Lee, X. F. Xu, J. S. Park, Y. Zheng, J. Balakrishnan, T. Lei, H. R. Kim, Y. I. Song, Y. J. Kim, K. S. Kim, B. Ozyilmaz, J. H. Ahn, B. H. Hong, S. Iijima, *Nat. Nanotechnol.* **5**, 574 (2010).
14. K. S. Novoselov, A. K. Geim, S. V. Morozov, D. Jiang, Y. Zhang, S. V. Dubonos, I. V. Grigorieva, A. A. Firsov, *Science* **306**, 666 (2004).
15. Y. B. Zhang, Y. W. Tan, H. L. Stormer, P. Kim, *Nature* **438**, 201 (2005).
16. C. Lee, X. Wei, J. W. Kysar, J. Hone, *Science* **321**, 385 (2008).
17. R. R. Nair, P. Blake, A. N. Grigorenko, K. S. Novoselov, T. J. Booth, T. Stauber, N. M. R. Peres, A. K. Geim, *Science* **320**, 1308 (2008).
18. Y.-J. Kim, J. H. Lee, G.-C. Yi, *Appl. Phys. Lett.* **95**, 213101 (2009).
19. J. H. An, E. Voelkl, J. W. Suk, X. S. Li, C. W. Magnuson, L. F. Fu, P. Tiemeijer, M. Bischoff, B. Freitag, E. Popova, R. S. Ruoff, *ACS Nano* **5**, 2433 (2011).
20. K. Kim, Z. Lee, W. Regan, C. Kisielowski, M. F. Crommie, A. Zettl, *ACS Nano* **5**, 2142 (2011).
21. P. Y. Huang, C. S. Ruiz-Vargas, A. M. van der Zande, W. S. Whitney, M. P. Levendorf, J. W. Kevek, S. Garg, J. S. Alden, C. J. Hustedt, Y. Zhu, J. Park, P. L. McEuen, D. A. Muller, *Nature* **469**, 389 (2011).
22. J. H. Lee, E. K. Lee, W. J. Joo, Y. Jang, B. S. Kim, J. Y. Lim, S. H. Choi, S. J. Ahn, J. R. Ahn, M. H. Park, C. W. Yang, B. L. Choi, S. W. Hwang, D. Whang, *Science* **344**, 286 (2014).

23. W. I. Park, D. H. Kim, S. W. Jung, G. C. Yi, *Appl. Phys. Lett.* **80**, 4232 (2002).

24. W. I. Park, G.-C. Yi, M. Y. Kim, S. J. Pennycook, *Adv. Mater.* **14**, 1841 (2002).

25. Y.-J. Kim, J. Yoo, B.-H. Kwon, Y. J. Hong, C.-H. Lee, G.-C. Yi, *Nanotechnology* **19**, (2008).

26. Y. J. Hong, J. Yoo, Y. J. Doh, S. H. Kang, K. J. Kong, M. Kim, D. R. Lee, K. H. Oh, G. C. Yi, *J. Mater. Chem.* **19**, 941 (2009).

27. J. Jo, H. Yoo, S. I. Park, J. B. Park, S. Yoon, M. Kim, G. C. Yi, *Adv. Mater.* **26**, 2011 (2014).

28. X. K. Lu, H. Huang, N. Nemchuk, R. S. Ruoff, *Appl. Phys. Lett.* **75**, 193 (1999).

29. Y. J. Kim, H. Yoo, C. H. Lee, J. B. Park, H. Baek, M. Kim, G. C. Yi, *Adv. Mater.* **24**, 5565 (2012).

30. S. D. Hersee, X. Sun, X. Wang, *Nano Lett.* **6**, 1808 (2006).

31. M. K. Kelly, O. Ambacher, B. Dahlheimer, G. Groos, R. Dimitrov, H. Angerer, M. Stutzmann, *Appl. Phys. Lett.* **69**, 1749 (1996).

32. E. Yablonovitch, T. Gmitter, J. P. Harbison, R. Bhat, *Appl. Phys. Lett.* **51**, 2222 (1987).

33. J. Yoon, S. Jo, I. S. Chun, I. Jung, H.-S. Kim, M. Meitl, E. Menard, X. Li, J. J. Coleman, U. Paik, J. A. Rogers, *Nature* **465**, 329 (2010).

34. M. D. McCluskey, L. T. Romano, B. S. Krusor, N. M. Johnson, T. Suski, J. Jun, *Appl. Phys. Lett.* **73**, 1281 (1998).

35. J. W. Ju, J. J. Zhu, H. S. Kim, C. R. Lee, I. H. Lee, *J. Korean Phys. Soc.* **50**, 810 (2007).

36. K. Chung, S. I. Park, H. Baek, J. S. Chung, G.-C. Yi, *NPG Asia Mater.* **4**, e24 (2012).

37. A. Miura, S. Shimada, *Mater. Res. Bull.* **41**, 1775 (2006).

38. A. Miura, S. Shimada, T. Sekiguchi, *J. Cryst. Growth* **299**, 22 (2007).

39. S. J. An, W. I. Park, G. C. Yi, Y. J. Kim, H. B. Kang, M. Kim, *Appl. Phys. Lett.* **84**, 3612 (2004).

40. Y. J. Hong, J. M. Jeon, M. Kim, S. R. Jeon, K. H. Park, G. C. Yi, *New J. Phys.* **11**, 13 (2009).

41. H. Yoo, K. Chung, Y. S. Choi, C. S. Kang, K. H. Oh, M. Kim, G. C. Yi, *Adv. Mater.* **24**, 515 (2012).

42. M. A. Reshchikov, H. Morkoc, *Journal of Applied Physics* **97**, (2005).

43. R. Armitage, W. Hong, Q. Yang, H. Feick, J. Gebauer, E. R. Weber, S. Hautakangas, K. Saarinen, *Appl. Phys. Lett.* **82**, 3457 (2003).

44. S. Fischer, C. Wetzel, W. L. Hansen, E. D. BourretCourchesne, B. K. Meyer, E. E. Haller, *Appl. Phys. Lett.* **69**, 2716 (1996).

45. M. A. Khan, D. T. Olson, J. M. Vanhove, J. N. Kuznia, *Appl. Phys. Lett.* **58**, 1515 (1991).

46. S. Bidnyk, B. D. Little, T. J. Schmidt, Y. H. Cho, J. Krasinski, J. J. Song, B. Goldenberg, W. Yang, W. G. Perry, M. D. Bremser, R. F. Davis, *Journal of Applied Physics* **85**, 1792 (1999).

47. G. P. Yablonskii, E. V. Lutsenko, V. N. Pavlovskii, V. Z. Zubialevich, A. L. Gurskii, H. Kalisch, A. Szymakowskii, R. A. Jansen, A. Alam, Y. Dikme, B. Schineller, M. Heuken, *Phys. Status Solidi A* **192**, 54 (2002).

48. M. Funato, K. Hayashi, M. Ueda, Y. Kawakami, Y. Narukawa, T. Mukai, *Appl. Phys. Lett.* **93**, 021126 (2008).

49. C.-H. Lee, J. Yoo, Y. J. Hong, J. Cho, Y.-J. Kim, S.-R. Jeon, J. H. Baek, G.-C. Yi, *Appl. Phys. Lett.* **94**, 213101 (2009).

50. Y. J. Hong, C.-H. Lee, A. Yoon, M. Kim, H.-K. Seong, H. J. Chung, C. Sone, Y. J. Park, G.-C. Yi, *Adv. Mater.* **23**, 3284 (2011).

51. K. Kishino, K. Nagashima, K. Yamano, *Appl. Phys. Express* **6**, 012101 (2013).

52. Y. Tchoe, J. Jo, M. Kim, J. Heo, G. Yoo, C. Sone, G.-C. Yi, *Adv. Mater.* **26**, 3019 (2014).

53. J. K. Hyun, S. X. Zhang, L. J. Lauhon, *Ann. Rev. Mater. Res.* **43**, 451 (2013).

54. Y. J. Hong, W. H. Lee, Y. P. Wu, R. S. Ruoff, T. Fukui, *Nano Lett.* **12**, 1431 (2012).

55. Q. Li, J. B. Wright, W. W. Chow, T. S. Luk, I. Brener, L. F. Lester, G. T. Wang, *Opt. Express* **20**, 17873 (2012).

56. R. Koester, J. S. Hwang, C. Durand, D. L. S. Dang, J. Eymery, *Nanotechnology* **21**, 015602 (2010).

57. S.-M. Ko, J.-H. Kim, Y.-H. Ko, Y. H. Chang, Y.-H. Kim, J. Yoon, J. Y. Lee, Y.-H. Cho, *Cryst. Growth Des.* **12**, 3838 (2012).

58. W. Shan, R. J. Hauenstein, A. J. Fischer, J. J. Song, W. G. Perry, M. D. Bremser, R. F. Davis, B. Goldenberg, *Phys. Rev. B* **54**, 13460 (1996).

59. K. Chung, H. Beak, Y. Tchoe, H. Oh, H. Yoo, M. Kim, G. C. Yi, *APL Mater.* **2**, 7 (2014).

60. E. Kuokstis, J. W. Yang, G. Simin, M. A. Khan, R. Gaska, M. S. Shur, *Appl. Phys. Lett.* **80**, 977 (2002).

61. H. Sirringhaus, N. Tessler, R. H. Friend, *Science* **280**, 1741 (1998).

62. J. Yang, A. Banerjee, S. Guha, *Sol. Energy Mater. Sol. Cells* **78**, 597 (2003).

63. U. Ozgur, Y. I. Alivov, C. Liu, A. Teke, M. A. Reshchikov, S. Dogan, V. Avrutin, S. J. Cho, H. Morkoc, *Journal of Applied Physics* **98**, 041301 (2005).

64. S. R. Forrest, *Nature* **428**, 911 (2004).

65. S. Nakamura, *Science* **281**, 956 (1998).

66. D. P. Bour, N. M. Nickel, C. G. Van de Walle, M. S. Kneissl, B. S. Krusor, P. Mei, N. M. Johnson, *Appl. Phys. Lett.* **76**, 2182 (2000).

67. C. J. H., Andrei Zoulkarneev, Sun Il Kim, Chan Wook Baik, Min Ho Yang, Sung Soo Park, Hwansoo Suh, Un Jeong Kim, Hyung Bin Son, Jae Soong Lee, Miyoung Kim, Jong Min Kim , Kinam Kim, *Nat. Photonics*, On publication (2011).

68. S. Nakamura, *Solid State Commun.* **102**, 237 (1997).

69. H. Yoo, K. Chung, S. I. Park, M. Kim, G. C. Yi, *Appl. Phys. Lett.* **102**, 4 (2013).

70. S. Nakamura, M. Senoh, T. Mukai, *Japanese Journal of Applied Physics Part 2-Letters* **30**, L1708 (1991).

71. Z. Y. Fan, H. Razavi, J. W. Do, A. Moriwaki, O. Ergen, Y. L. Chueh, P. W. Leu, J. C. Ho, T. Takahashi, L. A. Reichertz, S. Neale, K. Yu, M. Wu, J. W. Ager, A. Javey, *Nat. Mater.* **8**, 648 (2009).

72. Y. M. Song, Y. Z. Xie, V. Malyarchuk, J. L. Xiao, I. Jung, K. J. Choi, Z. J. Liu, H. Park, C. F. Lu, R. H. Kim, R. Li, K. B. Crozier, Y. G. Huang, J. A. Rogers, *Nature* **497**, 95 (2013).

73. J. H. Choi, E. H. Cho, Y. S. Lee, M. B. Shim, H. Y. Ahn, C. W. Baik, E. H. Lee, K. Kim, T. H. Kim, S. Kim, K. S. Cho, J. Yoon, M. Kim, S. Hwang, *Adv. Opt. Mater.* **2**, 267 (2014).

74. C. J. Yu, Y. H. Li, X. Zhang, X. Huang, V. Malyarchuk, S. D. Wang, Y. Shi, L. Gao, Y. W. Su, Y. H. Zhang, H. X. Xu, R. T. Hanlon, Y. G. Huang, J. A. Rogers, *Proc. Natl. Acad. Sci. U. S. A.* **111**, 12998 (2014).

75. J. Yoo, Y. J. Hong, H. S. Jung, Y. J. Kim, C. H. Lee, J. Cho, Y. J. Doh, L. S. Dang, K. H. Park, G. C. Yi, *Adv. Funct. Mater.* **19**, 1601 (2009).

Appendix

Position controlled growth of GaN micro-rods

In this dissertation, vertically aligned 1D GaN microstructures were randomly formed on graphene layers since nucleation sites on the graphene layers could not be controlled yet. However, the position control of microstructures on the graphene layers would provide a great advantage for improving device performance because of the ability to uniformly control the heights and thicknesses of the individual microstructures over the entire surface of the substrates. For the preliminary study of the position controlled growth of 1D GaN micro-rods on graphene films, GaN film coated *c*-Al_2O_3 substrates with a SiO_2 mask layer were employed to investigate the selective area growth conditions of the 1D GaN microstructures.

Figure A.1a schematically shows the basic concept of the position controlled growth of GaN micro-rods. For the substrate preparation, 50-nm-thick SiO_2 layers were coated on *n*-GaN film grown *c*-Al_2O_3 substrates. Then, the SiO_2 mask layers were patterned into 500-nm-diameter hole array using lithography, such as nanoimprint lithography and *e*-beam lithography. The mask layer preparation and patterning were carried out by JunBeom Park and Hongseok Oh in our laboratory. After preparing the SiO_2 mask layer on the substrate, GaN micro-rods can be grown only on the hole openings because of the growth selectivity between GaN and SiO_2 layers. Figure A.1b shows a typical surface morphology of position controlled GaN micro-rods grown on the patterned

substrates. GaN micro-rods exhibited almost uniform surface morphologies, including height, diameter, and spacing. In addition, GaN micro-rods were grown selectively on every hole openings.

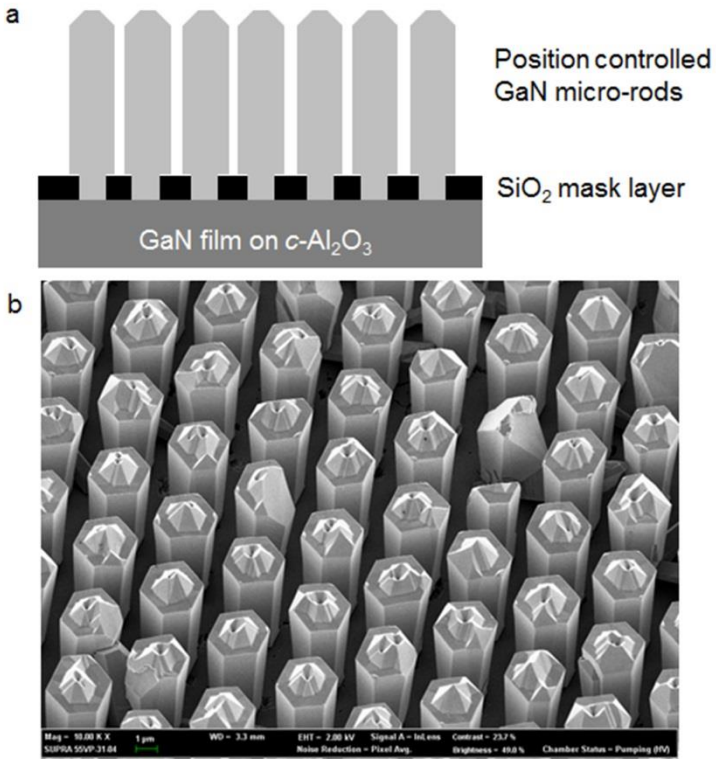

Fig. A.1. (a) Schematic illustration and (b) FE-SEM image of position controlled growth of GaN micro-rods on SiO_2 mask layer coated *n*-GaN/*c*-Al_2O_3 substrates.

For the position controlled growth of 1D GaN microstructures, accurate control of growth parameters is strongly required because the growth conditions strongly affected to the growth direction, growth yield, and surface morphology. Additionally, since GaN micro-rods were grown with high silicon doping in this study, the growth morphology were largely influenced by the DTBSi flow rates, which is the precursor of the silicon. For this reason, position controlled growth of

GaN micro-rods were investigated at various growth conditions. As shown in Fig. A.2, GaN micro-rods were grown with a three sequential steps of H_2 heat treatment, nucleation, and micro-rod growth. The effect of growth parameters in each step will be discussed.

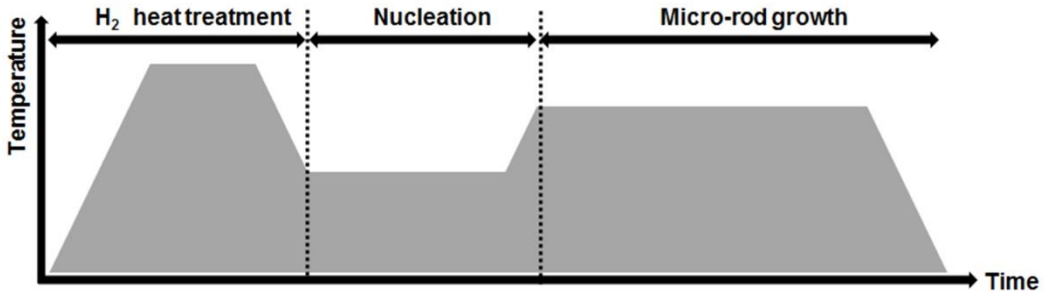

Fig. A.2. Sequential steps of GaN micro-rod growth on patterned SiO_2/*n*-GaN/*c*-Al_2O_3 substrates.

To grow position controlled GaN micro-rods, H_2 heat treatment process was firstly performed on the substrates. In this growth step, the effect of NH_3 injections and H_2 heat treatment time were investigated. Figures A.3a and A.3b show GaN microstructures grown without and with NH_3 flow rates at the H_2 heat treatment process, respectively. Without NH_3 flow rates, GaN micro-rods with a high aspect ratio could be grown on the substrates. However, GaN pyramids were grown on the hole opening when NH_3 flow injected during the heat treatment process. Additionally, the GaN micro-rods in Fig. A.3a showed poor vertical alignment presumably because of the relative high growth temperature of the GaN micro-rods. The vertical aligned GaN micro-rods can be obtained at GaN micro-rod growth temperature of 950-1050˚C.

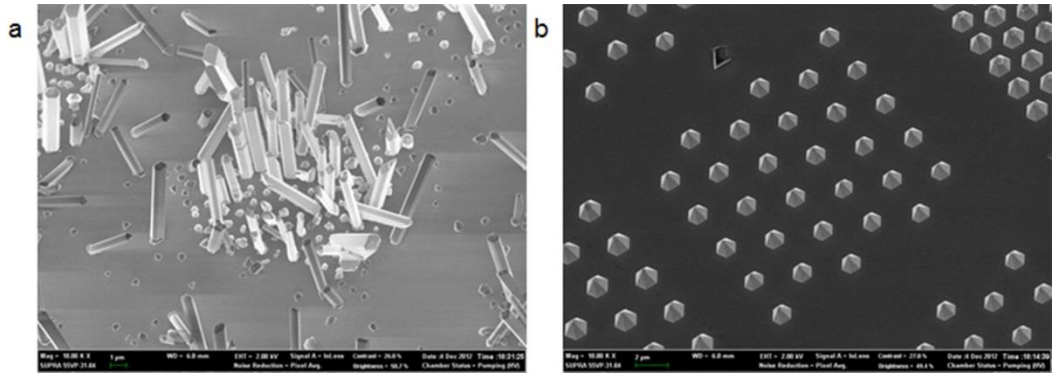

Fig. A.3. GaN micro-rods (a) without and (b) with NH_3 injection during H_2 heat treatment process.

Figure A.4 shows the effect of H_2 heat treatment time on the GaN micro-rod growths. When the heat treatment time was relatively short of 1 min, GaN micro-rods were rarely grown on the hole openings, as shown in Fig. A.4a. However, if heat treatment were performed for 10 min on the substrates, GaN micro-rods were grown on every holes (Fig. A.4b). Meanwhile, Fig. A.4c showed the growth yield was suppressed at 30-min-time heat treatment.

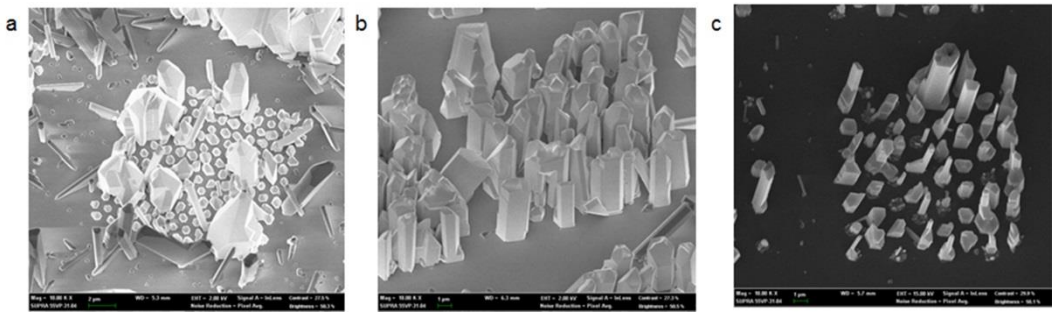

Fig. A.4. GaN micro-rods grown at various H_2 heat treatment times of (a) 1 min, (b) 10 min, and (c) 30 min.

Following by H_2 heat treatment process, GaN nucleation layers were deposited on the hole openings at nucleation steps. According to experimental results, the nucleation temperature and time largely affected to the uniform and regular growth of GaN micro-rods. Figures A.5a, A.5b, and A.5c show GaN micro-rods grown at various nucleation temperatures of 800, 750, and 700˚C, respectively. At nucleation temperature of 800˚C, GaN micro-rods were vertically well aligned normal to the substrate. However, as the nucleation temperature decreased, many GaN micro-rods showed random growth directions. In addition, GaN micro-rods were rarely grown at the nucleation temperature of 700˚C. Additionally, the growth morphology of GaN micro-rods were investigated at various tiled views, as shown in Fig. A.6. Figures A.6a and A.6b shows GaN micro-rods grown with nucleation temperatures of 800 and 850˚C, respectively. Although the 30˚-tilted FE-SEM images (top images) exhibited no observable differences in the growth direction, the plan-view FE-SEM images (bottom images) clearly showed the vertical growth of the GaN micro-rods. Specifically, at nucleation temperature of 800˚C, two or three GaN micro-rods were grown in one hole with random growth directions, while GaN micro-rods grown at nucleation temperature of 850˚C exhibited much improved growth alignments.

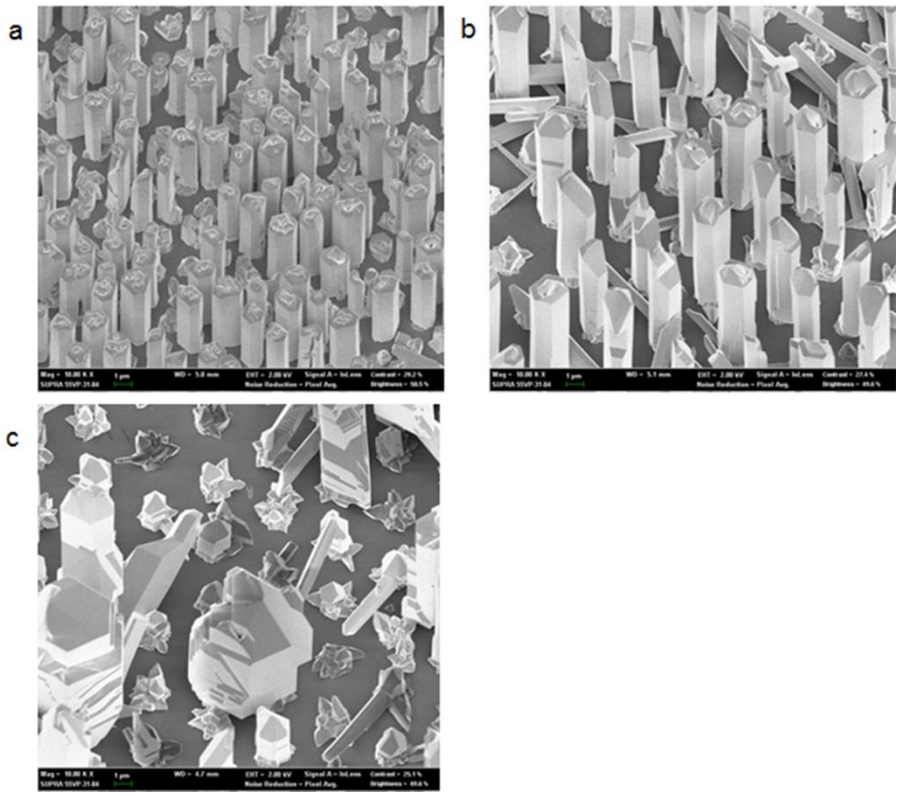

Fig. A.5. GaN micro-rods grown at various nucleation temperatures of (a) 800, (b) 750, and (c) 700˚C.

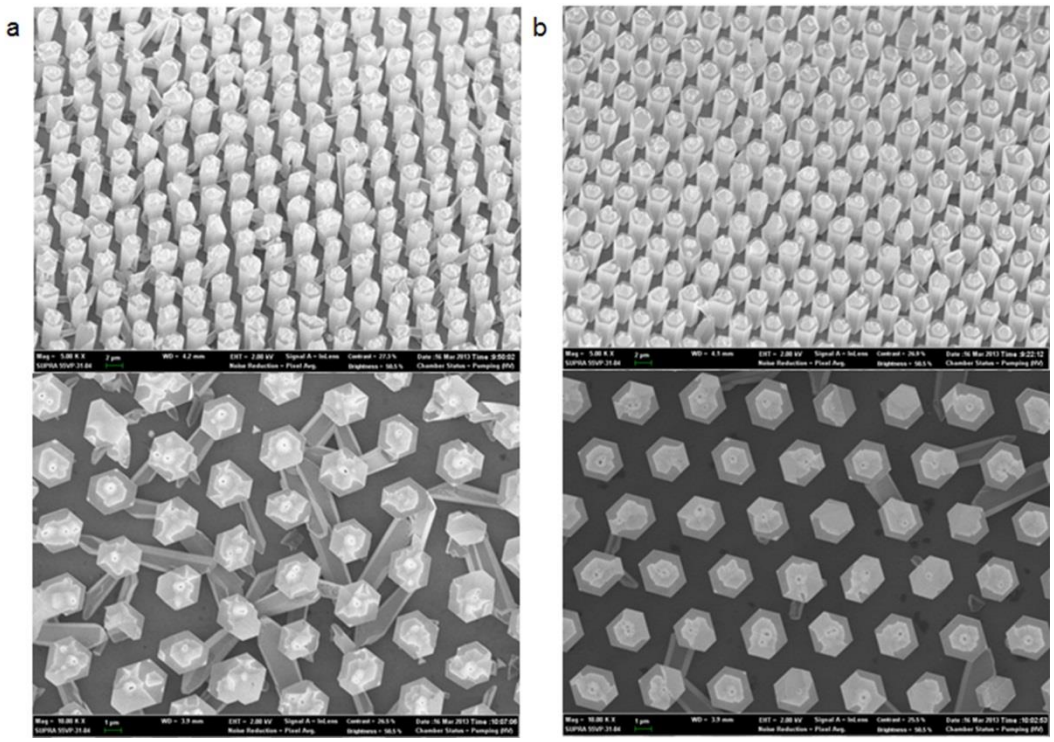

Fig. A.6. 30˚-tilted-views (top images) and plan-views (bottom images) of GaN micro-rods grown with nucleation temperatures of (a) 800 and (b) 850˚C.

In addition to the nucleation temperature, GaN micro-rods were grown at various nucleation time. Figures A.7a and A.7b show GaN micro-rods with nucleation times of 1 min and 3 min, respectively. Although GaN micro-rods were vertically well aligned on the substrates regardless of the nucleation time, the growth morphology showed large differences, such as surface morphology, diameter, and length. To investigate the effect of nucleation time on the uniform growth of GaN micro-rods, mean diameter and mea length of the GaN micro-rods were plotted as a function of nucleation time, as shown in Figs. A.7c and A.7d, respectively. The GaN micro-rods with 3-min-nucleation showed slightly larger diameter compared to those of GaN micro-rods with 1-min-nucleation presumably

due to the long growth time. Additionally, relatively long GaN micro-rods were grown at nucleation time of 1 min, which resulted in the large mean length. Nevertheless, the error bars both in diameter and length clearly reveals that the uniform growth of GaN micro-rods at 3-min-nucleation.

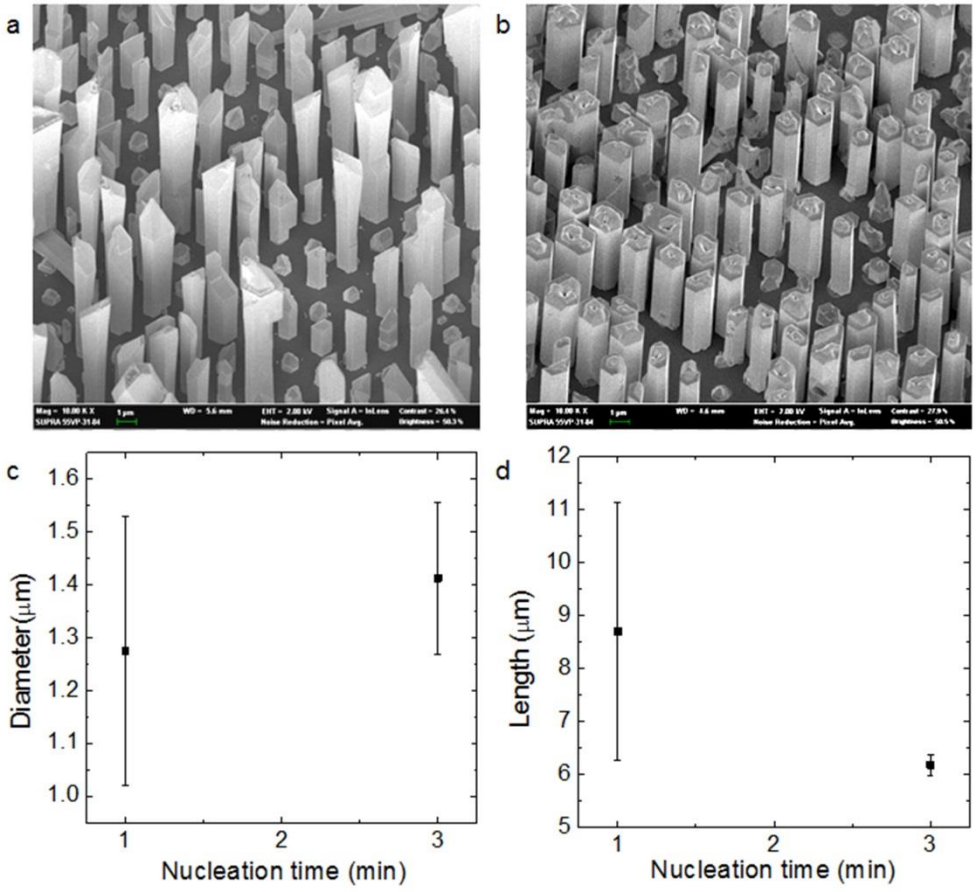

Fig. A.7. FE-SEM images of GaN micro-rods with nucleation times of (a) 1 min and (b) 3 min. (a) Diameter and (b) length of the GaN micro-rods at various nucleation time.

After growing GaN nucleation layer on the hole openings, highly Si-doped GaN micro-rods were selectively grown on the nucleation layer coated substrates at the final micro-rod growth process. Since V/III ratio is important to grow 1D GaN micro-rods, the GaN microstructures were grown at various NH_3 flow rates of 100, 300, and 1000 sccm, as shown in Figs. A.8a, A.8b, and A.8c, respectively, while TMGa flow rates kept constant at 15 sccm. The GaN micro-rods with NH_3 flow rates of 100 sccm exhibited rough surface morphology. However, the surface morphology showed drastic improvements with increasing NH_3 flow rate at 300 sccm, where the GaN micro-rods exhibited smooth sidewalls and uniform growth morphology. For further increasing the NH_3 flow rate to 1000 sccm, however, irregular GaN microstructures were grown.

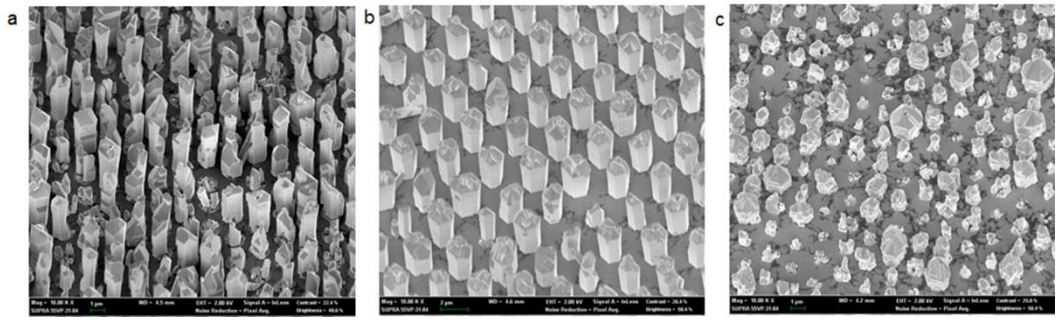

Fig. A.8. GaN micro-rods grown on the hole patterned substrates at various NH_3 flow rates of (a) 100, (b) 300, and (c) 1000 sccm.

Additionally, the surface morphology of GaN micro-rods was investigated at various DTBSi flow rates, as shown in Fig. A.9. At low DTBSi flow rates, GaN micro-disks were grown on the substrates, where the diameter is larger than the height. As increasing the DTBSi flow rates, the surface morphology drastically changed to micro-rods, indicating that high Si concentration significantly

improved the vertical growth of GaN microstructures. At optimum Si concentration, the GaN micro-rods exhibited a high aspect ratio as well as uniform and smooth sidewalls. However, when the Si concentration increased further, the GaN micro-rods showed irregular and rough sidewalls. In addition, GaN microstructures could not be grown at very high Si concentration.

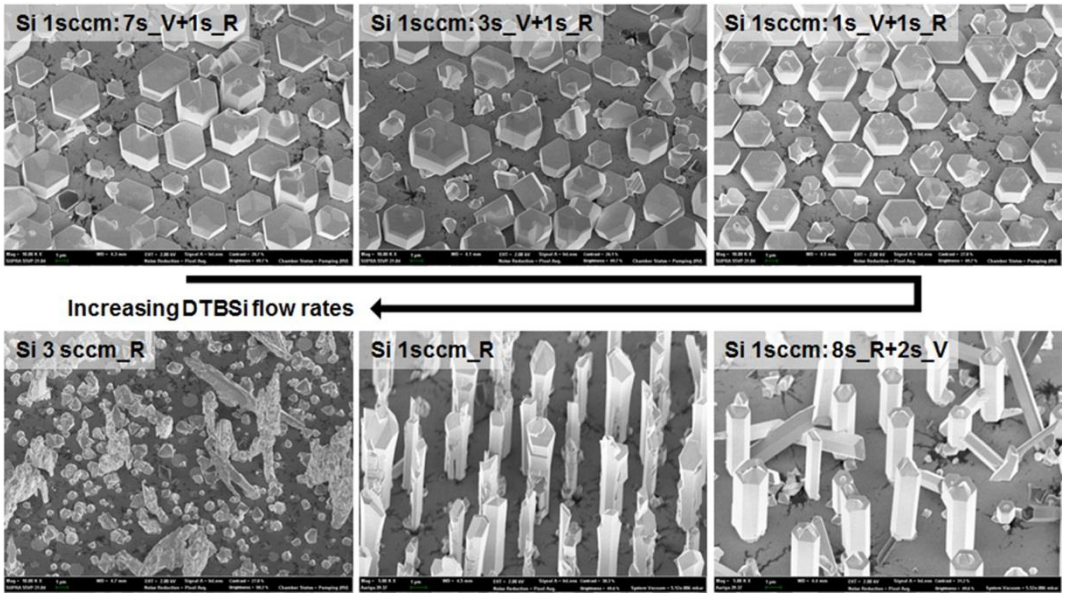

Fig. A.9. Surface morphologies of GaN micro-rods at various DTBSi flow rates.

GaN micro-rods were selectively grown on the patterned substrates with different hole spacing. When the hole-to-hole distance was 1 μm, as shown in Fig. A.10a, GaN micro-rods exhibited large differences in their diameter, length, and surface morphology. In addition, the GaN microstructures did not showed regular array presumably due to the short hole to hole distance. However, the GaN micro-rods with hole spacing of 2 μm clearly show regular intervals, indicating the position controlled growth of the micro-rods (Fig. A. 10b). Nevertheless, the GaN micro-rods showed large difference in their growth height. This problem was

overcome by increasing the hole spacing. Figure A.10c shows position controlled GaN micro-rods grown on 4-μm-distance hole array. The GaN micro-rods exhibited excellent growth selectivity and uniform surface morphology. The growth morphology improvement with increasing hole-to-hole distance is presumably due to the relatively large diameter of GaN micro-rods. Additionally, GaN micro-rods were grown on large-size holes, as shown in Fig. A.10d, where the hole diameter was 3 μm. When the hole size is larger than the diameter of typical GaN micro-rods, two or three GaN micro-rods were grown on individual holes.

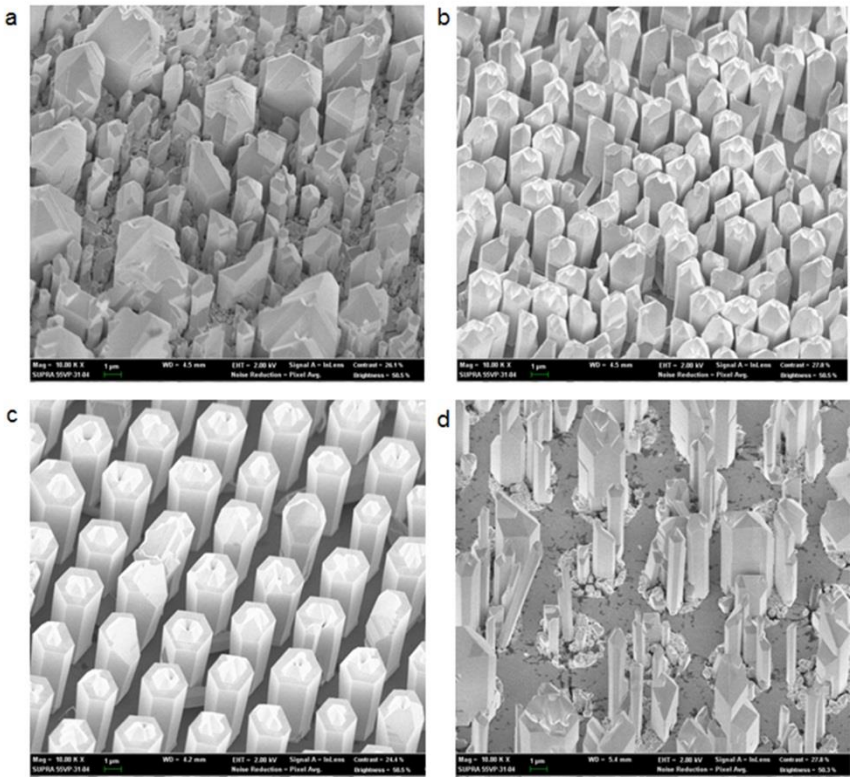

Fig. A.10. GaN micro-rods with various hole-to-hole distances of (a) 1 μm, (b) 2 μm, and (c) 4 μm. GaN micro-rods with 3-μm-diameter hole patterns.

After optimizing the growth conditions of position controlled GaN micro-rods on GaN/*c*-Al_2O_3 substrates, SiO_2 mask layers were prepared on the graphene substrates for the selective area growth. Figure A.11a shows a method to grow position controlled GaN micro-rods on graphene films. CVD graphene films were transferred onto SiO_2/Si substrates, and then SiO_2 mask layer was coated on entire graphene surface. Subsequently, the SiO_2 hole patterns were prepared by *e*-beam lithography and etching process, similar to those prepared on GaN/*c*-Al_2O_3 substrates. Additionally, ZnO nanowalls were selectively grown on the exposed graphene surfaces in order to improve the GaN layer nucleation. The ZnO nanowalls were coated by a thin GaN layer prior to the GaN micro-rod growth. Finally, GaN micro-rods were grown on SiO_2 mask layer coated GaN/*c*-Al_2O_3 and CVD graphene/SiO_2/Si substrates simultaneously for the morphology comparison.

Figures A.11b and A.11c show GaN micro-rods grown on GaN/*c*-Al_2O_3 substrates and on CVD graphene/SiO_2/Si substrates with SiO_2 mask layers, respectively. On GaN/*c*-Al_2O_3 substrates, GaN micro-rods were selectively grown with high growth yield. Furthermore, the micro-rods showed regular surface morphology over the entire SiO_2 patterns. On CVD graphene/SiO_2/Si substrates, GaN micro-rods exhibited fairly good growth selectivity, where the GaN microstructures were only grown on the ZnO nanowall coated graphene surfaces. However, the growth yield was much poor compared to those grown on GaN/*c*-Al_2O_3 substrates. Although GaN micro-rods were grown on both substrates simultaneously, the actual growth and nucleation temperature were not same because of the different substrate thermal conductivities. Additionally, the nucleation process of GaN micro-rods on patterned graphene substrates are not

fully investigated yet. Nevertheless, I believe that these problems, such as low yield growth, can be eventually solved by optimizing further growth condition.

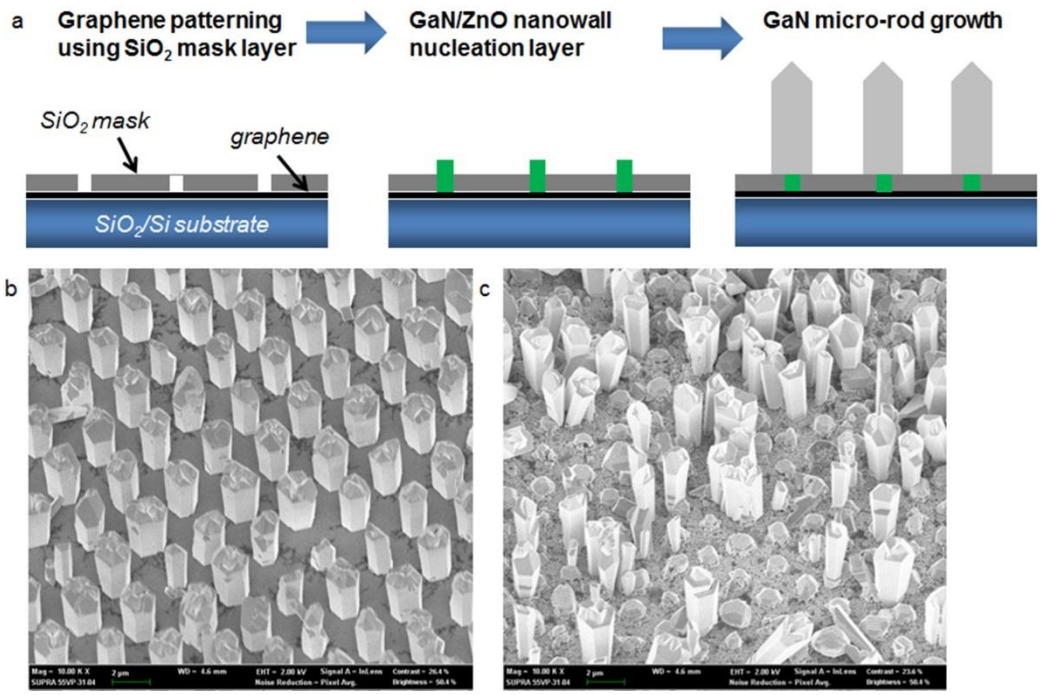

Fig. A.11. (a) Schematic illustration of a method to prepare position controlled GaN micro-rods on graphene substrates. FE-SEM images of GaN micro-rods grown on (b) GaN/*c*-Al_2O_3 and on (c) CVD graphene/SiO_2/Si substrates with SiO_2 mask layers.

국문 초록

LED, 태양 전지, 레이저, 트랜지스터 등 현재 사용되고 있는 대부분의 고효율 광소자, 전자소자들은 반도체 기술의 뛰어난 발전에 바탕을 두고 있다. 그리고 이런 반도체 기술 중 큰 축이 되는 하나는 에피탁시(epitaxy)이다. 에피탁시는 고품질의 반도체 소재를 성장하는 기술로, 유기금속화학기상증착법 (metal-organic chemical vapor deposition, MOCVD), 분자선에피탁시 (molecular beam epitaxy, MBE), 펄스레이져증착법 (pulsed laser deposition, PLD)등 선진화된 장비들로 이를 구현 할 수 있다. 이런 에피탁시 기술을 이용하면, 불순물과 결함이 매우 적은 단결정 반도체 소재를 제조할 수 있을 뿐만아니라, 반도체 소재의 밴드갭을 조절할 수 있어 고효율 반도체 소자 제조에 매우 유용하게 이용될 수 있다. 고효율 LED에 사용되는 양자 우물 구조나 HEMT 같은 매우 빠른 전자이동도를 가진 전자소자에 사용되는 2차원 전자가스 등이 모두 이런 밴드갭 조절을 통해 구현된 것들이다.

에피탁시 기술은 현재까지도 매우 중요하게 사용되고 있는 반도체 기술로 2014년 노벨 물리학상에서도 이를 보여준다. 노벨 물리학상의 수상자인 나카무라 교수와 그의 동료들은 에피탁시 기술을 이용하여 사파이어 기판 위에 고품질의 단결정 질화갈륨 박막을 제조할 수 있었고, 고품질의 양자우물구조 제조와 p형 도핑된 질화갈륨 박막을 후속적으로 제조하여 고효율, 저전력 발광 소자를 개발할 수 있었다. 그리고 현재 질화갈륨 LED는 산업 전반의 발광소자로 이용될 만큼 커다란 파급 효과를 가져왔다.

반면, 현재 고품질의 반도체 소재들은 3 차원 단결정 벌크 기판 상에 에피탁시 기술로 성장되어 왔다. 하지만 이런 벌크 기판들은 단단하고, 부러지기 쉽고, 대면적 공정 제조가 어려우며, 또한 반도체 소재와 강한 결합으로 붙어있기 때문에 반도체 소자의 응용성을 국한하는데 매우 큰 영향을 끼친다. 더욱이, 현재는 유연하고 대면적인 광소자, 전자소자들이 디스플레이, 태양 전지 등 많은 산업 분야에 필요한데 3 차원 벌크 기판의 사용은 이런 산업 전반적인 추세를 따라가는 데에 극복해야 할 가장 큰 난관으로 여겨지고 있다. 이에 본 연구에서는 그래핀과 같은 2 차원 층상 구조의 소재를 반도체 성장 기판으로 사용하여 이동가능하고, 유연한 광소자를 제조하였다.

다양한 2 차원 층상 소재들 중 그래핀은 고품질의 반도체 소재를 성장할 수 있는 기판으로써 많은 가능성을 가지고 있다. 우선, 그래핀은 벌집 모양의 육각 결정 구조를 가지고 있어서 질화갈륨과 산화아연과 같은 wurtzite 결정 반도체 소재들과 좋은 조화 격자를 가질 수 있다. 고품질의 반도체 소재를 성장하기 위해서는 이런 조화 격자 맞춤이 매우 중요한 요소이다. 또한, 그래핀은 매우 다양하고 뛰어난 기능성들을 반도체 소자에 부여할 수 있다. 유연성, 전기전도성, 열전도성, 대면적 공정성, 투명성 등이 이런 대표적인 장점들이다. 또 다른 장점으로 강조하고 싶은 것은 그래핀은 다른 물질들과 약한 상호작용으로 결합하는 특성을 가지고 있기 때문에, 그래핀 상에 반도체 소자를 제조하게 되면, 반도체 소자 역시 쉽게 떼어내거나 붙일 수 있는 소자로 응용될 수 있다는 것이다. 이런 이유로 그래핀을 기판으로 사용했을 때, 반도체 소자는 기판의 제약 없이 대면적, 유연한 소자로 응용이 가능해진다.

하지만 그래핀 상에 반도체 소재를 성장하는 일은 기존의 반도체 소자 성장 기술로 쉽게 달성할 수 없다. 이는 그래핀 기판과 기존의 반도체 성장 기판의 차이 때문에 비롯된다. 사파이어 기판과 같은 기존의 반도체 성장 기판은 표면에 많은 dangling bond 들을 가지고 있어, 반도체 소재들이 기판에 처음 성장될 때 쉽게 핵생성을 할 수 있고, 고품질의 반도체 소재를 성장할 수 있다. 하지만, 그래핀은 표면에 결함이 없는 한 dangling bond 가 거의 없는 특성을 가지고 있기 때문에 쉽게 반도체 소재들을 핵생성 시킬 수 없고, 이에 따라 고품질의 반도체 박막을 성장하는 일이 매우 어려웠다. 이런 문제점을 해결하기 위해서 본 연구에서는 그래핀 기판 상에서도 핵 생성이 잘 이뤄질 수 있는 성장 기술을 개발하여 고품질의 질화갈륨 반도체 박막을 성장하였다.

우선, 그래핀 상에 고밀도 핵생성이 이뤄질 수 있도록 산소 프라즈마 처리를 해준다. 산소 플라즈마는 그래핀을 에칭하는 역할로 많은 dagling bond 들을 그래핀 상에서도 만들 수 있다. 이 후, 산화아연 나노 구조물을 그래핀 상에 성장하여 질화갈륨 반도체 박막 성장에 필요한 핵생성을 해준다. 마지막으로 질화갈륨 반도체 박막을 그 위에 성장하게 되면, 그래핀-산화아연 나노구조물-질화갈륨 박막의 에피탁시 관계 형성으로 인해 고품질의 반도체 질화갈륨 박막이 그래핀 상에서도 제조할 수 있게 된다. 이 성장 기술을 이용하여 처음으로 고품질의 반도체 박막이 그래핀 상에서 에피탁시 관계를 가지고 성장될 수 있다는 것을 보여주었다.

앞서 보여준 에피탁시 성장 기술을 이용하면, 다양한 그래핀 기판 상에서도 고품질 질화갈륨 반도체 박막을 성장할 수 있다. 그래파이트 덩어리에서 scotch tape 을 이용하여 떼어내는 방법으로 준비한 그래핀에서 뿐만 아니라 화학기상증착법 (chemical vapor deposition, CVD)으로 합성한 그래핀에서도 매끄럽고 평평한 표면 형상을 가진 질화갈륨 반도체 박막들을 성장할 수 있었다. 또한, 다양한 광학적, 구조적 분석법을 통해 기존에 3 차원 단결정 벌크 기판에서 성장된 질화갈륨 박막과 비견될 만큼의 뛰어난 소재 특성을 보여주었다. 더욱이, 그래핀에서 성장된 질화갈륨 박막은 탄소 불순물에 대한 영향을 거의 찾아볼 수 없었다. 만약, 그래핀의 탄소 불순물들이 질화갈륨에 섞여 있었다면 도핑이 어려워지므로 반도체 소자로 응용될 수 없었겠지만, 본연구에서는 질화갈륨/그래핀 이종구조를 이용한 p-n 접합 광소자들을 제조할 수 있었다.

본 연구에서는 그래핀 기판의 장점을 보여줄 수 있는 광소자들을 제조하였다. 그 대표적인 예로 이동가능한 LED 이다. 그래핀 기판 상에 LED 를 제조하기 위하여 인듐질화갈륨/질화갈륨 양자우물층이 포함된 p-n 접합구조 질화갈륨 박막을 성장하였고, 강한 청색 발광 LED 를 제조할 수 있었다. 또한 그래핀 기판의 전사성을 이용하여, 그래핀 상에 제조된 광소자들을 쉽게 금속, 유리, 플라스틱 등 다양한 기판에 이동시켜 구동할 수 있었다.

더욱이, 그래핀은 사파이어 기판과 같은 기존의 반도체 성장 기판보다 훨씬 큰 면적으로 제조할 수 있기 때문에 대면적 소자 제조에 매우 유리하다. 그 예로 본 연구에서는 쿼츠 기판에 질화갈륨-그래핀

이종구조를 이용하여 박막 LED 를 제조하였다. 쿼츠 기판과 같은 비정질 기판은 수십 인치 크기의 면적으로 쉽게 제조할 수 있을 뿐만 아니라 단결정 기판보다 저렴하다는 장점이 있어서, 대면적 디스플레이 같은 곳에서 매우 필요한 기판이라 할 수 있다. 하지만 이런 비정질 기판상에서 성장된 질화갈륨 반도체 박막은 에피탁시 관계를 형성하기 어렵기 때문에 고품질로 제조하기 매우 어렵다. 반면, 대면적 그래핀은 쿼츠 표면을 모두 덮을 수 있을 정도로 크게 제조될 수 있고, 그래핀이 코팅된 비정질 기판 상에서는 에피관계를 가진 박막 LED 를 성장할 수 있었다. 또한 쿼츠 기판에서 성장된 LED 의 밴드갭 조절을 통하여 청색과 녹색의 발광 소자를 구현하였다.

반면, 그래핀이 플라즈마 노출에 쉽게 식각되는 특성을 이용하여, 질화갈륨/그래핀 이종구조 기반의 광소자 어레이(array)를 제조할 수 있었다. 임의의 기판 위에 전사된 그래핀은 포토리소그래피와 산소 플라즈마 처리를 통해 다양한 크기의 그래핀 어레이로 제조될 수 있었고, 또한 질화갈륨이 그래핀 패턴상에 선택적으로 성장되는 조건을 탐색하여, 대면적이고 일정한 크기를 갖는 질화갈륨 미세구조물 어레이를 제조할 수 있었다. 이렇게 준비된 질화갈륨/그래핀 이종구조 어레이는 쉽게 다른 기판에 이동시킬 수 있고, 대면적 공정이 가능하다는 장점들을 보여줄 수 있을 뿐만 아니라, 마이크로 크기의 소자 형태를 가지고 있어서, 유연한 광소자로 이용될 수 있었다.

본 연구에서는 반도체 박막뿐만 아니라 1 차원 질화갈륨 미세구조물들도 그래핀 상에서 성장시킬 수 있는 기술을 개발하였다. 1 차원 미세구조물들은 높은 종횡비, 매우 작은 직경, 넓은 표면적, 개별

소자에 다양한 결정면을 가지는 등 매우 흥미로운 특성을 지닌 반도체 소재들이다. 특히, 이런 1 차원 미세구조물들은 작은 직경으로 인해 단결정 기판뿐만 아니라. 금속, 유리 등의 기판 상에서도 기판의 제약을 거의 받지 않고 고품질로 성장할 수 있다. 뿐만 아니라, 1 차원 미세구조물이 수직으로 정렬된 어레이 구조는 휘어지거나 구부릴 때 데미지가 거의 없어서 유연한 광소자 또는 전자소자 제조하는 데 뛰어난 장점을 가지고 있다. 하지만 이런 1 차원 미세구조물의 장점을 소자에 응용하기 위해서는 쉽게 떼어내거나 구부릴 수 있는 기판에 준비할 수 있어야 하는데, 본 연구에서는 1 차원 미세구조물을 그래핀 기판에 수직 성장하는 방법으로 유연한 광소자를 제조할 수 있는 기술을 확보했다. 질화갈륨 미세구조물들은 그래핀 기판 전면적에 수직으로 성장되어 있었고, 성장 밀도도 균일하게 분포되어 있었다. 또한, 구조적인 분석을 통하여 그래핀에서 성장된 질화갈륨 미세구조물들이 단결정으로 성장되어 있는 것을 확인할 수 있었고, 광학적인 분석을 통해서 광소자로서의 응용이 가능함을 입증하였다. 이에, 그래핀에 성장한 1 차원 질화갈륨 미세구조물을 이용하여 유연한 LED 를 제조하였다.

유연한 LED 를 구현하기 위해서, 인듐질화갈륨/질화갈륨 양자우물 구조가 포함되어 있는 p-n 접합 1 차원 질화갈륨 미세구조물을 제조하였다. 박막 LED 와 마찬가지로, 1 차원 미세구조물 LED 는 그래핀 상에서 제조되었기 때문에, 쉽게 기판에서 떼어내거나 붙일 수 있어서 유연한 플라스틱 기판에 전사할 수 있었다. 더욱이 본 연구에서 LED 로 사용된 소재들은 1 차원 미세구조물과 그래핀으로 뛰어난 유연성을 기대할 수 있었다. 유연성 측정 결과, 그래핀에서 제조된 1 차원

LED 들은 1000 번 이상의 구부림에도 안정적인 작동을 하는 것을 확인할 수 있었다.

요약하면, 본 연구에서는 그래핀과 무기물 반도체가 에피 관계로 결합되어 있는 이종 구조를 제조하고, 이를 이용한 신기능 소자를 제조하는 연구를 수행하였다. 특히, 그래핀이 가지고 있는 뛰어나고 독창적인 물리적 특성들을 반도체 소자인 LED 에 접목하여 무기물 기반의 이동가능하고, 대면적 저비용 공정에 유리하고, 유연성을 지닌 광소자를 제조할 수 있었다.

Curriculum Vitae

Personal Information

Name: Kunook Chung

Nationality: South Korea

Address: Dept. of Physics and Astronomy, Seoul National University,
599 Gwanak-ro, Gwanak-gu, Seoul 151-742, South Korea

Phone: +82 2 877 2651 (Lab), +82 10 3099 5716 (Cell)

E-mail: cnjoy199@snu.ac.kr, kunookc@gmail.com

Education

Mar. 2009. – Feb. 2014.	Ph.D. in Physics, SNU, Seoul, South Korea. Advisor: Prof. Gyu-Chul Yi (Dept. of Physics and Astronomy, and Inst. of Applied Physics, SNU)
Mar. 2001. – Feb. 2009.	B.S. in Physics, SNU, Seoul, South Korea.

Awards and Scholarship

2011–2014	TJ Park Ph.D. Scholarship, POSCO TJ Park Foundation.
2011	Brain Korea fellowship, Dept. of Physics and Astronomy, SNU.
2013	Brain Korea fellowship, Dept. of Physics and Astronomy, SNU.

Research Interests

- Epitaxial growth and position controlled growth of inorganic semiconductor thin films, micro- and nanostructures on various substrates including graphene.

- Heteroepitaxy, band-gap control, and doping in inorganic semiconductors for high performance optoelectronics.
- Fabrication of transferable and flexible optoelectronic devices using inorganic semiconductor/graphene hybrid heterostructures.

Experimental Experience and Skills

1. Material growth

- Metal organic chemical vapor deposition for nitride semiconductors: GaN, $In_xGa_{1-x}N$, $Al_xGa_{1-x}N$ thin films, 1D GaN micro- and nanostructures, GaN/$In_xGa_{1-x}N$ quantum structures, GaN/ZnO heterostructures, and GaN hetroepitaxy on graphene and *c*-Al_2O_3 substrates.
- Metal organic chemical vapor deposition for ZnO: 1D ZnO nanostructures including ZnO nanowalls and nanorods
- Chemical vapor deposition for graphene: CVD graphene on Cu and Ni films

2. Device fabrication

- GaN-based optoelectronic devices including LEDs and photovoltaic devices.
- Apparatus: photolithography and e-beam lithography, thermal and e-beam evaporators, sputter, electroplating, plasma etching system including reactive ion etching (RIE), rapid thermal annealing.

3. Characterization

- Material characterization: electron microscopy (FE-SEM, SEM), AFM, temperature-dependent and power-dependent PL, CL, Raman spectroscopy, XRD, TEM, EBSD, room temperature Hall measurement.

- Device characterization: EL, LED output power measurement, photovoltaic measurement.

Publications

1. Kunook Chung, Chul-Ho Lee, and Gyu-Chul Yi, Transferrable GaN layers grown on ZnO-coated graphene layers for optoelectronic devices, ***Science***, **330**, 655 (2010).
2. Hyobin Yoo, Kunook Chung, Yong Seok Choi, Chan Soon Kang, Kyu Hwan Oh, Miyoung Kim, Gyu-Chul Yi, Microstructures of GaN thin films grown on graphene layers, ***Adv. Mater.***, **24**, 515 (2012).
3. Min Hwa Kim, Kunook Chung, Dae Young Moon, Jong-Myeong Jeon, Miyoung Kim, Jinsub Park, Yasushi Nanishi, Gyu-Chul Yi and Euijoon Yoon, Catalyst-free metal-organic chemical vapor deposition growth of InN nanorods, ***J. Nanosci. Nanotechnol.***, **12**, 1645 (2012).
4. Kunook Chung, Suk In Park, Hyeonjun Baek, Jin-Seok Chung and Gyu-Chul Yi, High-quality GaN films grown on chemical vapor-deposited graphene films, ***NPG Asia Mater.***, **4**, e24 (2012).
5. Hyeonjun Baek, Chul-Ho Lee, Kunook Chung, and Gyu-Chul Yi, Epitaxial GaN microdisk lasers grown on graphene microdots, ***Nano Lett.***, **13**, 2782 (2013).
6. Hyobin Yoo, Kunook Chung, Suk In Park, Miyoung Kim, and Gyu-Chul Yi, Microstructural defects in GaN thin films grown on chemically vapor-deposited graphene layers, ***Appl. Phys. Lett.***, **102**, 051908 (2013).

7. Kunook Chung, Hyeonjun Beak, YoungbinTchoe, Hongseok Oh, Hyobin Yoo, Miyoung Kim and Gyu-Chul Yi, Growth and characterizations of GaN micro-rods on graphene films for flexible light emitting diodes, ***APL Materials***, **2**, 092512 (2014).
8. Hyeonjun Baek, Jerome K. Hyun, Kunook Chung, Hongseok Oh, and Gyu-Chul Yi, Selective excitation of fabry-perot or whispering-gallery mode-type lasing in GaN microrods, ***Appl. Phys. Lett.***, **105**, 201108 (2014).
9. Kunook Chung and Gyu-Chul Yi, Design of large-scale and flexible GaN microstructure light emitting diodes using two-dimensional graphene dot array, in preparation.
10 Kunook Chung and Gyu-Chul Yi, Position controlled growth of highly Si-doped GaN micro-rods, in preparation.

International Conference Presentations

1. International Workshop on Nitride Semiconductors (IWN), Sapporo, Japan. (Oct. 2012)

   Oral presentation: "GaN-based visible light-emitting diodes on a chemical vapor deposited graphene film".
2. 16th International Conference on Metal Organic Vapor Phase Epitaxy (ICMOVPE-XVI), Pusan, South Korea. (May. 2012)

   Poster: "GaN-based visible light-emitting diodes on a chemical vapor deposited graphene film".

3. MRS Spring Meeting, SanFrancisco, USA. (Apr. 2012)

   Oral presentation: “GaN-based visible light-emitting diodes on a chemical vapor deposited graphene film”.

4. 7th International Conference on Advanced Materials and Devices (ICAMD), Jeju, South Korea. (Dec. 2011)

   Poster: “GaN-based visible light-emitting diodes on a chemical vapor deposited graphene film”.

5. International Symposium Physics of Semiconductors and Applications (ISPSA), Jeju, South Korea. (Aug. 2011)

   Oral presentation: “Transferrable GaN Layers Grown on ZnO-coated Graphene Layers for Optoelectronic Devices”.

6. Materials Research Society Spring Meeting, SanFrancisco, USA. (Apr. 2011)

   Oral presentation: “Transferrable GaN Layers Grown on ZnO-coated Graphene Layers for Optoelectronic Devices”.

National Conference Presentations

1. TJ Park Science Symposium, POSCO Center, Seoul, South Korea. (Jul, 2013)

   Oral presentation: “Light-emitting diodes fabricated on graphene films”

Patents

-Registered

1. Gyu-Chul Yi, Kunook Chung, “Optoelectronic Device and Method for Manufacturing the Same”, South Korea, *1012674500000* (2013.05.20)
2. Gyu-Chul Yi, Kunook Chung, Chul-Ho Lee, “Electronic Device and Manufacturing Method Thereof”, South Korea, *1013093080000* (2013.09.10).

3. Gyu-Chul Yi, Kunook Chung, Chul-Ho Lee, “Light Emitting Device and Method for Manufacturing the Same”, South Korea, *1012172100000* (2012.12.24).

- Applied

1. Gyu-Chul Yi, Kunook Chung, “Optical Device and Method for Manufacturing Same”, US, *KR-2012-006484*, (2012.08.14).
2. Gyu-Chul Yi, Kunook Chung, Chul-Ho Lee, “Electronic Device and Manufacturing Method Thereof”, PCT, *KR-2012-002886*, (2012. 04.14).
3. Gyu-Chul Yi, Kunook Chung, Chul-Ho Lee, “Light-emitting Element and Method for Manufacturing Same”, US, *KR-2011-007461*, (2011.10.07).
4. Gyu-Chul Yi, Kunook Chung, “Thin Film Device”, South Korea, *10-2010-0051029* (2010.05.31).